PCM-based Ceiling Panels for Passive Building Indoor Cooling: Experimental and Numerical Study

A thesis submitted for the degree of

Master of Philosophy (MPhil)

by

Mr Shufan Yang

U6104095

Primary Supervisor: Dr Xiaolin Wang

Chair Supervisor: Dr Xiaolin Wang

Associate Supervisor: Dr Yongling Zhao

School of Engineering

College of Engineering, Computer Science, and Cybernetics

The Australian National University

August 2023

This thesis is an account of research undertaken between August 2021 and August 2023 through the College of Engineering, Computer Science, and Cybernetics at the Australian National University.

This thesis contains no material which has been accepted for the award of any other degree of diploma in any university. To the best of the author's knowledge, it contains no material previously published or written by another person, except where due reference is made in the text.

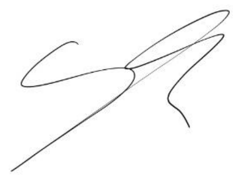

Shufan Yang

01 August 2023

Acknowledgement

The completion of this work could not have been possible without the participation, assistance, and support of a number of individuals and organisations. They are sincerely appreciated and gratefully acknowledged below:

I would like to appreciate sincerely to my primary and chair supervisor Dr Xiaolin Wang for her supervision, leading, and support throughout my MPhil program. Dr Wang is highly responsible for my research progressing and always willing to provide me with help when I encountered questions or doubts. The professional guidance and reasonable judgment of Dr Wang really facilitated my study and work during my candidature. It was a pleasure to work with Dr Wang, and this thesis could not have been possible without her great efforts.

I would also like to express my gratitude towards Dr Yongling Zhao and Dr Juan Felipe Torres who offered me insightful suggestions to overcome various difficulties and optimise the deliverables of my work with their knowledge and expertise. They always picked time from their busy scheduling to meet and talk with me, even outside of the standard working hours.

I would also like to thank Yuxuan Zhang, Shuqi Xu, and Junxiang Zhang for the sharing of their technical experience and research equipments to fulfil or support my research need. My appreciation also goes to the admin team and technical service team of the School of Engineering, where the administrative and technical support really helped my work.

Thanks also go to my fellow graduate students and colleagues, especially Wilhiam de Carvalho, Sophie Burgess, and Sam Coggins for our relaxing talks over the lunch break with endless joy. The sharing of the life stories and experience added colours to our study.

I would like to thank all the course convenors that I worked with for their kind offer of the tutoring opportunities, which improved and enhanced my professional skills. Appreciation also goes to all my fellow tutors, with whom the courses were delivered smoothly.

I would like to appreciate the anonymous reviewers of the paper I have published during my candidature for their valuable feedback. The quality of the paper was assured with their comments and feedback.

Last but not least, I wish to express my deepest appreciation and love to my partner Han Zhang, who provided me with solid supports and care during my candidature. I also thank my parents and grandparents back in China for their financial support which allowed me to study and pursue degrees abroad for more than 7 years. Every bit of my achievement and success was based on their love, encouragement, and support. Moreover, I appreciate the time of my elderly grandparents, where we had long talking about my study, work, and life over the countless phone calls.

Abstract

To relieve the upsurge of the energy demand associated to building indoor cooling, passive cooling employing phase change materials (PCMs) has been proposed as a promising technique to stabilise indoor air temperature fluctuation and reduce building energy demand. PCMs can exchange a large amount of latent heat during the melting and solidification processes, which can be utilised in line with the discharging and charging processes of a cooling system. The use of encapsulated PCM ceiling panels in buildings has immense application potential for passive cooling, which has attracted investigations in recent years.

The geometry selection of the PCM ceiling panel is vital as it determines the exposed surface area to the surrounding air and the natural convection, and therefore the heat transfer rate to/from the PCM, which generally suffers from low thermal conductivity. The first part of this study builds on the geometric optimisation of enclosed PCM capsules driven by natural convection, aiming to investigate the phase change behaviour and thermal performance of encapsulated PCM ceiling panels of different geometries. Here, the presented study focuses on the conjugate heat transfer phenomena through the surrounding air, panel shell, and PCM. A mixture of lauric, capric, and oleic acids was selected as PCM encapsulated in a thin-shell enclosure made of acrylonitrile butadiene styrene plastic, which forms the aesthetic panels attached to the ceiling. A computational fluid dynamics model was validated using full-scale experimental data and further employed to analyse the discharging process and design considerations of the PCM ceiling panels. The effects of various influencing factors were explored, such as panel volume, the initial temperature difference between PCMs and surrounding air, shell thickness, and geometrical features. The results indicate that the panel comprised of a pyramid array is more advantageous than the tetrahedral-based panel in terms of thermal performance, where the average melting rate is 20.8% higher when the panel volume is 250 mL.

In addition, tweaking the geometric features of the panel will largely impact its thermal performance as the effective heat transfer area and natural convection conditions are varied. Finally, it was found that hanging the panel to the ceiling will effectively enhance the heat transfer compared to directly attaching it to the ceiling. The results complement the knowledge body of macro-encapsulated PCM ceiling panels in terms of thermal performance and geometric optimisation. The effects of geometric features on the thermal performance of the PCM ceiling panels are studied in a more holistic manner.

The second part of this study builds on the prior numerical investigations on the phase change behaviour and thermal performance of individual encapsulated PCM ceiling panel of different geometries, aiming to further investigate the thermal performance of multiple encapsulated PCM ceiling panels (i.e. PCM ceiling panels array) in an outdoor storage enclosure with negligible thermal mass. A mixture of lauric and capric acids was selected as PCMs encapsulated in self-designed thin-shell panels. Through additional simulations, the performance of PCM panels under realistic varying ambient temperature were investigated and compared to that under constant ambient temperature. Through a holistic experiment, the panel performance was evaluated with metrics of indoor-outdoor temperature difference and indoor temperature homogeneity, considering the effects of outdoor temperatures and solar irradiations. It was found that the PCM panels reduced the daily average indoor-outdoor temperature difference by 88.4% under similar daily weathers and generally reduced the indoor-outdoor temperature difference for the studied days. With PCM panels, the indoor temperature can sometimes be lower than the outdoor temperature, which is not possible without PCM. The vertical temperature gradient showed better homogeneity in the upper part, which was evidenced by both experiment and simulations. This study complements to the current research on PCM ceiling panels for building passive cooling under real working conditions.

Table of Contents

List of Figures

List of Tables

Nomenclature

Abbreviations

TES	Thermal energy storage
PCM	Phase change material
CFD	Computational fluid dynamics
DSC	Differential scanning calorimetry
DTA	Differential thermal analysis

Variables

ρ_{PCM}	Density of PCM	[kg m^{-3}]
ρ_{air}	Density of air	[kg m^{-3}]
$\mathrm{A}_{\mathrm{mush}}$	Mush zone constant	
λ_{PCM}	Thermal conductivity of PCM	[W m^{-1} K^{-1}]
λ_{shell}	Thermal conductivity of panel shell	[W m^{-1} K^{-1}]
$c_{p,l}$	Specific heat of liquidus PCM	[kJ kg^{-1} K^{-1}]
$c_{p,s}$	Specific heat of solidus PCM	[kJ kg^{-1} K^{-1}]
$c_{p,\mathrm{shell}}$	Specific heat of panel shell	[kJ kg^{-1} K^{-1}]
h_{sen}	Sensible enthalpy	[kJ kg^{-1}]
L	Latent heat of fusion	[kJ kg^{-1}]
m	Mass of PCM	[g]
T_{liquidus}	Liquidus temperature of PCM	[K]
T_{solidus}	Solidus temperature of PCM	[K]
T_{PCM}	Temperature of PCM	[K]
T_{air}	Temperature of air	[K]
T_{shell}	Temperature of panel shell	[K]
t	Time	[min]

Chapter 1 – Introduction

1.1 Background and Motivation

In recent decades, the electricity consumption has substantially increased as the global population grows. Among all the sectors with substantial growth such as agriculture, industry, transport, and infrastructure, industrial and building sectors have contributed significantly to the increase of global electricity consumption [1]. The building sector corresponds to 30–40% of the total global electricity consumption, where majority of the building energy consumption corresponds to the heating, ventilation, and air conditioning (HVAC) for either residential or commercial buildings [2]. In United State, 6% of the total electricity production is consumed by the air conditioners, which creates a cost of 29 billion USD to homeowners annually. This also results in an annual carbon dioxide emission of approximately 117 million metric tons [3]. According to *Australia's air conditioning usage statistics 2022*, 64% of the Australian people rely on the air conditioners in the summer months, which costs a collective 2.4 billion AUD [4]. The energy costs for air conditioning are overwhelming, which brings environmental challenges such as depletion of the ozone sphere, intensification of global warming, and greenhouse effect [5]. As a result of excessive carbon emissions and global warming, the rise in average atmospheric temperature would further intensify the energy demand for space indoor cooling, which triggers a wretched cycle.

Another factor that contributes to the demand of indoor cooling is to do with the emerging building constructions. The emerging construction techniques have made the lightweight-design buildings to dominate, which have reduced thermal mass compared to the conventional buildings [6]. The reduced thermal mass makes the buildings to have lower thermal inertia, where the thermal energy is much easier to penetrate into or be extracted from the building interior. Therefore, the indoor temperature becomes more sensitive to the external temperature change.

The electricity consumption for the air conditioning of residential and commercial buildings not only brings the environmental challenges but also poses a great burden on the electricity grid, where the high peak transmission stress on the grid infrastructure may cause some negative effects such as overloading or even power failure. In addition, the peak electricity rate will increase as the large peak electricity demands, which makes air conditioning less affordable to the building owners or users.

Therefore, overcoming the challenges of substantial energy demands for building indoor cooling and reduce the burden of electricity grid infrastructure at the peak hours with an effective approach is of great significance. In recent years, numerous building cooling options integrated with renewable energy have been proposed to mitigate the different environmental concerns as results of the over usage of air conditioning. Among all the environmentally-friendly options, passive cooling technologies have been proposed as a promising pathway to provide thermal comfort with the lowest energy cost possible, and support to the environment and ecosystem. Passive cooling technologies employ the low-temperature ambient as a cooling sink to mitigate the indoor temperature rise. As there is no mechanically assisted system, passive cooling technologies can maintain indoor thermal comfort with minimal or no energy cost. Thermal energy storage is an exemplary approach for passive cooling, and PCMs are widely adopted in thermal energy storage since PCMs can exchange a large amount of latent heat during the phase change process in narrow temperature ranges. PCMs absorb heat during the endothermic melting process while releasing heat during the exothermic solidification process. PCM-based thermal storage can be an effective complement to the overall thermal mass of building envelopes, where the incorporation of PCMs into building envelopes can reduce the energy demand for cooling, smoothen indoor temperature fluctuation, and improve the thermal comfort of building occupants [7]. Furthermore, this also benefits the electricity grid infrastructure and end-users by reducing the burden over the peak hours and lowering the electricity expense, respectively.

In the current available literature, it is proved that PCMs can be incorporated into different building envelopes or building materials to form PCM-filled wallboards, PCM walls, PCM floors, PCM ceilings, PCM windows, and PCM shutters by many different incorporation methods [7]. Among all the PCM-based applications, PCM ceilings are recognised to be more advantageous and deployable for several reasons: The ceiling has large area of contact for exchanging the heat between the interior and exterior; more direct interaction with vertical thermal plumes can be achieved [8]; the indoor furniture arrangement and layout are not affected; the effective indoor area for human activities is not reduced. Thus, effective control of heat exchange through PCM ceilings or PCM ceiling panels is promising for building indoor thermal management. To achieve this, an extensive analysis on the geometric configurations of the PCM ceilings or PCM ceiling panels is essential to thoroughly understand their thermal performance. In addition, it is desirable if the PCM ceiling panels are flexible in terms of the PCM amount, position, and layout to obtain benefits in performance not achieved in otherwise static configuration. As discussed in the following chapters, most PCM ceiling panels are macro-encapsulated, where PCMs are filled into the hollow panel before sealing and being attached to the ceiling. In this case, the panel serves as a container for PCMs. However, within the current available literature, there is a lack of analysis on the geometric configurations of the PCM ceilings although the understanding of the effects of the geometry on thermal performance is rather vital. Besides, the PCM amount, position, and layout of the PCM ceiling panels are static in most of the available literature [9]. In addition, the current research on PCM ceiling panels mainly focuses on the residential and commercial buildings, these examples have relatively decent thermal mass from the construction materials. However, there is no research on the PCM ceiling panels for the indoor cooling of outdoor storage enclosures or machine rooms with very low or negligible thermal mass. Nevertheless, the cooling for these examples is also essential from the perspective of reducing thermal degradation and fire safety of the stored materials or ensuring machines' safe operation.

From a previous study, it is proved that CFD numerical modelling can be employed to study the melting behaviour of PCMs encapsulated in capsules with different geometries. Based on this previous study, the presented study extends and focuses on demonstrating the passive building indoor cooling using macro-encapsulated PCM ceiling panels, with an emphasis on the CFD-based geometric optimisation of the ceiling panels and the real-world applicability of PCM ceiling panels in an outdoor storage enclosure. The mixture of the capric and lauric acid was adopted as the PCMs due to the reason that different phase change temperatures can be achieved by varying the proportions of the two acids. In this study, through both simulation and experimental work, the following research questions are addressed:

1. What are the effects of geometric features on the thermal performance of macro-encapsulated PCM ceiling panels?
2. For multiple PCM ceiling panels with optimised geometry, what cooling efficacy can they provide to an outdoor storage enclosure in the area with large day-night temperature difference?

Overall, the aims and objectives of this thesis are to optimise the geometric configuration of the macro-encapsulated PCM ceiling panels using CFD numerical modelling and investigate the thermal performance (i.e. cooling efficacy) of the panel array with the optimised geometry configuration in an outdoor storage enclosure.

1.2 Thesis Outline

This thesis gives a comprehensive insight into the thermal performance of PCM ceiling panels. It includes a simulation work on how the geometric features of macro-encapsulated PCM ceiling panels can affect the thermal performance by considering the conjugate heat transfer and an experimental study to prove the applicability of PCM ceiling panels for the indoor cooling of an outdoor storage enclosure in the area with high day-night temperature difference. A CFD model is developed and validated to analyse the effects of different geometric features on the thermal performance of PCM ceiling panels. Moreover, this study provides data on the full-scale working conditions of PCM ceiling panels for passive cooling, which can be used as a reference for future industrial real-world implementations.

Chapter 2 includes detailed introduction and the thorough review of the current literature on the topic of building passive cooling technologies. It covers the context, background, motivation, and common methodologies in this research topic. This chapter serves as an usher to the thesis work by summarising the current studies on the topic of building passive cooling and identifying the knowledge gap to be filled.

Chapter 3 introduces a simulation work to optimise the geometric configuration of the individual PCM ceiling panel and study the effects of its geometric features on the thermal performance, considering conjugate heat transfer. The numerical model was developed in the commercial software package Ansys Fluent 2020 R2, and validated with full-scale experiment. The validated numerical model was then used to investigate the different influencing factors on the thermal performance of the individual PCM ceiling panel.

To further investigate the passive cooling potential of PCM ceiling panels in the low-thermal-mass building envelope, an experimental study was carried out on-site in the city of Canberra, where the day-night temperature difference is relatively large due to its geographical location and climate. This experimental study is introduced in Chapter 4. Based on the optimal geometric configuration obtained from the simulation work in Chapter 3, a PCM ceiling panel array consisting multiple individual PCM ceiling panels was mounted to the ceiling of an outdoor storage enclosure (i.e. a metal shed). The metal shed has very low thermal mass with the major heat gain to be solar irradiation. The internal PCM temperature, indoor temperature, and outdoor temperature were measured at multiple measurement points. By analysing the measured data, the PCM ceiling panels were proved to be an effective thermal mass add-on to those buildings or rooms with poor thermal inertia. The indoor temperature fluctuations can be smoothened with reduced peak indoor temperature.

Chapter 5 summarises the main findings of the thesis work and wraps it up into a conclusion. It reiterates that PCM ceiling panels are a promising approach for passive building indoor cooling. This approach only relies on the day-night temperature swing and therefore the cooling is achieved at no extra energy costs. In addition, this is also a safe and non-toxic approach with the minimal impact to the building mechanical structures. Finally, some recommended future works are included in this chapter.

1.3 Publications and Extracurricular Work

The partial work of this MPhil thesis presented in Chapter 3 has been published, while the remainder of this MPhil thesis presented in Chapter 4 is to be published.

A significant part of this work is in determining the optimal geometric configuration of the PCM ceiling panels. Therefore, the author carried out a simulation work on the discharging process of the PCM ceiling panels to investigate and determine the optimal geometric configuration of the PCM ceiling panels. This part of work includes the development and validation of a CFD model. The results of this part of work are presented in a journal paper – 'PCM-based ceiling panels for passive cooling in buildings: A CFD modelling'. *Energy and Buildings* 2023; 285:112898.

The author gave a 30-min guest lecture talk on the CFD modelling of PCM ceiling panels in the course *ENGN3338 Aerodynamics* to 3rd-year undergraduate students within School of Engineering, College of Engineering, Computer Science, and Cybernetics, Australian National University (ANU), in August 2022. The author also tutored the courses *ENGN3224/6224 Fluid mechanics and heat transfer* in 2022, *ENGN3338 Aerodynamics* in 2022 and 2023, and *ENGN2222 Engineering Thermodynamics* in 2023.

Chapter 2 – Building Thermal Management and Indoor Passive Cooling

2.1 Building as a Thermodynamic System

Thermodynamics reveal the correlation between energy and temperature. A better understanding about building energy consumption and thermal comfort can be gained with the thermodynamic principles. For a building, all the thermodynamic interactions between different systems are essentially governed by the laws of thermodynamics. Ideally, the building design approach is supposed to ensure the all-year thermal comfort with minimum consumptions of energy. In optimum, the building envelope possesses appropriate thermal insulation and storage characteristics, so that the influence of external temperature change to the indoor temperature could be mitigated by decaying or delaying. Therefore, the indoor air temperature can be maintained at a comfortable level for building occupants without the use of any heating or cooling units [10]. However, the building is a very complex thermodynamic system, where numerous thermodynamic interactions exist. The building thermodynamics are impacted by both external and internal factors, so the aforesaid perfection is usually hard to achieve. The external factors are typically determined by the local climate and geography, which include solar irradiation, wind speed, humidity, and air temperature. The internal factors include internal heat sources and indoor space arrangement. Thus, on top of fulfilling the basic requirements for mechanical considerations, it is vital to design the building based on the considerations of specific climate, locality, and its functionality. Items such as material selection of building envelope, room size, wall thickness, and occupation rates should be carefully considered in the design stage of the building, in order to achieve the optimal thermal performance with the minimum assistance of cooling or heating units. Notably, the building envelope, functioning as the boundary of interior and exterior, is an essential component in terms of heat exchange. Hence, the thermophysical properties of the building envelope plays the key role in determining the indoor thermal comfort [11].

2.2 Lightweight/heavyweight-design buildings

The fundamental philosophy in building constructions is evolving as time going by. The lightweight-design buildings are becoming more popular in recent years, as they show a lot of advantages over the heavyweight-design buildings. Heavyweight construction materials are mainly masonry such as brick, concrete, tiles, rammed earth, and mud brick, while lightweight construction materials normally include steel and wood frame [12]. The main components and thermophysical properties of common lightweight and heavyweight construction materials are summarised in Table 2.1 below.

Table 2.1. Thermophysical properties of common lightweight and heavyweight construction materials [13] [14] [15].

Material	Classification	Main component	Thermal conductivity (W m^{-1} K^{-1})	Specific heat capacity (kJ kg^{-1} K^{-1})	Density (kg m^{-3})
Concrete	Heavyweight	Aggregates (coarse/fine)	0.6–3.3	1.0	2000
Brick	Heavyweight	Silica	0.73	0.8	1700
Tile	Heavyweight	Clay	0.6–1.7	0.85	2000
Steel	Lightweight	Iron	45	0.48	7800
Timber	Lightweight	Cellulose	0.14	1.2	650

Compared to heavyweight-design buildings, lightweight-design buildings allow fast construction, high flexibility in renovation, and easy transportation of materials with an overall low cost. In addition, the production of lightweight construction materials is low in the energy consumption as well as the residual waste. Thereby, the lightweight-design buildings are advantageous from the perspective of cost effectiveness and environmental load [16]. Although lightweight-design buildings show advantages over heavyweight-design buildings from the dimensions of material production, material transportation, construction speed, and retrofitting flexibility, they are, however, usually defective from the dimension of building thermal comfort. The thermal mass and insulation capability of the building are two determining factors of building thermal comfort, which is influenced by the intrinsic properties of the building construction materials such as specific heat capacity, thermal conductivity, and density. On top of the intrinsic properties of building construction materials, the building thermal comfort can be also impacted by the openings of the building envelope such as glazing, lovers, and ventilations. Specific heat capacity determines how much heat or thermal energy that the material with unity mass can store when the temperature varies by one degree Celsius. The material with high thermal mass usually possess high specific heat capacity. Thermal conductivity determines how fast the heat can transport through the material. Ideally, the construction materials are supposed to possess moderate thermal conductivity, so that the building can manifest certain insulation capability, while the absorption and releasing of the heat can be cooperative with the cooling and heating cycles of the building. Density is the mass of material with unity volume. High material density can guarantee the high mass at the fixed volume, which is favourable for achieving high thermal mass [15]. The lightweight-design philosophy in building constructions would typically result in the low thermal mass and inappropriate thermal insulation of the building envelope, where the building envelope has low capability in absorbing, storing, and releasing thermal energy. In this case, the building indoor temperature is very sensitive to the external temperature change, and the resultant indoor temperature fluctuation will have negative impact on thermal comfort of the building occupants. For example, in the daytime of summer season, the outdoor temperature rises due to the solar irradiation. The indoor temperature of lightweight-design buildings will be highly vulnerable to this outdoor temperature rise and therefore rise with shorter time lag compared to the heavyweight-design buildings due to the low thermal mass of the building envelope. The heat transfers through the building envelope from exterior to interior with low delay or decay, which elucidates the low thermal inertia of the building envelope. Consequently, the building will be problematic for overheating or overcooling, with the corresponding poor thermal comfort affecting the health and wellbeing of the building occupants [17]. In this case, there is considerable demand for the deployment of cooling or heating appliance such as air conditioner to adjust and control the indoor thermal conditions. As such, the lack of thermal mass in lightweight-design buildings will lead to the overwhelming energy cost on heating and cooling, which is unbeneficial both environmentally and financially [18].

2.3 Building Passive Cooling Technologies

As the escalating global warming and greenhouse effect, the building thermal management tend to be more inclined to indoor cooling than indoor heating. As opposed to the high-energy-cost active cooling, the passive cooling technologies employ the low-temperature ambient as a cooling sink to extract coolness and therefore mitigate the indoor temperature rise due to various heat sources such as direct solar gain and internal heat gain. The low-temperature ambient serves as a medium to prevent the heat away from the indoor environment. As there is no mechanically assisted system, passive cooling technologies could maintain the indoor thermal comfort in an environmentally-friendly manner with the lowest energy cost possible. In general, passive cooling technologies can be classified into three categories: heat protection, heat modulation, and heat dissipation [18]. Heat protection is the technique to protect the building from the direct solar gain, which is dominant source of the incoming heat. Heat protection can be further classified into microclimate and solar control, where landscaping, active vegetation, water surface, and shading are frequently used methods. In heat modulation, the heat gain is modulated by the thermal mass of the building structure, which depends on the energy storage capacity of the building envelops. Heat dissipation comprises convective cooling, which takes air as heat sink; evaporative cooling, which takes water as heat sink; and radiative cooling, which takes sky as heat sink. It disposes the excessive heat of a building to a low-temperature environmental sink by thermal coupling, which would provide effective cooling effects in a short period of time or shift the nocturnal coolness for diurnal cooling demand [18]. A holistic classification of passive cooling technologies is presented in Figure 2.1 below.

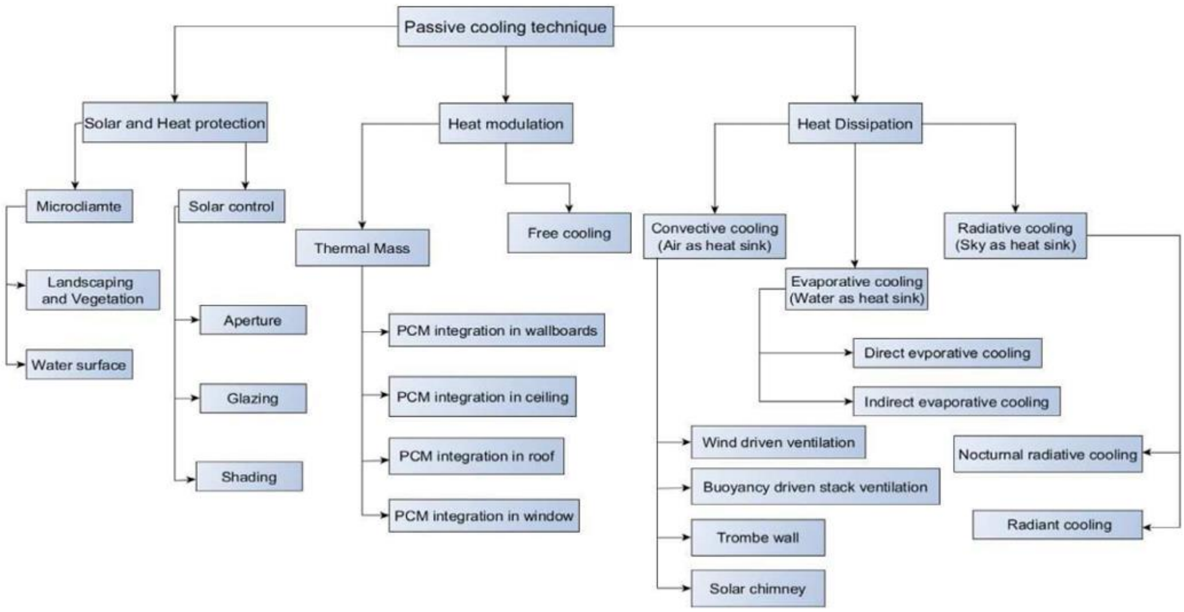

Figure 2.1. Holistic classification of passive cooling technologies [18].

Obviously, the heat modulation relies heavily on the thermal mass of the building envelope, where the thermal mass is to do with the thermophysical properties of the building construction materials. For lightweight-design buildings, the building envelope is typically unable to provide sufficient thermal mass for the purpose of heat modulation. Therefore, the additional thermal energy storage is required as complements to the existing building envelope to achieve the purpose of heat modulation for passive cooling.

2.4 Building Thermal Energy Storage

Thermal energy storage (TES) complements to the shortage of lightweight-design buildings not having sufficient thermal mass. TES is beneficial when incorporated into the building envelope or blended into the existing cooling systems. When being incorporated into the building envelope, TES can improve the thermal mass of the building substantially and provide additional thermal inertia to the heat gain, which realises the purpose of heat modulation; when being blended into the existing cooling systems, it utilises the temperature difference between the daytime and night to enable the load shifting. That is, the cooling capacity is accumulated at night, where the low-temperature ambient is employed as a heat sink, and then deployed for cooling services in the daytime. By accessing the off-peak inexpensive electricity rate, it also helps to reduce the total electricity costs and mitigate the electricity grid peak load, which realises demand management. In addition, the incorporation of TES into the existing building cooling systems can also reduce the on-off cycles of the cooling systems, which prolongs the system lifetime [19]. In the context of this study, we mainly focus on the incorporation of TES to the building envelope, with which the building will have an overall enhanced resisting ability to heat transfer from the exterior to the interior by natural means such as conductive, convective, and radiative heat transfer, as well as phase change process [20]. Common TES technologies for buildings include sensible heat TES, latent heat TES, and thermochemical TES. The first two technologies are usually implemented in the passive systems while the third technology is usually implemented in the active systems [21]. In the following context, the TES technologies for passive systems will be elaborated. Overall, the incorporation of TES technologies can effectively improve the building energy efficiency.

2.4.1 Sensible Heat TES

Sensible heat TES is realised by the temperature variation of the storage medium without the occurrence of the change of aggregate state (i.e. the storage medium remains solidus, liquidus, or gaseous). That is, the phase change temperature of the storage medium is beyond the temperature range within which the heat exchange occurs. The process of sensible heat TES is usually slow, so it takes the system a long time to store the thermal energy. The amount of thermal energy stored is determined by three factors: the specific heat capacity of the storage medium, the mass of the storage medium, and the temperature different between the initial and final states of the storage medium. Mathematically, this relationship can be expressed as:

$$Q = C_{\mathrm{p}} m (T_{\mathrm{final}} - T_{\mathrm{initial}}) \tag{2.1}$$

where Q is the amount of thermal energy stored, C_{p} and m is the specific heat capacity and mass of the storage medium, T_{final} and T_{initial} are the final and initial temperature of the storage medium, respectively.

In building passive cooling, the sensible heat TES is usually implemented by applying solid or liquid storage medium to the building envelope or peripherals [22]. Sensible heat TES is simple, inexpensive, and safe. However, the storage capacity is limited by the specific heat capacity of the storage medium. Large amount of storage medium is required to meet the storage demand if the medium has relatively low specific heat capacity [23].

2.4.2 Latent Heat TES

Latent heat TES is realised by the phase change process of the storage medium. During the entire process of heat exchange, the aggregate state of the storage medium gets changed either isothermally or within a narrow temperature band. Thereby, the thermal energy is stored in the latent form. For example, the aggregate state of the storage medium is changed from solid to liquid when the ambient temperature rises over the melting point of the storage medium. In this process, the chemical bonds break so that the phase change is triggered. For solid-liquid latent heat TES, which is the most common latent heat TES for passive cooling, the amount of thermal energy stored can be mathematically expressed as:

$$Q = C_{\mathrm{p,s}} m (T_{\mathrm{solidus}} - T_{\mathrm{initial}}) + mL + C_{\mathrm{p,l}} m \left(T_{\mathrm{final}} - T_{\mathrm{liquidus}}\right) \tag{2.2}$$

where Q is the amount of thermal energy stored; $C_{\mathrm{p,s}}$ and $C_{\mathrm{p,l}}$ are the specific heat capacity in solid and liquid states, respectively; m is the mass of the storage medium; T_{solidus} is the highest temperature at which the material is completely solid; T_{liquidus} is the lowest temperature at which the material is completely liquid; L is the latent heat of fusion; T_{final} and T_{initial} are the final and initial temperature of the storage medium, respectively. In the Equation (2.2), the first term refers to the sensible heat of the solid phase, the second term refers to the latent heat of fusion, and the third term refers to the sensible heat of the liquid phase.

Compared to sensible heat TES and thermochemical TES, latent heat TES manifests high storage density, relative low volume change, and minor temperature change [24], which is advantageous to serve as complements to the thermal mass of the building envelope.

2.5 Phase Change Materials

Phase change materials (PCMs) play an important role as the storage medium in latent heat TES. The occurrence of latent heat TES must encompass the phase change temperature of the PCMs. PCMs can exchange a large amount of latent heat during the phase change process either isothermally or within a narrow temperature band. For example, the PCMs change from solid state to liquid state in the process of melting. The melting process is endothermic which absorbs heat. The absorbed heat breaks the chemical bond between the PCM molecules, so the aggregate state of the PCMs changes from solid to liquid. Conversely, the PCMs change from liquid state to solid state in the process of solidification. The solidification process is exothermic which releases heat. The heat release triggers the crystallisation of the PCMs, where the aggregate state of the PCMs changes from liquid back to solid. Ideally, the PCMs are incorporated into the building envelope as latent heat TES, and the phase change cycles are in line with the charging and discharging processes of the passive cooling system. In this case, PCMs help to reduce the energy demand for air conditioning and smoothen indoor temperature fluctuations when incorporated into various building components or envelopes [7]. From the current literatures, PCMs are proved to be effective complements of thermal mass to the building envelope, with which the building envelope can have increased thermal inertia for maintaining the thermal comfort with minimum energy costs possible. In this section, the characteristics of PCMs will be covered to better understand the practical deployment as latent heat TES for building passive cooling.

2.5.1 Classification of PCMs

Generally, the PCMs can be classified by the change of aggregate states during the phase change process: solid-solid PCMs, liquid-gas PCMs, and solid-liquid PCMs. It is recognised that solid-liquid PCMs are the most suitable for latent heat TES for building passive cooling when they are incorporated to the building envelope or components [7] [25]. In addition, the solid-liquid PCMs are usually further classified based on the material types: organic PCMs, inorganic PCMs, and eutectics. The eutectics comprise inorganic-inorganic eutectics, organic-organic eutectics, and organic-inorganic eutectics. In the following context, the word 'PCMs' solely refers to solid-liquid PCMs unless otherwise specified. The classification tree of PCMs is shown in the Figure 2 below.

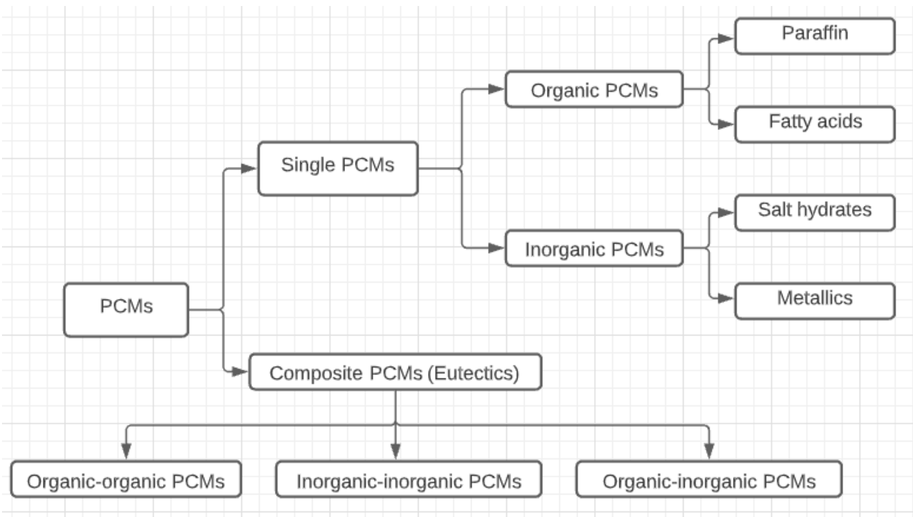

Figure 2.2. Classification tree of PCMs.

2.5.1.1 Organic PCMs

The organic PCMs comprise paraffin and fatty acids. Organic PCMs are thermally and chemically stable, and they are available in large phase change temperature ranges. Organic PCMs show good compatibility with other materials and do not suffer from supercooling and phase separation. Furthermore, organic PCMs can maintain the TES capability under multiple melting-solidification cycles. However, the key disadvantages of organic PCMs include low thermal conductivity, relatively large volume change during phase change, and flammability. The low thermal conductivity would largely impact the TES performance and efficiency, the volume change may cause PCM leakage, and the flammability would impact the fire safety of the system [7] [25]. Molecularly, paraffin is considered as straight-chain n-alkanes, with the generic chemical formula of '$CH_3(CH_2)_nCH_3$' [26]. It is the most inexpensive organic PCMs among all the available options [27]. Paraffin possesses considerable latent heat of fusion ranging from 120 to 210 kJ kg^{-1}, with a melting point ranging from 20 to 70℃. However, the low thermal conductivity (typically around 0.2 W m^{-1} K^{-1}) and volume expansion during melting are the two key defects that limit its applications [25]. Fatty acids differ from the paraffin in terms of the molecular constitution, with the generic chemical formula of '$CH_3(CH_2)_nCOOH$'. Compared to paraffin, fatty acids are typically available in relatively smaller phase change temperature ranges. During the melting process, fatty acids experience less volume expansion than paraffin [25].

2.5.1.2 Inorganic PCMs

The inorganic PCMs comprise salt hydrates and metallics. Inorganic PCMs are usually inexpensive in price. They usually have high thermal conductivity, considerable latent heat of fusion, and relatively small volume change during phase change. In addition, inorganic PCMs are usually non-flammable, which benefits the system in terms of the fire safety. However, they suffer from supercooling, phase separation, and corrosivity to the facilities [7] [25]. Salt hydrates are advantageous inorganic PCMs due to the high TES density of about 240 kJ kg^{-1} and the relatively high thermal conductivity of about 0.5 W m^{-1} K^{-1}. However, apart from the common disadvantages of inorganic PCMs, the high TES density of salt hydrates will degrade after multiple phase change cycles due to the irreversible formation of lower salts during the congruent melting. When it comes to the metallics, they typically possess high melting point, which makes them merely applicable in the context of latent heat TES for building passive cooling [25] [28].

2.5.1.3 Composite PCMs (Eutectics)

As the combination of two types single PCMs, the composite PCMs (eutectics) have a sharper and lower melting temperature, and they usually yield a higher volumetric TES density compared to their single PCM component alone [7]. There is almost no phase segregation during the phase change process for eutectics [28]. Especially, the organic-inorganic eutectics would combine the advantages of single organic and inorganic PCM components, which manifest outstanding performance in TES. However, there is a lack of research on the eutectics so far, more research on eutectics is required to enrich the available information about their thermophysical properties, phase change behaviours, and TES performance.

2.5.2 PCMs Selection Criteria for Building Passive Cooling

As there are numerous types of available PCMs, it is essential to be selective when applying PCMs into building envelope or components for passive cooling. Since PCMs complement to the thermal mass of the existing building envelope as a buffer to the heat gain, multiple characteristics and properties of PCMs need to be considered before they are actually implemented to achieve the optimal thermal performance. The key properties to be considered in this context include thermodynamic properties, kinematic properties, chemical properties, cost-effectiveness, and environmental impact [29].

2.5.2.1 Thermodynamic Properties

The thermodynamic properties are the most crucial as the phase change TES for passive cooling is a thermodynamic interaction including multiple heat transfer processes. Firstly, the phase change temperature of the PCMs should be in the appropriate range depending on the local climates and geography. In addition, the PCMs are supposed to have high latent heat of fusion, high specific heat capacity, high density, and moderate thermal conductivity. Furthermore, it is desirable that the PCMs have low vapour pressure at the operational temperature, so that the issues of inhibiting melting and containment problems can be effectively mitigated. Lastly, it is also expected that the PCMs can melt congruently with minimum change in volume.

2.5.2.2 Kinematic Properties

The PCMs should possess high reaction or nucleation rate to avoid supercooling, and therefore, the high rate of crystal growth could facilitate the heat restoring from the storage unit.

2.5.2.3 Chemical Properties

Firstly, in terms of materials, the PCMs should be stable, non-toxic, non-explosive, non-flammable, and non-corrosive. These properties help to maximise the system safety and prolong the system lifetime. In addition, it is desirable that the PCMs are reversible in melting-solidification cycles. Last but not least, it is also expected that the PCMs can undergo multiple melting-solidification cycles with no degradation on the storage capacity and heat transfer performance. These properties help to maximise the system performance and storage efficiency.

2.5.2.4 Cost-effectiveness and Environmental Impact

The PCMs are supposed to be inexpensive in the cost and widely available. This would help with the affordability as typically large amount of PCMs will be required to be incorporated into the building envelope. It is also favourable that the PCMs are recyclable and not harmful to the environment when being disposed.

The total costs of the PCM-based passive cooling applications are mainly driven by the cost of raw PCMs, the cost of matrices/encapsulations, and the cost of peripherals. In general, the total costs of different applications can vary a lot depending on the system complexity, market availability of PCMs and other supporting materials, as well as the labour cost for installations. As such, the unit cost of some common PCMs are summarised in Table 2.2 below [30].

Table 2.2. Unit cost of some common PCMs [30].

PCM	Unit Price (USD/kg)
Paraffin wax	1.88–2
Fatty acids	1.43–1.76
Calcium chloride	0.13–0.2
Biocrude	0.22–0.29
Laboratory-grade eicosane	53.90

2.5.3 Thermophysical Properties Measurements of PCMs

The thermophysical properties of PCMs are the most important, as they directly determine the TES performance and the amount of thermal mass the PCMs can provide. Thus, an accurate measurement of the thermophysical properties of PCMs is vital. In this section, several common measurement methods for thermophysical properties will be presented and compared.

2.5.3.1 Differential Scanning Calorimetry (DSC)

The differential scanning calorimetry (DSC) technique enables the measurement of the latent heat of fusion, specific heat capacity, and phase change temperature of the PCMs. DSC technique measures the amount of heat absorbed or released by the PCMs with respect to the temperature change. During the measurement process, the sample with unknown properties is tested alongside with a reference sample with all properties known. Then, under the identical condition, the difference in amount of heat required to increase the same temperature of the two samples is measured as a function of temperature. The thermophysical properties of the sample are then obtained by comparing the difference in the added heat. Apart from measuring the thermophysical properties of PCMs, DSC can also help to measure the thermophysical properties of PCM composites such as PCM wallboards. In addition, the PCM distribution within the wallboards and the impact of multiple thermal cycling on the thermophysical properties of the PCMs can be examined [7]. However, DSC technique also has several limitations: Some heat transfer components such as convective component in the sample are neglected; the temperature profile of the sample is non-uniform; it may take a long time to heat or cool the samples; the measured specific heat capacity is dependent on the sample mass and heating rate; the DSC facility is expensive and complex, which requires ongoing maintenance and calibration; the phase change process cannot be visually observed [11]. Overall, DSC technique is the most popular for measuring the thermophysical properties of PCMs.

2.5.3.2 Differential Thermal Analysis (DTA)

Differential thermal analysis (DTA) technique is opposite to the DSC technique in terms of the mechanism. During the measurement process, same amount of heat is applied to the sample with unknown properties and the reference sample with known properties. DTA measures the temperature difference between the two samples subject to the same amount of heat, and the thermophysical properties of the sample of interest can be therefore obtained [7] [11].

2.5.3.3 T-history Method

Zhang and Jiang [31] proposed a simple method called T-history method to determine the phase change temperature, thermal conductivity, specific heat capacity, and latent heat of fusion for PCMs. The thermophysical properties of the sample of interest are obtained by comparing its temperature-time curve with that of a reference sample [11]. The trials of T-history method also revealed good agreement between the trial results and the experimental data from the literature [7]. The T-history method is advantageous over the conventional calorimetric methods, DSC and DTA with the following features: T-history method is compatible with samples of large amount; the experimental setup is simple; it allows simultaneous thermophysical properties measurements of multiple samples of interest; the phase change process can be visually observed [11]. Several authors improved the T-history method subsequently. Hong et al. [32] refined several inappropriate assumptions in the original proposal of Zhang and Jiang [31] to improve the T-history method. Peck et al. [33] improved the accuracy of the T-history method by adjusting the orientation of the test tube to be horizontal, and therefore the temperature difference along the longitudinal direction of the test tube can be minimised.

2.5.4 Heat Transfer Enhancement

Although PCMs can exchange large amount of thermal energy during the phase change process thanks to their high latent heat of fusion, the low thermal conductivity is problematic, which constrains the heat transfer and therefore slows down the charging and discharging processes of the passive cooling system. The low heat transfer rate is unbeneficial to the real-world PCM-based passive cooling systems. Thus, integrating the heat transfer enhancement techniques to the system becomes essential. The common heat transfer enhancement techniques include dispersing high-conductivity particles into PCMs, incorporating high-conductivity porous matrix into PCMs, introducing fibrous materials such as carbon fibres into PCMs, placing metal pin-fin structures into PCMs, and enlarging the heat transfer surface area by encapsulations [11]. Parsazadeh and Duan [34] studied the melting of nanoparticle enhanced PCMs in a shell-and-tube TES system using both numerical and statistical approaches. The results revealed that the incorporation of nanoparticles can effectively increase the heat transfer rate. Murry and Groulx [35] investigated the phase change and energy characteristics within a cylindrical latent heat TES system. Their results showed that the dispersion of nanoparticles can reduce the melting time of the PCMs if the cavities are large. Py et al. [36] introduced a graphite matrix for the paraffin wax by employing capillary forces. The impregnation of graphite matrix resulted in higher thermal conductivity and more stable power output. Boomsma et al. [37] discovered that the thermal resistances of a compact heat exchanger with open-cell metal foams are much lower than that of the best commercial heat exchanger. Nakaso et al. [38] employed carbon fibre cloths to extend the heat transfer area in a latent heat TES tank. The experimental results revealed that the carbon fibre cloths of 0.4% volume can improve the heat exchange rate in the storage tank. Stritih [39] enhanced the heat transfer in a paraffin-based TES system by implementing fins as the media. The simulation results showed the time dynamics of heat accumulation within the PCMs, which concluded the distance between the fins as the most influential factor.

2.6 PCM-based Latent Heat TES for Building Thermal Management

In the last section, the characteristics of PCMs are thoroughly discussed and we understand that PCMs can serve as the storage medium in latent heat TES owning to the considerable latent heat of fusion (i.e. enthalpy). In this section, we will look at the versatile applications of PCMs in the context of building thermal management. The PCMs can be integrated into either active systems or passive systems. For active cooling systems, PCMs enable load shifting and demand management, which reduce the overall electricity costs and the peak grid load. In this case, the lifetime of the active systems can be prolonged and the chiller can be downsized. For passive cooling systems, PCMs serve as effective complements of thermal mass to the existing building envelope and structures, as discussed in previous sections. With the incorporation of PCMs, the building envelope can have increased thermal mass and the thermal comfort can be enhanced for the built environment. In this section, we mainly focus on the applications of PCMs in the passive systems. The impregnation methods of PCMs and various PCM-based passive strategies for building thermal management will be introduced. Some PCM-based passive cooling strategies are presented in Figure 2.3 and Figure 2.4 below. In addition, Table 2.3 presents a summary of containing matrices and PCMs used in literature.

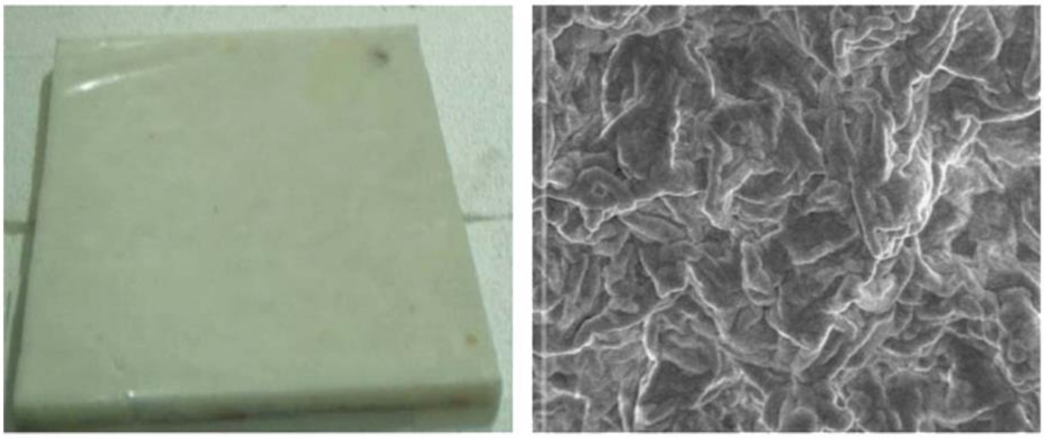

Figure 2.3 Shape-stabilised PCM plate [7].

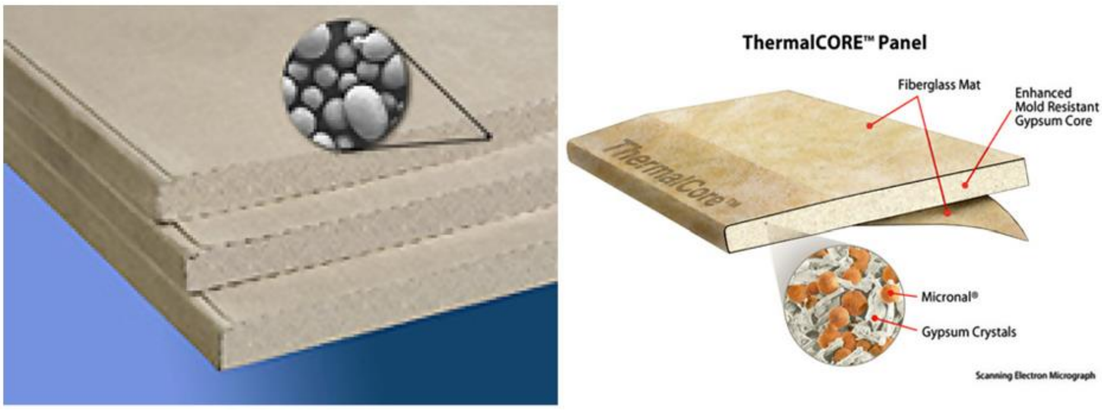

Figure 2.4 Gypsum wall board with PCM (left) and thermal CORE phase-change drywall (right) [7].

Table 2.3 Containing matrices and PCMs used in literature [7].

Containers	PCMs	Percentage of PCMs (%)
Gypsum board	Butyl stearate	~25
Gypsum board	Mixture of butyl stearate-palmitate	~20
Gypsum board	Eutectic mixtures of capric acid and lauric acid	26
PVC panel	Polyethylene glycol	–
Concrete	Micronal1PCM (from BASF)	–
Stainless steel panel	(48% CaCl2 + 4.3% NaCl + 0.4% KCl + 47.3% H_2O	–
Copolymer	Paraffin wax	60
CSM panel with brick	RT27; SP 25 A 8	–
Gypsum board	MPCM 28D	23, 30 40
Aluminium	Paraffin A22; Paraffin A26	–
Honeycomb panel	Mixture of Tetradecane and Octadecane	–
Concrete (Regular block; Autoclaved block)	Butyl stearate (Autoclaved block)	5.6
	Unicere 55 (Autoclaved block)	8.6
	Unicere 55 (Regular block)	3.9

2.6.1 Impregnation Methods of PCMs

The incorporation or impregnation methods of PCMs is key to the passive strategies for building thermal management, as they determine how the PCMs will be introduced into the building envelopes or construction materials. The most common and promising incorporation methods include direct incorporation, immersion, and macro-encapsulation [7]. Apart from these common incorporation methods, there are also advanced and novel incorporation methods such as micro-encapsulation and shape-stabilisation. A good understanding of the advantages and disadvantages of these incorporation methods is essential when it comes to the real-world implementations.

2.6.1.1 Direct Incorporation

Direct incorporation is as simple as indicated by the naming: The PCMs are directly added into the construction materials such as gypsum, concrete, or plaster when they are in slurry state during their production [40]. Direct incorporation is the most economical method to introduce PCMs into the construction materials. However, the drawbacks are the leakage of PCMs after discharging and the incompatibility with construction materials.

2.6.1.2 Immersion

For immersion, the building construction materials such as brick, concrete block, and gypsum board are immersed into the liquid-state PCMs, where the PCMs will be absorbed into the pore volumes of the construction materials with the assistance of capillary force. Similar to direct incorporation, immersion also suffers from leakage and is not suitable for long-term use.

2.6.1.3 Macro-encapsulation

Macro-encapsulation is an incorporation method where the PCMs are loaded and encapsulated into a container before being incorporated into building envelopes. The container includes tubes, spheres, panels, or other receptacles. The design of the container or enclosure is essential and should be application-dependent, as the geometric and thermal characteristics of the container will directly impact the heat transfer within the PCMs and therefore affect the thermal performance of the enclosed PCMs [41]. In optimum, the container is supposed to facilitate the heat transfer during the phase change process of the enclosed PCMs. In addition, the container should also avoid material loss, corrosion, and volume change of PCMs. By macro-encapsulation, the leakage and flammability issue of PCMs can be mitigated, and it will less affect the mechanical strength of the building envelopes or structures. However, macro-encapsulation is usually complicated to be integrated into building materials, and it leads to poor thermal conductivity and edge solidification [42].

2.6.1.4 Micro-encapsulation

Micro-encapsulation can be considered as an improved and scaled-down version of macro-encapsulation, where PCM particles or droplets are encapsulated in a film to maintain the shape. The film is normally made of high-molecular-weight polymers, which is thin and sealed. The PCM particles or droplets coated with the film are similar as the core enclosed in the shell, with a scale of micrometre or millimetre. The leakage issue can also be avoided by micro-encapsulation. Compared to macro-encapsulation, micro-encapsulation is easier and more economic to be integrated into the building construction materials such as cement, lime, mortar, and concrete. Some research revealed that micro-encapsulation technique can enhance the heat transfer of the PCMs due to the increased heat exchange surface area and mitigate the volume change of PCMs during the phase change process [43] [44]. However, some researchers raised the concern that the incorporation of micro-encapsulated PCMs might affect the mechanical strength of the building structure [45]. Further investigation on micro-encapsulation could be on its fire safety, thermal stability, and impact to the building mechanical strength [7].

2.6.1.5 Shape-stabilisation

Shape-stabilisation is another novel incorporation method of PCMs, in which PCMs (e.g. paraffin) are dispersed into another phase of supporting material (e.g. high-density polyethylene) to form a stable composite material. The supporting material will have a higher melting temperature than the selected PCMs, and therefore the supporting material will not melt when PCMs change the phase from solid to liquid. Thus, the supporting material can hold the PCMs so that there will be no leakage issue during the PCM melting. Furthermore, by introducing the supporting material, the formed composites will possess an enhanced thermal conductivity and specific heat, as well as the capability of undergoing multiple thermal cycles [7]. Compared to macro-encapsulation and micro-encapsulation, shape-stabilised PCMs do not need any container, but it can still hold the PCMs and prevent it from leaking when it melts down. According to this characteristic of the shape-stabilised PCMs, Zhang et al. [46] proposed the potential applications of the shape-stabilised PCMs as building inner linings such as inner walls, ceiling, and floor, which helps to enhance the thermal mass of the building envelopes and smoothen the indoor temperature fluctuations.

2.6.2 PCM-based Passive Cooling Strategies

There are various building applications employing PCMs as latent heat TES for passive cooling. These applications can be categorised into PCM-based building construction materials and PCM-based building envelopes or structures. For PCM-based building construction materials, the PCMs are usually incorporated during the production of the materials by direct incorporation or immersion, examples include PCM bricks, PCM mortars, and PCM concrete. For PCM-based building envelopes or structures, the PCMs are usually incorporated afterwards by encapsulation or shape-stabilisation, examples include PCM wallboards, PCM walls, PCM Tromble wall, PCM floors, PCM ceilings, PCM shutters, and PCM windows [7] [11].

2.6.2.1 PCM Bricks

As a heavyweight construction material, bricks are typically made of clay and have relatively high thermal mass in its original form [47]. Adding PCMs to the bricks can further improve the overall thermal mass, so that the indoor temperature fluctuation of the built environment can be smoothened and the indoor thermal comfort of the building occupants can be further guaranteed. Mahdaoui et al. [48] employed numerical modelling technique to evaluate the thermal behaviour of a brick wall impregnated with PCMs and assess the thermal response of the PCM-impregnated brick. The study was carried out in Moroccan regions, where the ambient temperature is varied by 20 degrees Celsius during a day in the season of summer. To improve the building thermal comfort under such extreme weather, they proposed to incorporate PCMs into the 12-hole hollow brick. A 2-D model was adopted assuming the air flow and heat transfer is laminar, and the numerical model was properly validated with the experimental results. The numerical results were in a good agreement with the experimental data. They concluded that the impregnation of PCMs into the brick can reinforce the thermal storage capacity and insulation power of the brick, and therefore stabilise the indoor temperature fluctuation. Elnajjar [49] presented a numerical modelling-based study on PCM-embedded brick material, to save the energy demand for cooling purpose in United Arab Emirates. The author proposed three types of PCMs to be included in the brick: n-Octadecane, n-Eicosane, and P116. The results revealed that the PCM P116 with the highest melting temperature among all candidates showed the best performance in energy saving. In addition, the author also pointed out that the results of one-day evaluation might be misleading, so that a longer period of analysis and evaluation is required in order to ensure appropriate PCM selection. Saxena et al. [50] carried out experimental study to investigate the performance of PCM-incorporated bricks by assessing the change in temperature difference and heat flow, under the composite climate of Delhi. It was found that the temperature fluctuation can be reduced by up to 10℃ when two types of PCMs (Eicsosane and OM35) were incorporated into bricks. The two types of PCMs were found to achieve solidification in the night, which ensures effective cyclic utilisation. Thus, the two PCMs were concluded to be suitable for application in Delhi. Yang et al. [51] investigated the thermal performance of PCM concrete hollow bricks in summer season using hot-box method. Their results revealed that filling PCMs in the internal side was better than the external side. This was because the external side was directly exposed to the ambient and the resultant rapid melting of PCMs is not beneficial. The PCMs would melt slowly if filled in the internal side as the air layer in the block could attenuate the penetration of the heat. When PCMs were filled in the internal side, the amplitude of indoor average temperature was decreased by 10%, the indoor average temperature was decreased by 23.7%, and the indoor average heat flux was decreased by 12.4%. Gao et al. [52] proposed filling PCMs into the hollow bricks to improve the thermal behaviour by latent thermal storage. A numerical model was built and validated with the full-scale experiment. The results showed that the filled PCMs can reduce the attenuation rate from 13.07% to 0.92%–1.93% and increase the delay time from 3.83 h to 8.83 h–9.83 h. The peak heat fluxes could be reduced from 45.26 W m^{-2} to 19.19 W m^{-2}–21.4 W m^{-2}. In addition, under the studied conditions, it is recommended that the phase change latent heat of PCMs should be lower than 125 kJ kg^{-1}. Overall, PCM bricks are the most common and fundamental PCM-based building construction materials. However, there is a lack of flexibility as the amount of PCMs is not tunable once the construction is completed.

2.6.2.2 PCM Mortars

Mortar is typically a mixture or combination of cement or other cementitious materials such as lime or alkali activated binders with fine aggregates such as river sands, crusher rock powder, or robo sand in the presence of adequate amount of water. Mortars are useful in bonding the bricks internally during the wall construction or plastering externally as the finishing layer. When the hydration reaction completes, the calcium silicate hydrate gels are formed, which brings sufficient mechanical strength to the mortar [53]. Guardia et al. [54] evaluated the thermal behaviour of a multi-layered building enclosure with five different compositions of PCM cement-lime mortars under heating and cooling cycles. The authors measured the temperature and heat flux on both sides of the multi-layered enclosure and the temperature on both sides of the PCM cement-lime mortar layer. The results revealed that the incorporation of PCM cement-lime mortar layer could delay the penetration of heat flux into the enclosure: During the heating cycle, the heat wave was delayed by 30 minutes and during the cooling cycle, the heat wave was delayed by 130 minutes compared to the case without PCMs. Furthermore, the authors also found that adding lightweight aggregates to PCM cement-lime mortar can improve the thermal insulation, and this can be used for both new buildings and energy rehabilitation of existing building enclosures. Orsini et al. [55] investigated the potential of PCMs in cement-based mortars. The performance of two innovative mortars made with the addition of 3% and 7% PCMs was compared to that of the traditional mortar. The mechanical and thermal performance of the PCM integrated mortar were thoroughly studied. The results showed that a rise from 3% to 7% of the PCM proportion would cause a 50% reduction of the indirect tensile strength, while the compression was reduced to a third. In addition, the thermal performance testing showed that the PCM integrated mortar manifests good insulation properties, making it suitable for building applications. Lucas et al. [56] carried out the characterisation studies of PCM lime mortar. The results indicated that the mechanical strength of the lime mortar was not reduced with the introduction of the PCMs. In their study, the PCMs were incorporated into the lime mortar using micro-encapsulation. The porosity, mechanical strength, and microstructure were characterised. The performance of the lime mortar with 20% PCMs was found to be superior to that with 10% PCMs. In addition, the porosity of the composite was found to increase as more PCMs were incorporated. Shadnia et al. [57] studied the mechanical and thermal properties of geopolymer mortar synthesised with low calcium fly ash and different amount of PCMs experimentally. The authors used scanning electron microscopy (SEM) imaging to identify the micro structure change of the geopolymer mortar after the incorporation of PCMs to investigate the effect of PCMs on the unit weight and compressive strength of geopolymer mortar. The thermal properties were also characterised using DSC analysis. The capability of PCMs in heat flow and temperature controlling was evaluated by using small cubicles built with geopolymer mortar slabs containing different amount of PCMs. The results elucidated that the incorporation of PCMs into the geopolymer mortar could decrease the total weight of the building, which is beneficial for the construction of lightweight buildings. In addition, the incorporation of PCMs could significantly increase the specific heat capacity of the geopolymer mortar, which enhances the heat transfer within the mortar. Furthermore, the testing with cubicles proved that the PCM-incorporated geopolymer mortar can be used in building walls to improve the overall thermal inertia of the building envelope and therefore achieve the thermal comfort. Cunha et al. [58] studied the behaviour of PCM-incorporated mortar under harsh physical conditions. The effect of high temperature on PCM-incorporated mortar was investigated. It was found that the exposure to high temperature would lead to a decrease in the flexural, compressive, and adhesion strengths for the mortar. The addition of PCMs to the mortar would decrease the mechanical strength of the mortar under all studied temperature ranges due to the presence of higher content of water and the increased microporosity. This study raised the concerns on the impact of PCMs to the mechanical strength of the mortar, which is worthwhile to consider before the actual implementation. In general, PCM mortar serves as bonding adhesives for the normal construction materials, which offers additional thermal mass. However, the impact to mechanical strength due to the introduction of PCMs and the PCM leakage would be concerning for real implementation.

2.6.2.3 PCM Concrete

Concrete is recognised as a greater carrier of for PCMs than other construction materials, thanks to its decent thermal conductivity (about 1.7 W m^{-1} K) and density [59]. Shen et al. [60] proposed using clastic light shale ceramsite (CLSC) to absorb the paraffin to prepare PCM-CLSC aggregate and PCM-concrete thermal storage blocks (PCM-CTSBs) with different PCM weightages. The authors also tested the absorption, compatibility, thermal, and mechanical properties of PCM-CLSC aggregate and PCM-CTSBs. The results showed that the PCM-CTSBs manifest greater thermal storage capacity than the ordinary concrete without PCMs. The average specific heat capacities of PCM-CTSBs increases as the PCM weightage increases. In addition, the discharging rate would be significantly impacted by the PCM weightage while the charging rate would be merely impacted. A considerable cyclicality was revealed as the PCM-CTSB completed numerous of charging-discharging cycles without any PCM leakage. The authors also suggested some future work on the long-term cyclic stability. Hakim et al. [61] determined the characteristics of thermal properties of a type of PCM-concrete composite, with the PCM namely beeswax. The beeswax-concrete composite has a measured thermal conductivity of 0.0211–0.0212 W m^{-1} K and diffusivity of 2.89×10^{-6} m^2 s^{-1}. During the experiment, the heat received at the inner walls of the ordinary concrete block was greater than that received at the inner walls of the beeswax-concrete, as the heat propagation was faster through the hollow concrete material than through the beeswax-concrete. The results revealed that the quality of beeswax will determine the thermal performance of beeswax-concrete, and this implementation would be promising for the purpose of reducing building energy demand and ensuring the thermal comfort. Niall et al. [62] developed two types of PCM-concrete composite panels and evaluated the effects that PCM had on the concrete properties. Micro-encapsulated paraffin was blended into the fresh concrete, then followed by vacuum impregnation of butyl stearate to form the first type of composite panel. Ground granulated blast-furnace slag (GGBS) was introduced as a partial cement replacement to form the second type of composite panel. The authors reported that the panel with 50% GGBS had a slightly higher thermal conductivity and manifested a considerable thermal storage capacity than the panel with no GGBS. The enhancement of thermal storage capacity decreased with the depth, which revealed the low thermal diffusivity of GGBS. The PCM concrete manifests some advantages than other PCM-based construction materials as the concrete complements to the low thermal conductivity of PCMs, and the enhanced thermal conductivity is beneficial to the heat transfer during the phase change processes. However, the PCM leakage is still an outstanding disadvantage for PCM concrete.

2.6.2.4 PCM Wallboards

PCM wallboards are recognised to be a cost-effective application, where PCMs are embedded into building structures such as gypsum board and plaster. The thermal characteristics of PCM wallboards are very close to the PCM alone [63]. Wang et al. [64] conducted a parametric study on the performance of PCM wallboards in air-conditioned lightweight buildings in Shanghai using EnergyPlus single-zone model. The studied city Shanghai has a climate pattern of hot summer and cold winter. The PCM wallboards were integrated to the exterior wall of rooms located in different orientations in the middle floor of high-rise building. The results revealed that the optimal melting temperature range of the PCMs should be 20–26℃, while the optimal melting temperature varies for different room locations. In addition, the optimal melting temperature also depends on the seasons. Under the seasonal optimal melting temperature, more total energy can be saved in summer, while a higher energy saving rate can be achieved in winter. Furthermore, the authors also suggested to implement active cooling technology or night ventilation to compensate the overheating and improve the PCM charging rate in summer. Evola et al [65] proposed a methodology to evaluate the effectiveness of PCM wallboards on improving the summer thermal comfort in lightweight buildings comprehensively. Several statistical indicators were developed to assess the thermal comfort and PCM wallboard effectiveness. These indicators can further aid the evaluation of PCM wallboard on improving the indoor thermal comfort in summer. The authors also carried out some simulations on a refurbished buildings implemented with PCM wallboards to validate the power of these indicators, the calculation of the indicators combined with the simulation can enable the interpretation of both PCM behaviour and efficacy. In addition, this proposed new methodology also prompts the appropriate selection of PCMs based on the range of phase change temperatures. In the presented case study, although the honeycomb PCM wallboards can provide decent thermal comfort for a lightweight building in southern France in summer but using PCMs with a 1℃ lower peak melting point is recommended by the authors. Yu et al. [66] fabricated PCM wallboards and attached them to the exterior surface of a test room to test their thermal performance against that of polystyrene plastic insulation wallboards. The selected PCM comprised organic alcohol PCMs and diatomite, which was formed by shape-stabilisation. The impact of wallboard location and the phase change temperature were investigated. Their results revealed that the high thermal insulation of the wallboard can prevent the heat transfer from exterior to interior in the daytime, but is not favourable for heat dissipation at night. In addition, the optimal phase change temperature also depends on the orientation of the wallboards on top of the outdoor meteorological conditions. Overall, using diatomite as a matrix for the organic alcohol PCMs can not only prevent the leakage but also enhance the compatibility between the composite PCMs and the building materials. Biswas et al. [67] developed innovative nano-PCM with PCMs supported by expanded graphite nanosheets, which is shape-stable and easy to incorporate into lightweight building envelope. Then, a prototype PCM-incorporated interior wallboard was built and tested in a hot-humid climate condition. Some additional simulations were conducted for the PCM wallboards and validated with the experimental results. From the modelling results, the highest annual reduction in wall heat gain was obtained with a 22℃ cooling set point for a south-oriented wall. However, the nano-PCM wallboard at 21℃ cooling set point reduced the peak heat gains and delayed the heat penetration during peak summer. In general, based on both experiments and simulations, the nano-PCM wallboard manifests great potential for reducing electricity demand for indoor cooling. Kuznik [68] carried out comparative study in a renovated office building to evaluate the potentials of PCM wallboards. Two identical rooms were monitored for approximately one year: one room was installed with PCM wallboards in the lateral walls and ceiling, while the other one without PCM was used for comparison. Their results showed that the PCM wallboards can be really effective if the air temperature is varying between the melting and freezing temperatures of the PCMs. By using the PCM wallboards, the thermal comfort is enhanced due to both air temperature and wall-surface temperature. Owning to the planer structure and simple installation, PCM wallboards are the most common PCM-based building structures and the phase change behaviour is relatively simple to model.

2.6.2.5 PCM Walls

Wang et al. [69] conducted numerical simulations to study a south-faced wall with internal PCM liner in hot summer weather in the city of Shanghai. The PCM wall in this study was expected to be able to reduce the abrupt penetration of heating loads due to high outdoor air temperature and solar radiation. The studied influencing factors included PCM type, PCM layer thickness, and the PCM positioning. The results showed that the PCM wall with optimised configurations could reduce the heat flow by 34.9% (i.e. 1481 kJ). In addition, it was also found that the heat transfer rate and average inner surface temperature could be substantially reduced by using PCM wall. The authors also proposed the windows as a thermal bridge connecting the indoor space and outdoor environment, which should be considered in practical implementations. He et al. [70] combined PCMs, micro-channel heat pipes (MCHPs), and radiative cooling (RC) to form an innovative RC-PCM-wall for building indoor cooling purposes. In this comparative study, the test room with RC-PCM-wall was compared to two reference rooms, one with conventional brick walls and the other one with normal PCM walls. The experimental results revealed that the test room would maintain a lower interior surface temperature on the south wall than the room with normal PCM walls, than the room with brick walls. However, the daily indoor average temperatures were not very different for these three rooms. The test room implemented with RC-PCM-wall took 16 hours to achieve the full melting of PCMs, while the reference room implemented with normal PCM walls took 2.3 hours longer to achieve so. By using RC-PCM-wall, a considerable amount of cooling loads can be saved from the south wall. Choi et al. [71] proposed a type of novel PCM wall with injected bubbles, where the density difference between PCM and bubbles caused the bubbles to move upward. This phenomenon led to the flow in the liquidus PCM and therefore the temperature stratification within the PCM was interfered, so that the PCM phase change can be triggered by the applied heat and the heat penetration within the PCM bulk can be reduced. The authors carried out a comparative experiment to evaluate the effects of bubble injection, with one cell injected with bubbles and the other one without injected bubbles. The results revealed that the injection of bubbles can yield a 11% more latent heat storage within PCM and a 28% less heat penetration across the PCM wall. In addition, the injection of bubbles can increase the average velocity of liquid PCM by 19 times higher than the case without bubble injection, which improved the temperature homogeneity within the PCM bulk. Overall, the proposed method brought great improvement in the thermal performance of PCM wall. Xie et al. [72] designed a thermal performance testing equipment and studied the intermittency of solar radiation on the PCM layer of the wall in a conditioned room both experimentally and numerically. From the results, the PCM layers on the internal surface of the wall could change the absorptivity of the wall and therefore improve the surface temperature, temperature rise rate, surface temperature difference, and heat flux in the discharging process. In addition, it was found that most of the thermal energy was stored within a short period of time, where the heat storage process was finished within two hours when the solar radiation was 600 W m^{-2}. Duan et al. [73] integrated the mixture of decanoic and lauric acid in the proportion of 55:45 into the Trombe wall to improve its thermal performance. The thermophysical properties of the PCM was tested and the thermal performance of a small-scale PCM-integrated Trombe wall was investigated by the authors experimentally. It was found that a large temperature gradient existed in the vertical direction of Trombe wall even if the absorber surface was heated evenly. Furthermore, the heat transfer through the PCM Trombe wall was a 2-D heat transfer process along the height and thickness directions of the wall. This was rather distinct when there was an intensive solar radiation.

2.6.2.6 PCM Floors

Ansuini et al. [74] proposed a pioneer study to integrate PCM into lightweight piped radiant floors for passive indoor cooling. The authors constructed the laboratory specimens of the PCM floor and developed an optimised finite element model to simulate the thermal performance of the PCM floor. A custom-designed steel matrix was inserted into the interior of the PCM radiant floor as a thermal diffuser, which reduced the stratified melting behaviour of granular PCM. Based on the simulation results, 25% of the water used for cooling can be saved when the PCM floor was used for radiant cooling in a 16 m^2 room in summer season. The PCM floor can provide a buffer of 2–3 days against the direct solar radiant gains and the internal gains in mid-season under typical living conditions. The authors also mentioned the essence of full-scale testing under real living conditions to further improve and tune the proposed technology. Royon et al. [75] optimised the PCM-embedded floor panel to resolve the PCM leakage issue under liquid state. A new component was derived from an existing slab with cylindrical cavities and the cavities were filled with a polymer-paraffin composite. The leakage issue can be avoided due to the composite and the insertion inside cavities. Both experimental and numerical studies were carried out, and the numerical model was validated by the experimental results. The authors also proposed a new indicator called 'PCM activity' to evaluate the amount of PCM to be used in the component. Under the given geometry and boundary conditions, an amplitude attenuation of 50% was achieved from the modelling. Jin et al. [76] proposed a novel double-layered PCM floor. There were two layers of PCMs with different phase change temperatures within the floor. The thermal performance of the PCM floor was analysed using the numerical model. The results showed that the energy released by PCM floor during peak hours increased by 41.1% and 37.9% for heating and cooling respectively, compared to the normal floor, when the latent heat of fusion of PCM was 150 kJ kg^{-1}. The authors also located the optimal melting temperatures of PCM for heating and cooling to be 38℃ and 18℃, respectively, where the optimal melting temperatures depend on the physical locations of the two PCM layers.

2.6.2.7 PCM Ceilings

Lu et al. [16] conducted experimental investigation on the PCM ceiling coupled with earth-air heat exchanger for building cooling, where the cooling capacity of soil and the energy storage capacity of PCM were combined. Their results showed that the peak temperature of the experimental room was reduced by 2.1℃ under 8-hour timed cold storage strategy and 2.7℃ under 12-hour timed cold storage strategy. In addition, the temperature and heat flux of the PCM ceiling were found to have the similar distribution characteristics under the two operation strategies. Riffat et al. [17] presented an experimental study on a novel PCM chilled ceiling panel in humid climate, where the PCMs were covered by a transparent membrane. It was found that the PCM chilled ceiling panel could maintain the cabinet temperature lower by 2–2.5℃ than the case without PCM up to 4.5 hours after the chiller was switched off. Furthermore, the transparent membrane cover helped to restrict convection to avoid condensation, so a lower capacity was evident. Velasco-Carrasco et al. [18] evaluated the thermal performance of the PCM ceiling panels experimentally. The results indicated that the PCM ceiling panels can maintain higher room temperatures compared to the condition without PCMs, and the PCMs could complete the thermal cycle as the PCM temperature dropped below the melting point after 6 hours. Koschenz et al. [10] introduced a thermally activated ceiling panel with PCMs for incorporation in light-weight and retrofitted buildings. It was shown that the high thermal energy storage capacity (300 Wh m^{-2} day^{-1}) during phase change could limit the overall panel thickness to less than 5 cm. By using simulation and experiments, it was proven that a 5-cm layer of micro-encapsulated PCM and gypsum surface could maintain a comfortable room temperature in standard office buildings. Jose et al. [19] studied the performance of suspended PCM ceiling panels for the cooling in office rooms. The performance was modelled using TRNSYS 17 and then compared to an all-air system and a thermally active building system. It was found that 15% of the energy saving and 30% of the peak cooling power reduction can be achieved by the PCM ceiling panels, compared to the all-air system. Rida et al. [20] explored the effects of geometric features on the thermal performance of a macro-encapsulated PCM ceiling panel using numerical modelling. Four different geometries of macro-encapsulated ceiling panels with identical PCM volume but different exposed surface areas were contrasted. It was concluded that the ceiling panels with higher exposed surface area yielded a higher heat transfer rate in both melting and solidification, while an 50% increase on the exposed-surface-area-to-volume ratio yielded a 20% increase on the melting speed. Jamil et al. [21] carried out a comparative study to investigate the feasibility of PCM as a retrofitting option to enhance occupant thermal comfort in an existing house in Melbourne. The study was conducted both experimentally and numerically. In the experiment, the indoor air temperatures of two rooms (one with PCM ceiling implemented and the other one without PCM ceiling) were recorded and compared. The experimental data was also used to validate a simulation model developed with EnergyPlus. The results indicated that the effectiveness of PCM in enhancing occupant thermal comfort depends on the behaviour of the occupants. The most efficient effect can be achieved when the windows were kept open during the previous nights, while internal doors remained closed all the time.

2.6.2.8 PCM Shutters

Silva et al. [84] proposed a hybrid study to investigate the thermal performance of PCM shutter by both experimental and numerical methods. The real-scale comparative experiment was carried out with two window shutters, one with PCMs and the other one without PCMs. Then, the experimental results were used to further validate the numerical model. The indoor temperature was used as a key metric to evaluate the accuracy of the numerical model. The results revealed that the PCM shutters manifested decent thermal behaviour in terms of free cooling: the average internal temperature for the compartment without PCM shutters ranged from 15 to 46℃, while that for the compartment with PCM shutters ranged from 18 to 42℃. This means the peak temperature in the compartment was reduced by 4℃ while the minimum temperature was increased by 3℃. In addition, it also showed that the PCM shutters can delay the penetration of the external heat gain. Alawadhi [85] used finite element method to evaluate the thermal performance of PCM shutter against that of the conventional foam shutter. The indoor space heat gain between the room with PCM shutter and the room with foam shutter was compared during typical working hours to show the cooling efficacy of the PCM shutter system. Furthermore, the author also carried out a parametric study to assess the effect of various design parameters. The results elucidated that the heat gain through windows can be reduced by 23.29% when the PCM with the highest melting temperature was deployed. The author concluded the optimal melting temperature of PCM should be close to the upper temperature limit of windows during the daytime and the quantity of PCM should be enough to absorb large quantity of heat during the daytime, so that the best thermal performance can be achieved. Silva et al. [86] carried out comparative experimental study to test a PCM shutter prototype during the summer season under Mediterranean climate zone. The indoor air temperatures, outdoor weather conditions, and the heat flux of the interior wall partition were monitored and analysed. The outdoor air temperature swing was between 13 to 25℃ and the average solar radiation was between 237 to 306 W m^{-2} during the entire course of the experiment. The results showed that the implementation of PCM shutter could regulate the indoor temperature by 18%–22%, and the maximum and minimum temperature decreased by 6% and 11%, respectively. In addition, the PCM shutter could reduce the maximum heat flux through the window by 10 W m^{-2}, which proved the efficacy of PCM shutter in thermal regulations.

2.6.2.9 PCM windows

Durakovic et al. [87] conducted experimental and numerical study on a PCM-based temperature-responsive window system, and the real cases under both natural environment and lab environment were analysed. The authors mathematically described and determined the impact of glazing cavity size on reducing the temperature fluctuations as well as its limitations. The results revealed that the PCM window system could achieve decent indoor cooling effect when the cavity thickness was 24 mm. On top of this, the simulation also showed the increase of PCM cavity thickness was beneficial from the perspective of A/C unload hours, but it was limited by the solid-liquid phase volume fraction. Therefore, the authors recommended the cavity thickness to be no more than 24 mm if the window is exposed to the radiation, while no more than 19 mm without the presence of radiation. Li et al. [88] realised the low thermal conductivity as the key defect of paraffin which would hinder its thermal performance when incorporated to the double-glazed windows as PCM windows. They proposed adding nanoparticles into PCMs to enhance the thermal conductivity and investigated the effects of nanoparticle volume fraction and particle diameter on the temperature difference between the interior surface of the window and indoor air. The results showed that the energy consumption increases with the nanoparticle volume fraction, but decreases with the particle diameter. The minimum energy consumption could be achieved when the nanoparticle concentration was 1% and nanoparticle diameter was 100 nm for all the seasons. More specifically, with the appropriate combination of nanoparticle volume fraction and size, the energy consumption can be reduced up to 1.5%, 2.0%, and 4.0% for summer, autumn, and winter seasons, respectively. King et al. [89] examined the thermal performance of a double-glazed PCM window and compared with a normal double-glazed window without PCMs. The technical grade paraffin was incorporated into a 12 mm gap within the window. Several building thermal features such as indoor thermal environment, inner glass temperature, energy consumption through glazed window, and transmittance of PCM window were thoroughly assessed. The PCM window provided a transmittance of more than 0.7 during daytime operation and it permitted good lighting to the room. The PCM window could reduce the indoor temperature fluctuation by 10℃ and the indoor peak temperature by 9℃. Overall, the energy consumption through the double-glazed window could be reduced by 3.76% when the PCM was incorporated.

2.7 Chapter Summary

In this chapter, we thoroughly discuss the properties, characteristics, and working mechanisms of PCMs, PCM impregnation methods, and various PCM-based cooling strategies. We understand that the latent heat of fusion of PCMs can be employed to store large amounts of thermal energy, which is beneficial when PCMs are used for cooling strategies. Among all the PCM-based cooling applications, PCM ceilings manifest a great potential for cooling due to the nature of vertical thermal plume, where the sinking of cold air is in line with the purpose of cooling. However, some knowledge gaps have been identified to be addressed from the existing literature to improve the applications of PCM ceilings or ceiling panels, and they were explored and addressed in this study:

1. For PCM ceiling panels, there is not a known study investigating the effects of the geometric features of the macro-encapsulated panel on the thermal performance.
2. In the existing literature, most of the study on PCM ceiling panels focuses on either commercial or residential buildings. There is not a known study investigating the cooling efficacy of PCM ceiling panels for low-thermal-mass architectures.

Chapter 3 – Modelling the Discharging Process of PCM Ceiling Panel

Although substantial research has been carried out on PCM-based thermal storage in buildings for passive cooling, as thoroughly introduced in Chapter 2, most of the applications are thermal storage devices added to existing building energy systems or the use of incorporated PCMs in building envelopes. However, the implementation is usually complex, especially for the renovated buildings [90]. In addition, the incorporation of PCMs will reduce the concrete mechanical strength and incur the leakage issue when PCM walls are deployed [91]. Thus, more flexible, effective and safer incorporation of PCMs in buildings should be proposed. Compared to the walls, ceilings exchange large amount of heat between the building interior and exterior due to their large area of contact and more direct interaction with vertical thermal plumes [8]. Hence, effective control of heat exchange through ceiling PCM panels is promising for building indoor thermal management. There are current studies about PCM ceilings of various configurations. However, the PCM amount, position, and layout are static and unchangeable in most of the available literatures [9]. Ideally, the thermal energy storage capacity is supposed to be subject to the season to ensure the all-year thermal comfort. Therefore, it is desirable if the PCM ceilings panels are flexible in terms of the PCM amount, position, and layout to obtain benefits in performance not achieved in otherwise static configuration. Furthermore, an extensive analysis on the geometric configurations of the PCM ceilings is essential to thoroughly understand their thermal performance, as there is a lack in the available literatures in terms of the analysis of the geometric configurations of the PCM ceilings.

In this chapter, the modelling work on the discharging process of PCM ceiling panel is presented. The numerical modelling was conducted using the commercial software Ansys Fluent 2020 R2. Firstly, A PCM ceiling panel is proposed with flexibility to the building users. The provided cooling effect and capacity can be adjusted by the amount, position, and layout of PCM panels on the ceiling according to the local climate and space requirement. Importantly, the PCM ceiling panels can be blended into existing ceiling lights and air conditioning terminals, working jointly with air conditioners to remove cooling load in the air-conditioned space. Based on the temperature difference between day and night, the charge of cooling capacity at night and discharge of cooling capacity in the daytime will provide free cooling to the users. Owing to its constant-temperature feature during phase change and the high energy storage density, the PCM panels can assist in stabilising the indoor temperature without occupying too much space or affecting the building structural requirements. An indicative illustration of the proposed PCM ceiling panel configuration is presented in Figure . Following the panel design, a computational fluid dynamics (CFD) model validated by full-scale experiment is built to predict and better understand the phase change behaviour of PCMs enclosed in the proposed ceiling panels. The melting behaviour and thermal performance of the PCM ceiling panels of various geometric configurations are thoroughly studied using the developed CFD model. The developed CFD model can help to optimise the selection of geometric configuration and better understand the heat transfer mechanism of the PCM ceiling panel. The initial temperature difference between PCMs and ambient air, panel shell thickness, panel distance to the ceiling, protrusion-to-base ratio, gap width, and panel volume are the investigated key influencing parameters. The melting time, normalised melting rate, liquid fraction and temperature variations are the key metrics used to evaluate the discharging performance. Based on authors' previous fundamental geometric analysis of a single PCM capsule's melting performance in air [92], the application aspect is elaborated and emphasised in the work presented in this chapter, with various design considerations analysed. The results can inform the actual full-scale implementation of the PCM ceiling panels, which will be covered in the next chapter.

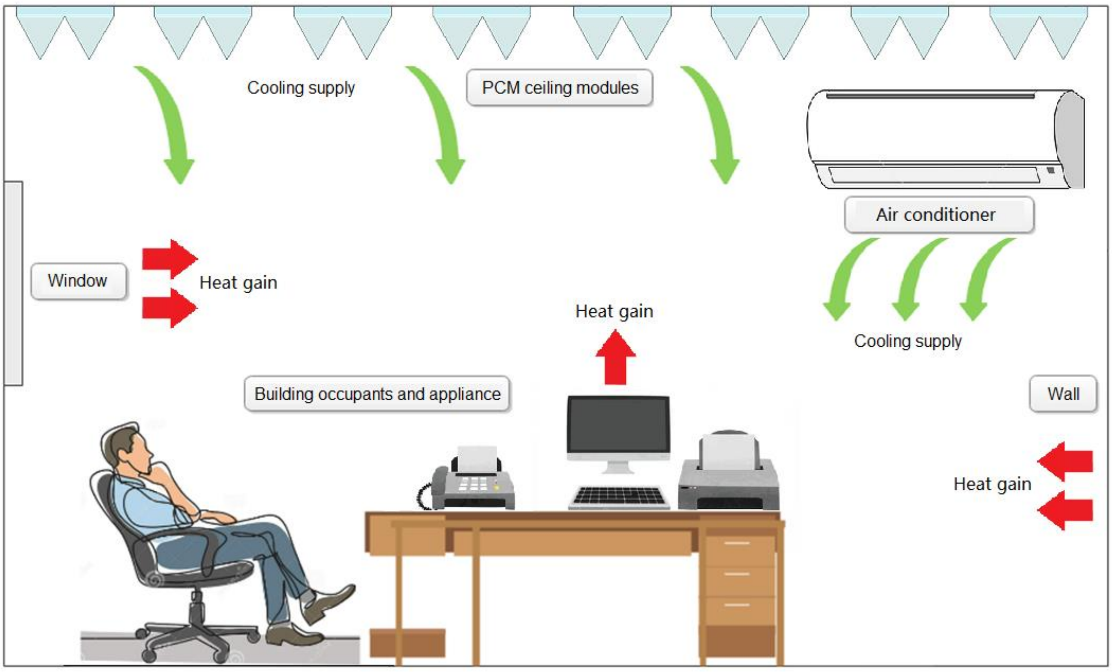

Figure 3.1 Indicative demonstration of the application [93] [94].

3.1 Simulation Background

3.1.1 Physics of CFD Model

In the present model, the conjugate heat transfers between air and panel shell, along with panel shell and PCMs are considered. Initially, the convective heat transfer occurs between the ambient air and the panel shell, where the ambient air with a higher temperature heats up the panel shell with a lower temperature. Then, the conductive heat transfer occurs between the panel shell and the contained frozen PCMs. The melting of the PCMs bulk occurs from the periphery to the core, where the local PCM close to the panel shell first turns into liquid. The heat transfer between the melted PCMs and the frozen PCMs is dominated by convection. During this process, the frozen core part of PCMs sinks towards the tip of the panel due to the density difference between the solidus and liquidus PCMs. Furthermore, the air in proximity to the panel decreases its temperature as the melting of the PCMs progresses. Thus, the density of the air near the panel increases, and therefore the air 'sinks' downwards forming an inverted plume in the panel shell. As the cooled air is denser than the ambient static freestream, it first sinks from the ceiling to the floor and then spreads sideways, creating a cooling effect for the room occupants.

Within the PCMs bulk, the entire melting process can be divided into three stages with associated heat transfer characteristics. In Stage 1, the temperature of the PCMs bulk is below the solidus temperature, where the only heat transfer mode within the solid phase is conduction. In Stage 2, the temperature of the local PCM regions gradually exceeds the solidus temperature, which triggers the phase change to liquid PCM and subsequent natural convection. As the developed PCMs are amorphous in the solid phase, the melting occurs over a temperature band rather than isothermally due to the nonexistence of the definitive lattice pattern [95]. The latent heat of melting is then discharged during Stage 2. After the temperature of PCMs bulk reaches the liquidus temperature, the Stage 2 ceases and the PCMs bulk is entirely in the liquid state. Subsequently, Stage 3 begins, where the heat is transferred from the panel shell to the liquidus PCMs. The absorbed heat is stored as sensible heat of the liquidus PCMs, and the temperature of the liquidus PCMs keeps increasing until approaches the ambient temperature. Natural convection within the cavity is also driven by temperature differences and the inclination of the cavity walls [96]. The temperature profile of the PCMs bulk during the phase change process is rendered in Figure , and the heat transfer during the Stage 2 of the melting process is depicted in Figure. As this is a low-temperature model (with temperatures well under 50°C) in the absence of external pressure differences (i.e. forced convection), then radiative heat transfer and mixed convection are heat transfer mechanisms that do not influence the PCM melting behaviour [97].

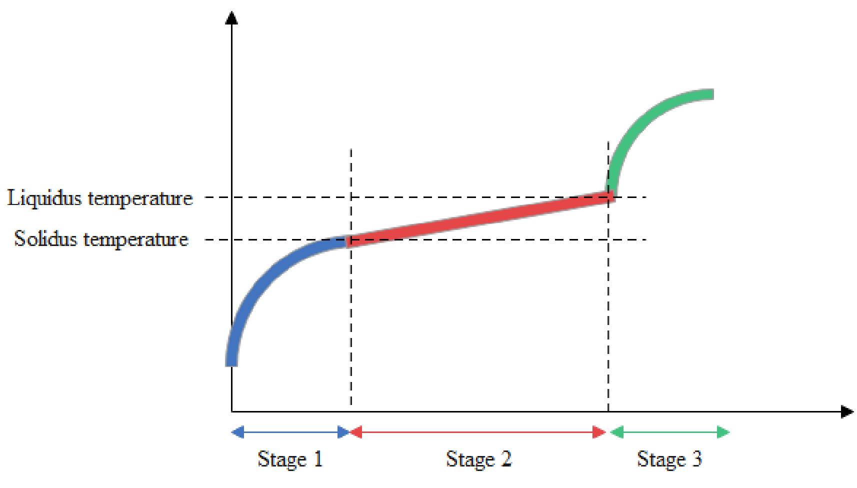

Figure 3.2 A qualitative temperature-time profile during PCMs melting.

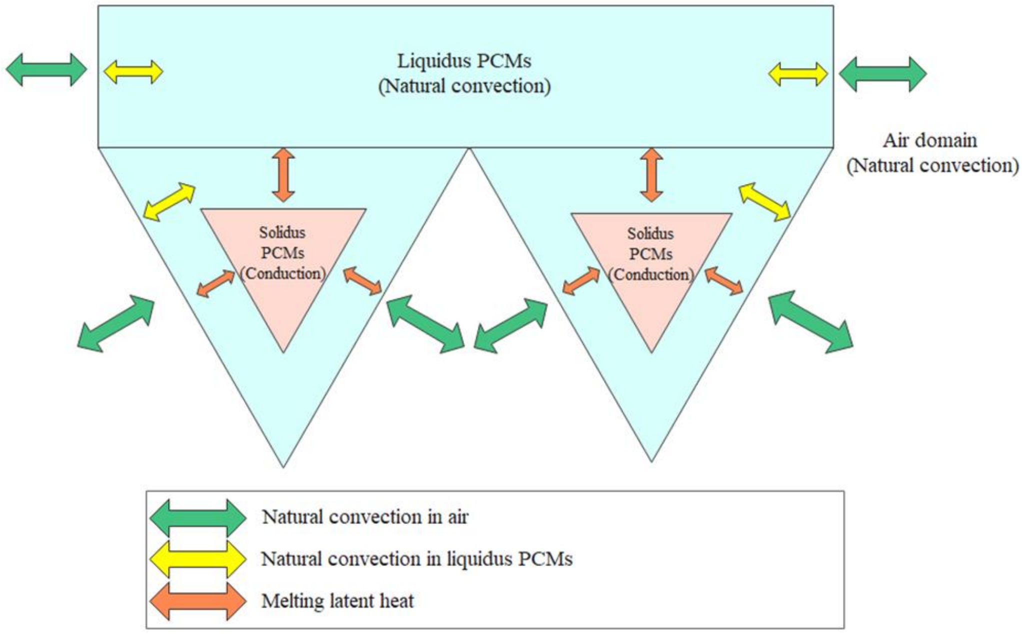

Figure 3.3 A schematic of heat transfer mechanism in Stage 2 of melting in the model [92].

In general, the discharging process of the aforementioned PCM ceiling panel includes multiple conjugate heat transfer processes in the modes of natural convection (i.e. between air and shell, between liquidus PCMs and solidus PCMs) and conduction (i.e. between shell and solidus PCMs). The driving force of the conjugate heat transfer is the temperature difference between the ambient air and the panel (i.e. shell and encapsulated PCMs). The described heat transfer processes are the same for the discharging processes of most of the macro-encapsulated passive PCM cooling applications, but the incoming direction of the cooled air is different as the PCM ceiling panel is fixed on the ceiling surface. As the heat transfer processes are highly dependent on the encapsulation methods, design, and positioning, a thorough understanding of the physics of the phase change process is vital for the implementation of the CFD model.

3.1.2 Assumptions of CFD Model

There are several assumptions made in the presented model: (1) the thermophysical properties of the PCM bulk are considered as constant value when the PCMs are in either solid or liquid state, while varying linearly between the solidus temperature and liquidus temperature during melting; (2) radiative heat transfer is neglected as the temperature difference between the PCMs and air domain is relatively small and their absolute temperatures are relatively low; (3) the surface of the panel in contact with the ceiling surface is adiabatic; (4) the initial temperatures of the PCMs and the panel shell are the same and uniform; and (5) there are no air gaps within the panel envelope. An enthalpy-porosity method was adopted for the presented physical model with the aforementioned assumptions to model the melting process of PCMs enclosed in the panel. This method treats the solid-liquid mushy zone as a “pseudo” porous medium, where the level of porosity is measured as liquid fraction. In other words, the liquid fraction represents the fraction of the cell volume that is in the liquid state, which is computed based on an enthalpy balance at each iteration. Therefore, the melting interface is not tracked explicitly in this technique [98]. The liquid fraction is denoted as γ, which is defined as

$$\gamma = \begin{cases} 0 & \text{when } T < T_{\text{solidus}} \\ \dfrac{T - T_{\text{solidus}}}{T_{\text{liquidus}} - T_{\text{solidus}}} & \text{when } T_{\text{solidus}} < T < T_{\text{liquidus}} \\ 1 & \text{when } T > T_{\text{liquidus}} \end{cases} \tag{3.1}$$

3.2 Experiment to Validate CFD Model

3.2.1 Selection of Phase Change Temperature

As discussed in Chapter 2, the phase change temperature is the most crucial parameter for any PCM-based cooling applications. Therefore, the selection of phase change temperature is essential and should be considered carefully in conjunction with local seasonal climate, cooling demand, building features, and many other factors. In general, the phase change temperature should be determined such that the balanced charging and discharging can be achieved. That is, to determine the phase change temperature, the local temperature variation should be measured over a decent period of time. Then, based on the temperature variation measurement, the phase change temperature can be determined such that the hours with temperature higher than the phase change temperature is roughly equal to the hours with temperature lower than the phase change temperature. In this study, as the validation experiments were carried out on site in a real-scale room, the phase change temperature of the PCM should be selected according to the local seasonal climate of the location for experiments. Considering the cost-effectiveness, the cooling load of PCM ceiling panels should be moderate. Otherwise, a very large PCM volume is required. Therefore, in the design of the study presented in this chapter, the PCM ceiling panels are supposed to work alone only in spring and autumn, while in summer and winter the PCM ceiling panels will mostly work jointly with the air conditioning system.

In this study, validation experiments were carried out in Canberra, Australia, during the season of autumn. Canberra is located at 35°16’55.2036’’S, 149°7’44.3928’’E [99] and holds an oceanic climate (Cfb) under the Koppen-Geiger classification. The average daily maximum and minimum temperature across spring and autumn are 19.3℃ and 6.5℃, respectively [100]. By averaging the maximum and minimum temperatures across spring and autumn, 13℃ is adopted as the phase change temperature for the PCM in this study. The number of hours with temperature over 13℃ in each month across spring and autumn of 2020 is summarised in Figure . The time portions of over 13℃ from March to November are 79.4% (March), 49.3% (April), 18.1% (May), 33.8% (September), 55.1% (October) and 75.1% (November). Thus, the two months to best adopt the passive cooling enabled by PCM panels are April and October, considering the relatively balanced charging and discharging hours for PCM panels [101].

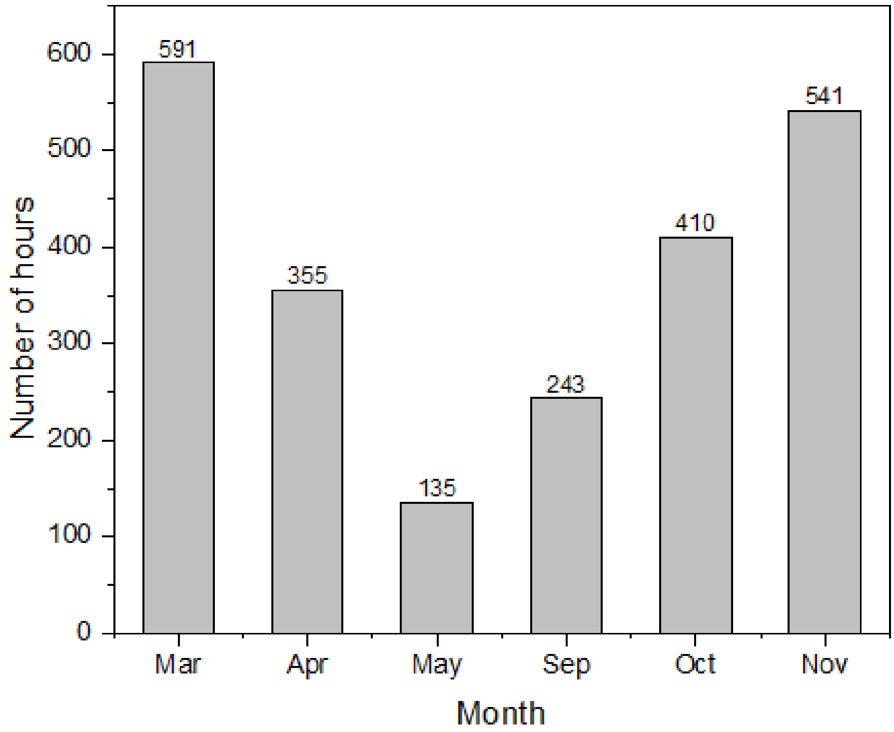

Figure 3.4 Number of hours in each month across spring and autumn with the temperature over 13℃ [101].

3.2.2 PCM Preparation and Screening

Wang et al. [102] proposed the mixture of capric and lauric (C-L) acid with organic additives as a promising energy storage material for high temperature cooling application. Their work showed that the eutectic point is 18.01℃, under the mole proportion of capric and lauric acid of around 70:30. By introducing extra organic additives, the phase change temperature of the C-L acid eutectic mixture can be further reduced. Among all the examined additives, oleic acid was recognised as the optimal additive since its influence on the phase change temperature of C-L acid eutectic mixture is the strongest. In addition, such combination of chemicals does not have outstanding toxicity, corrosivity, phase separation, and supercooling. The phase change temperature of the C-L acid eutectic mixture can reach 13℃ when the mole fraction of oleic acid is 0.1. The thermophysical properties of capric acid, lauric acid, and oleic acid are listed in Table . For the developed PCM, the thermophysical properties are listed in Table . All the thermophysical properties except for the thermal conductivity are obtained from the previous study of Wang et al [102], while the thermal conductivity of the PCM was measured using TEMPOS thermal conductivity analyser (shown in Figure). The thermophysical properties listed in Table are used for the simulation.

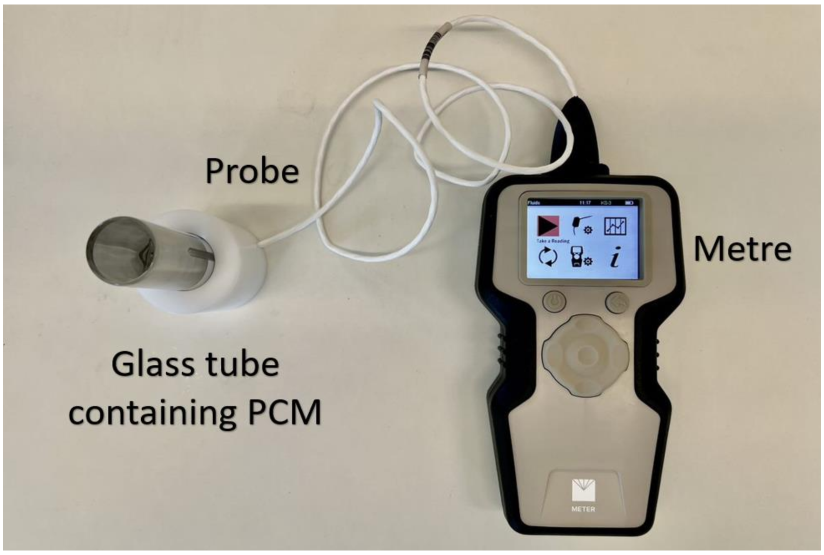

Figure 3.5 Thermal conductivity measurement using TEMPOS analyser.

Table 3.1 Thermophysical properties of capric acid, lauric acid, and oleic acid [102].

Name	Formula	Phase change temperature, °C	Thermal conductivity, W m^{-1} K^{-1}	Density, kg m^{-3}
Capric acid	$C_{10}H_{20}O_2$	36	0.149	886
Lauric acid	$C_{12}H_{24}O_2$	43	0.148	883
Oleic acid	$C_{18}H_{34}O_2$	16.3	–	870

Table 3.2 Thermophysical properties of the developed PCM.

Property	Value	Data source
Phase change temperature, K	286	[102]
Latent heat of fusion, kJ kg^{-1}	115	[102]
Density, kg m^{-3}	840	[102]
Thermal conductivity *l*, W m^{-1} K^{-1}	0.169	Measurement
Thermal conductivity *s*, W m^{-1} K^{-1}	0.183	Measurement
Specific heat *l*, kJ kg^{-1} K^{-1}	2.21	[102]
Specific heat *s*, kJ kg^{-1} K^{-1}	1.83	[102]

3.2.3 Fabrication of Panel Enclosure

Zhang et al. [92] studied the melting behaviour of the PCMs macro-encapsulated in the capsules of six different geometries, their results showed that the pyramidal and tetrahedral capsules yield the shortest melting time. Based on this finding, two enclosures were fabricated with acrylonitrile butadiene styrene (ABS) plastic using 3D printing technique, which represents the panel attached to the ceiling containing PCMs. The PCMs in the liquid state were filled into the enclosures with a dropper through a hole drilled on the enclosure surface. The hole was sealed using epoxy resin. That is, the macro-encapsulation was used as the PCM incorporation method. The geometry of enclosure A can be deemed as a cuboid topped with four pyramids, and that of enclosure B can be deemed as an extruded parallelogram topped with four tetrahedrons. The shell thickness is 1 mm for both enclosures. Each enclosure has an external volume of 250 mL and contains 170 g developed PCMs, yielding a total latent heat of 19.6 kJ. The cuboid/extruded-parallelogram base contains 50% of the total PCMs, while the pyramidal/tetrahedral protrusions contain another 50% of the total PCMs. The base surfaces of the enclosure A and B were well-insulated during the experiment, so the effective heat transfer area is defined as the total enclosure surface area excluding the base area (i.e. the effective heat transfer area is the area in contact with the ambient air). The appearance of the enclosures is presented in Figure with major dimensions labelled in Figure . The thermal and physical properties along with geometry features are summarised in Table .

Table 3.3 Thermophysical properties and geometry features of the enclosures.

<table>
<tr><th>Property</th><th>Enclosure A</th><th>Enclosure B</th></tr>
<tr><td>Material</td><td colspan="2">ABS plastic</td></tr>
<tr><td>Density, ρ</td><td colspan="2">1070 kg m^{-3}</td></tr>
<tr><td>Thermal conductivity, λ</td><td colspan="2">0.163 W m^{-1} K^{-1}</td></tr>
<tr><td>Specific heat, c_p</td><td colspan="2">1.99 kJ kg^{-1} K^{-1}</td></tr>
<tr><td>Surface area to volume ratio</td><td>1.33 cm^{-1}</td><td>1.41 cm^{-1}</td></tr>
<tr><td>Effective heat transfer area</td><td>232 cm^2</td><td>282 cm^2</td></tr>
</table>

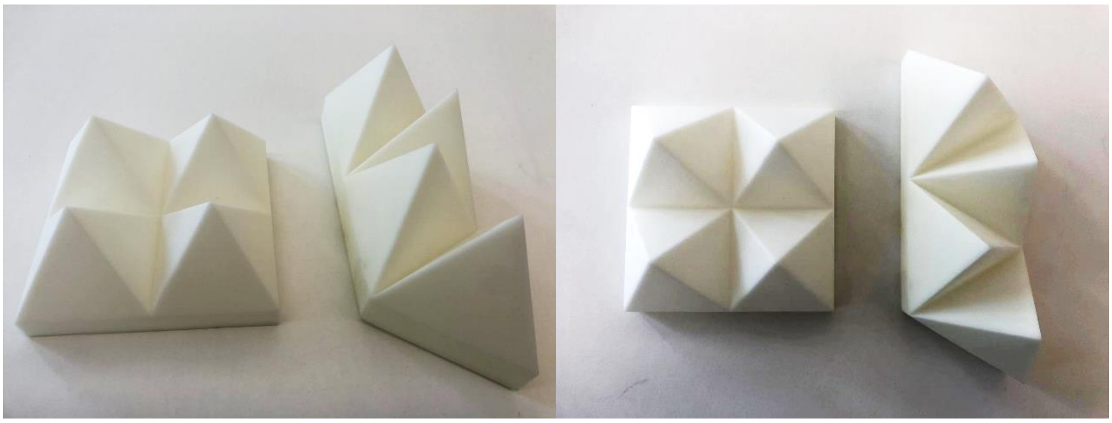

Figure 3.6 Photos showing the geometrical appearance of 3D printed enclosures with pyramid (left) and tetrahedron (right) shapes.

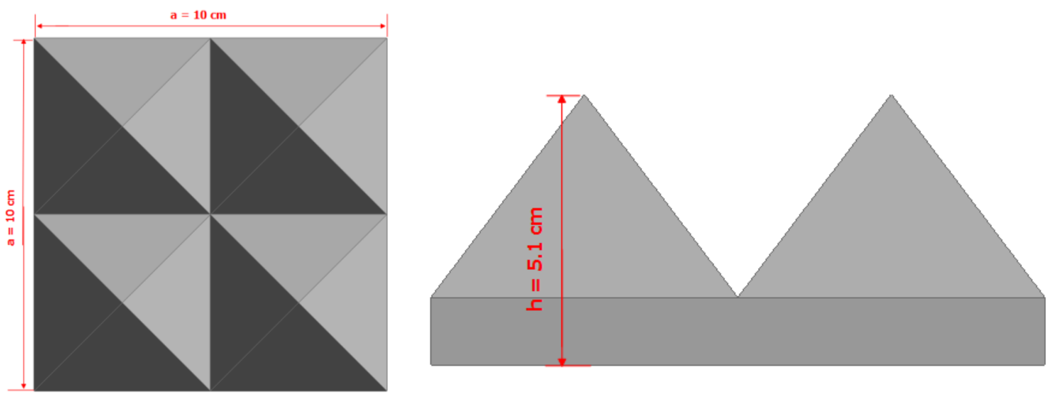

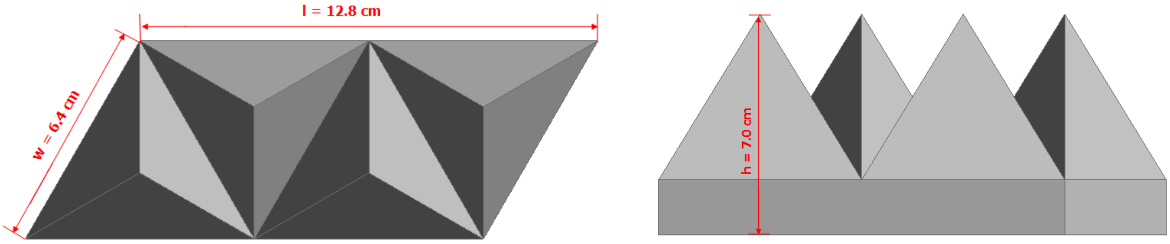

Figure 3.7 CAD design indicating the major dimensions.

3.2.4 Experimental Setup and Execution

The validation experiment was conducted in a well-insulated office room with a dimension of 3.51 m × 3.16 m × 2.25 m, where natural convection of air occurs due to density differences caused by the initially frozen PCM panel. The PCM panel was mounted to the centre of the office ceiling such that an inverted natural convection plume is generated for improved air circulation [8]. A rectangular polyethylene foam was attached between the base of the panel and the ceiling surface to set the base surface of the panel close to an adiabatic condition. The initial temperatures of the PCM panel and ambient air were 5℃ and 25℃, respectively. A schematic diagram of the experimental setup taking the pyramidal panel as an example is shown in Figure (a), with the panel size exaggeratedly enlarged to clarify the characteristic of the structure. An on-site photo of the pyramidal panel attached to the ceiling is shown in Figure (b). Three type-K thermocouples were fixed along the central vertical axis of one of the pyramidal/tetrahedral protrusions to record the internal temperature variations, and the data was recorded to a digital data logger. The accuracy of the type-K thermocouples is ± 0.75%. The top, middle, and bottom measuring points represented 1, 2/3 and 1/3 of the height of the pyramidal/tetrahedral protrusion, respectively, taking the pyramid/tetrahedron bases as a reference plane. The potential error of the experiment mainly came from the measurement error of type-K thermocouples and the possible minor deviation of the measurement points during the melting of PCMs.

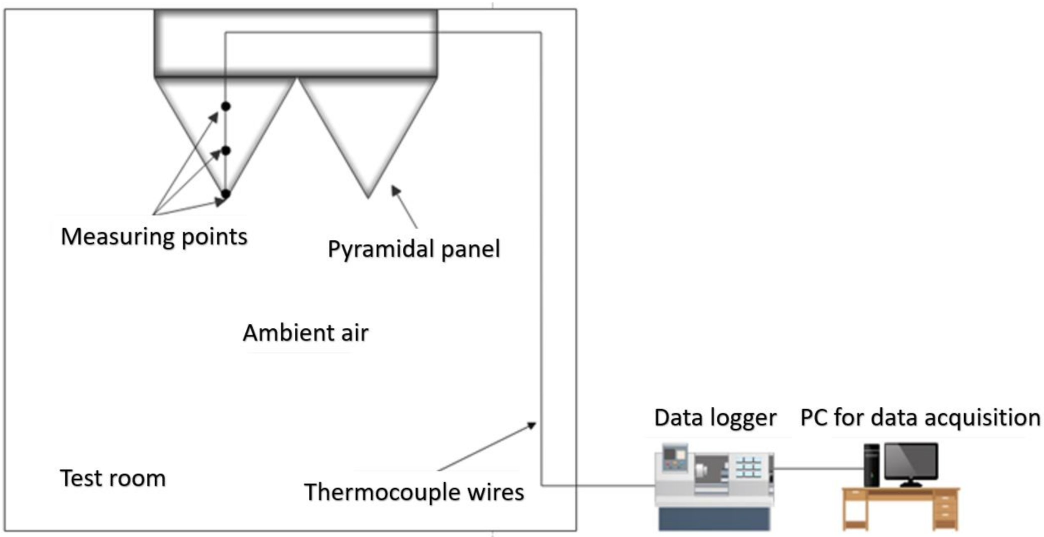

(a)

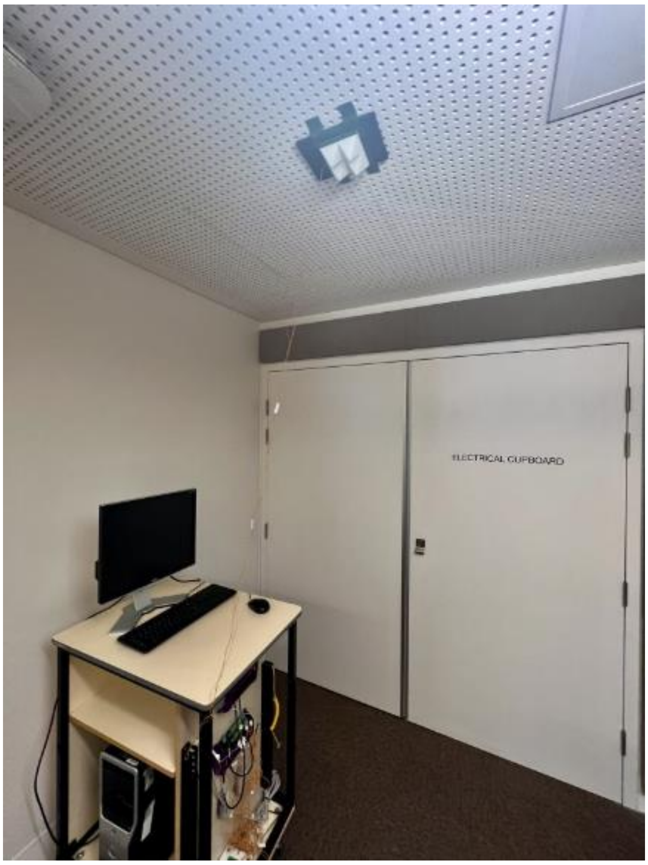

(b)

Figure 3.8 (a) Schematic of the experimental setup with the pyramidal panel as an example; (b) on-site photo showing the pyramidal panel attached to the ceiling with thermal couples fixed.

3.3 Governing Equations

3.3.1 Governing Equations for the Ambient Airflow

Eqs. (3.2) to (3.4) below represent the 3D continuity, conservation of momentum and energy for an incompressible turbulent flow, respectively [103].

$$\frac{\partial \rho}{\partial t} + \frac{\partial (\bar{u}_i)}{\partial x_i} = 0 \tag{3.2}$$

$$\frac{\partial (\rho \bar{u}_i)}{\partial t} + \frac{\partial}{\partial x_j}\left(\rho \bar{u}_i \bar{u}_j\right) = -\frac{\partial \bar{p}}{\partial x_i} + \frac{\partial}{\partial x_j}\left[\mu\left(\frac{\partial \bar{u}_i}{\partial x_j} + \frac{\partial \bar{u}_j}{\partial x_i}\right) - \frac{2}{3}\mu \frac{\partial \bar{u}_i}{\partial x_i}\delta_{ij} - \rho \overline{u_i' u_j'}\right] + \rho\beta(T - T_0)\vec{g} \tag{3.3}$$

$$\frac{\partial (\rho C_p \bar{T})}{\partial t} + \frac{\partial}{\partial x_j}\left(\rho \bar{u}_j C_p \bar{T}\right) = \frac{\partial}{\partial x_j}\left(\lambda \frac{\partial \bar{T}}{\partial x_j} + \frac{\mu_t}{\sigma_{h,t}} \frac{\partial \left(C_p \bar{T}\right)}{\partial x_j}\right) + \bar{u}_j \frac{\partial \bar{p}}{\partial x_j} + \frac{\partial \bar{u}_i}{\partial x_j}\left[\mu\left(\frac{\partial \bar{u}_i}{\partial x_j} + \frac{\partial \bar{u}_j}{\partial x_i}\right) - \frac{2}{3}\mu \frac{\partial \bar{u}_i}{\partial x_i}\delta_{ij} - \rho \overline{u_i' u_j'}\right] \tag{3.4}$$

where $\lambda, \rho, u, p, \beta, \mu_t$ and T represent the thermal conductivity, density, velocity, pressure, volumetric thermal expansion coefficient, turbulent viscosity, and temperature, respectively. The Reynold stresses in Eqs. (3.3) to (3.4) are calculated based on the work of Mwesigye et al. [104] as

$$-\rho \bar{u}_i \bar{u}_j = \mu_t \left(\frac{\partial \bar{u}_i}{\partial x_j} + \frac{\partial \bar{u}_j}{\partial x_i}\right) - \frac{2}{3}\left(\rho k + \mu_t \frac{\partial \bar{u}_k}{\partial x_k}\right)\delta_{ij} \tag{3.5}$$

Here, the turbulent kinetic energy, k, is written as [103]

$$k = \frac{1}{2}\left(\overline{u^2} + \overline{v^2} + \overline{w^2}\right) \tag{3.6}$$

In relation to turbulence modelling, the Realizable k-ε method is used due to its shorter run-time with sufficient accuracy for predicting the melting process, as well as the effectiveness in modelling turbulence of natural convection context of air [105] [106]. The turbulent dissipation rate ε and the turbulent kinetic energy k [104] are calculated by the following equations.

$$\frac{\partial(\rho k)}{\partial t}+\frac{\partial}{\partial x_j}\left(\rho k\bar{u}_j\right)=\frac{\partial}{\partial x_j}\left[\left(\mu+\frac{\mu_t}{\sigma_k}\right)\frac{\partial k}{\partial x_j}\right]+G_k-\rho\varepsilon$$

(3.7)

$$\frac{\partial(\rho\varepsilon)}{\partial t}+\frac{\partial}{\partial x_j}\left(\rho\varepsilon\bar{u}_j\right)=\frac{\partial}{\partial x_j}\left[\left(\mu+\frac{\mu_t}{\sigma_k}\right)\frac{\partial\varepsilon}{\partial x_j}\right]+\rho\varepsilon C_1 S-\rho C_2\frac{\varepsilon^2}{k+\sqrt{v\varepsilon}}$$

(3.8)

where G_k is the production of turbulent kinetic energy, and is derived from [104]

$$G_k=-\rho\overline{u_i'u_j'}\frac{\partial\bar{u}_j}{\partial x_i}=\mu_t S^2$$

(3.9)

Here, μ_t is defined as [104]

$$\mu_t=\rho C_\mu\frac{K^2}{\varepsilon}$$

(3.10)

The constant values of C_1,η,S,C_2 and σ_k used in the Eq. (3.8) are expressed as

$$C_1=\max\left[0.43,\frac{\eta}{\eta+5}\right],\eta=S\frac{k}{\varepsilon},S=\sqrt{2S_{ij}S_{ij}},C_2=1.9,\sigma_k=1$$

(3.11)

where S_{ij} is the fluid linear deformation rate. For the solid zone (ABS panel shell), the energy equation is given as

$$\frac{\partial(\rho_s C_{P,s}T)}{\partial t}=\nabla\cdot(\lambda_s\nabla T)$$

(3.12)

3.3.2 Governing Equations for the PCMs

For the PCM in the panel, the 3D governing equations corresponding to a laminar flow are

$$\frac{\partial\rho}{\partial t}+\frac{\partial(\rho u_i)}{\partial x_i}=0$$

(3.13)

$$\frac{\partial(\rho u_i)}{\partial t}+\frac{\partial}{\partial x_j}\left(\rho u_i u_j\right)=-\frac{\partial\bar{p}}{\partial x_i}+\frac{\partial}{\partial x_j}\left[\mu\left(\frac{\partial u_i}{\partial x_j}+\frac{\partial u_j}{\partial x_i}\right)\right]+\rho\beta(T-T_0)\vec{g}+S'$$

(3.14)

$$\frac{\partial(\rho H)}{\partial t} + \frac{\partial}{\partial x_j}(\rho u_j H) = \frac{\partial}{\partial x_j}\left(\lambda \frac{\partial \bar{T}}{\partial x_j}\right)$$

(3.15)

where S' and T represent the source term and temperature, respectively. The influence of natural convection is considered for both the PCMs in the liquid phase and the air. Boussinesq approximation is adopted in the presented model, and the density can be expressed by

$$\rho_{\mathrm{PCM}} = \rho_{\mathrm{ref,\ PCM}} \left[1 - \beta_{\mathrm{PCM}}(T - T_{\mathrm{ref,\ PCM}})\right]$$

(3.16)

$$\rho_{\mathrm{air}} = \rho_{\mathrm{ref,\ air}}\left[1 - \beta_{\mathrm{air}}(T - T_{\mathrm{ref,\ air}})\right]$$

(3.17)

For the PCMs, the specific enthalpy (H) is defined by the sum of the sensible enthalpy (h_{sen}), and latent heat (ΔH), which is written as:

$$H = h_{\mathrm{sen}} + \Delta H$$

(3.18)

where h_{sen} and ΔH are found by

$$h_{\mathrm{sen}} = h_{\mathrm{ref}} + \int_{T_{\mathrm{ref}}}^{T} c_p dT$$

(3.19)

$$\Delta H = \gamma L$$

(3.20)

where h_{ref} and T_{ref} represent the reference enthalpy and reference temperature of the PCMs, c_p represents the specific heat, and L represents the latent heat.

As the mushy zone region is treated as a porous medium in the enthalpy-porosity technique, and the level of porosity decreases as PCMs solidify. The source term S' in Eq. (3.14) characterises the momentum sink due to the reduced porosity in the mushy zone, which is given by

$$S' = \frac{(1-\gamma)^2}{(\gamma^3 + \varepsilon)} A_{\mathrm{mush}} u$$

(3.21)

where A_{mush} is the mushy zone constant which measures how fast the velocity of fluid reaches zero during the liquid solidification. In the presented study, A_{mush} is set to 10^6 for both pyramidal and tetrahedral panels, so that an optimal agreement can be achieved between the experimental results and the modelling results. In addition, ε is set to 0.001 to ensure the denominator to be non-zero.

3.4 Initial and Boundary Conditions of the Model

The boundary conditions of the model are defined as follows.

For the ambient air, the boundaries of the air domain (i.e. walls) are set to adiabatic. In addition:

$$u_i = 0, \frac{\partial p}{\partial n} = 0 \tag{3.22}$$

where n is the direction normal to the surface. For the k-ε turbulent model, the standard wall functions are taken. In this method, the turbulent kinetic energy equation is solved through the whole air domain considering the boundary condition $\partial p / \partial n = 0$. Then, the turbulent dissipation rate is calculated for all wall adjacent cells using the following equation

$$\varepsilon_P = \frac{C_\mu^{3/4} k_P^{3/2}}{\kappa y \mathrm{p}} \tag{3.23}$$

where κ stands for von Karman constant (0.4187) and y denotes the distance from the wall, respectively. Besides, subscript P represents the nearest nodes to the wall. The coefficient C_μ is chosen to be 0.09.

For the interface between PCMs and the panel shell:

$$\lambda_{\mathrm{shell}} \nabla T_{\mathrm{shell}} = \lambda_{\mathrm{PCM}} \nabla T_{\mathrm{PCM}}, u_i = 0 \tag{3.24}$$

where λ_{shell} and T_{shell} are the thermal conductivity and temperature of the panel shell, respectively, λ_{PCM} and T_{PCM} are the thermal conductivity and temperature of the PCMs, respectively.

The initial conditions of the model are defined as follows.

For the ambient air:

$$T = T_\infty, u_i = 0, k = 0.3 \text{ m}^2 \text{ s}^{-2}, \varepsilon = 0.5 \text{ m}^2 \text{ s}^{-3} \tag{3.25}$$

For the PCMs:

$$T = T_{0,\mathrm{PCM}} \tag{3.26}$$

For the panel shell:

$$T = T_{0,\mathrm{shell}} \tag{3.27}$$

Here, $T_{0,\text{PCM}}$ and $T_{0,\text{shell}}$ refer to the initial temperatures of the PCMs and the panel shell. The initial temperatures for both the PCMs and the panel shell are set to 278.15 K.

The governing equations were solved by the commercial software Ansys Fluent 2020 R2 using finite volume method. The pressure-velocity was decoupled using the semi-implicit technique for pressure-linked equations (SIMPLE) algorithm [107]. In the continuity, momentum, and energy equations, diffusion and convection terms were discretised using second-order up-wind schemes. The absolute residual was set to 10^{-6} to achieve a convergence solution for the energy equation. Other residual values corresponding to velocity components, turbulent dissipation rate, turbulent kinetic energy and continuity were set to 10^{-3}.

3.5 Mesh Independence Study

The physical geometry model was divided into an unstructured tetrahedron-dominated mesh. The mesh quality has been assured with the maximum skewness being less than 0.84 and the minimum orthogonal quality being greater than 0.16. The mesh of the entire modelled domain is shown in Figure (a) and the mesh of the PCM ceiling panel is shown in Figure (b). The mesh of the PCM ceiling panel has a higher density than the air domain since the panel has a much smaller physical volume than the air domain but the PCMs contained in the panel are the core objective of interest in this study.

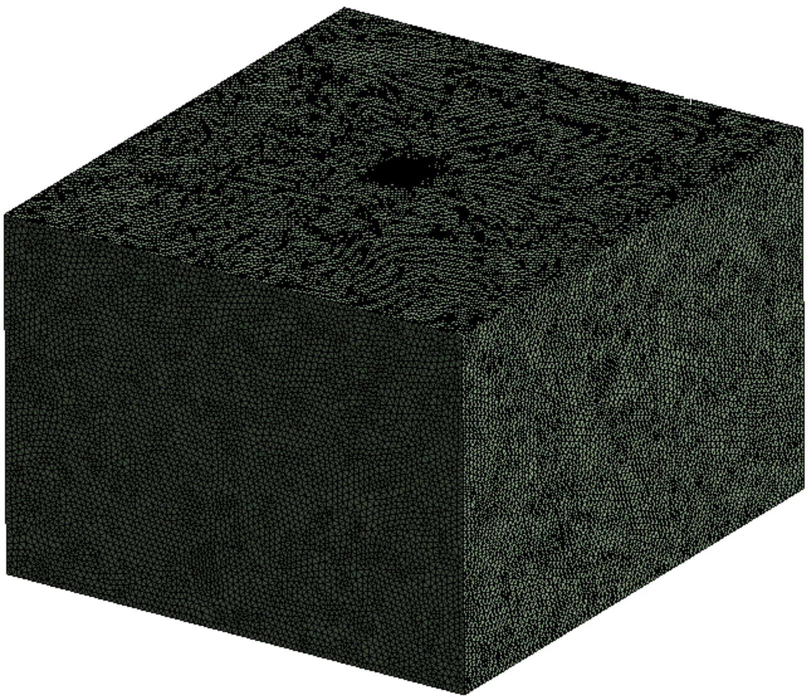

(a)

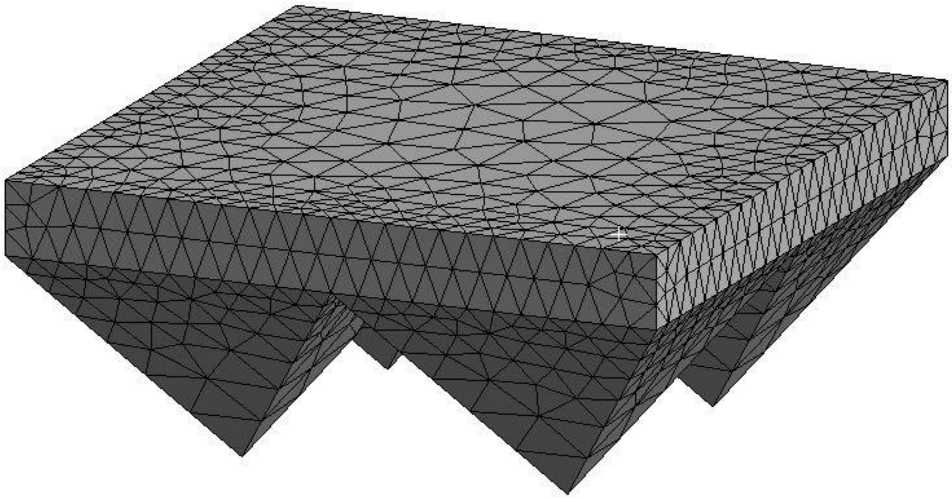

(b)

Figure 3.9 (a) Mesh of the entire modelled domain and (b) mesh of the PCM ceiling panel.

The mesh independence study was conducted before the extensive simulations, so that the minimum number of cells can be found to ensure both computation speed and result accuracy. The transient liquid fraction over the entire melting process was selected as an indicator for the results obtained with a different number of cells. The variation of liquid fraction for the pyramidal panel is shown in Figure 3, with the time-step size being 0.5 s. It can be noted that the curves with the cell number 1.1×10^6 and 1.7×10^6 almost coincide, which reveals the prediction of liquid fraction of the PCMs during the melting process will be independent of the cell number when it is close to or greater than 1.1×10^6. Hence, the cell number of 1.1×10^6 was adopted for further simulations. Similarly, the mesh independence study for the tetrahedral panel was also conducted, and the cell number of 1.1×10^6 was also adopted for the simulations.

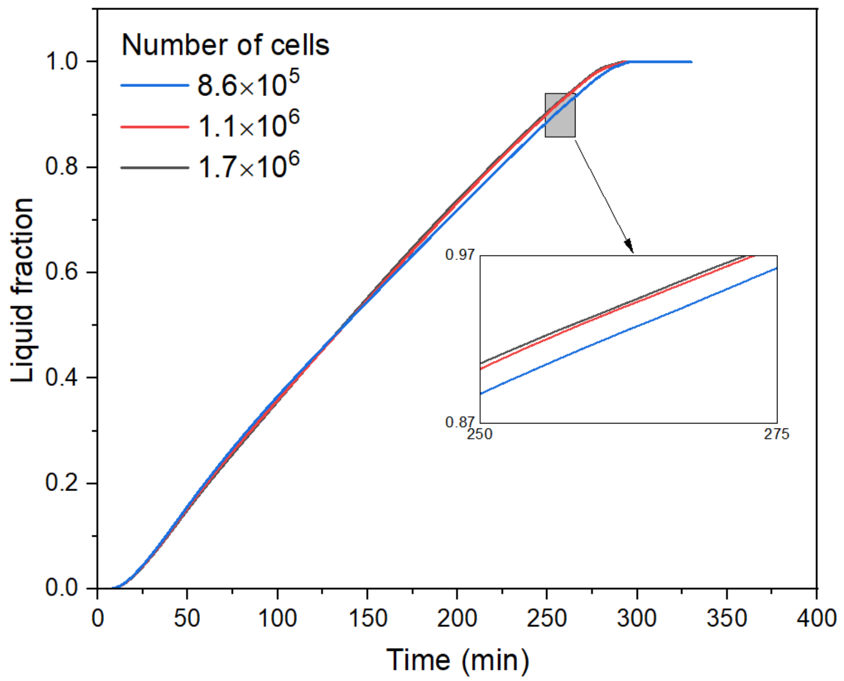

Figure 3.10 Transient liquid fraction variation of the pyramidal panel with a different number of meshes.

3.6 CFD Model Validation

To assess the accuracy of the CFD model for the purpose of validation, the modelling results were compared to the experimental results The accuracy of the CFD model is reflected by computing the relative error between the modelling results and the experimental results. The relative error is calculated using Equation (3.28).

$$RE = \frac{1}{N}\sum_{i=1}^{N} \frac{\left|T_{i,\mathrm{CFD}} - T_{i,\mathrm{EXP}}\right|}{T_{i,\mathrm{EXP}}} \tag{3.28}$$

where $T_{i,\mathrm{CFD}}$ stands for the temperature predicted by the CFD model, $T_{i,\mathrm{EXP}}$ stands for the measured temperature during the experiment, and N stands for the number of total data pairs compared.

A comparison of the temporal variation in temperature (at the three measurement points) during the melting process is conducted between experiments and simulations, as shown in Figure , for both pyramidal and tetrahedral panels. Figure depicts the entire three-stage melting process. The temperature profiles obtained by the experiment and simulation have a fairly good agreement overall for both pyramidal and tetrahedral panels. In Stage 1 (before reaching the solidus temperature), the temperature increase in the modelling results is more rapid than that in the experimental results. This discrepancy can be attributed to various factors: (1) lack of the accuracy of the PCM thermophysical properties that are considered in the CFD model, which does not account for the temperature dependence of such properties when the PCM is either in solid or liquid form. For example, the thermal conductivity and specific heat of the PCM are assumed to be constant in the CFD model when the PCM is entirely solid (i.e. Stage

1, before reaching the solidus temperature). However, in fact, the thermal conductivity and specific heat of the PCM may actually be temperature dependent. The lack of accuracy of the PCM thermophysical properties considered in the CFD model is highly likely to contribute to the discrepancy in Stage 1; (2) the numerical model underestimates the thermal contact resistance in a real experimental setup, where air gaps may decrease the effective thermal conductivity. That is, the effect of the thermal contact resistance in the real experiment cannot be accounted for in the CFD model, and the underestimated overall thermal contact resistance led to a stronger heat transfer and therefore a faster increase in temperature. Despite these apparent discrepancies, the qualitative aspects of the melting behaviour were accurately grasped by the model together with accurate quantitative predictions of the melting time (average ± 8.3%) for all monitored locations.

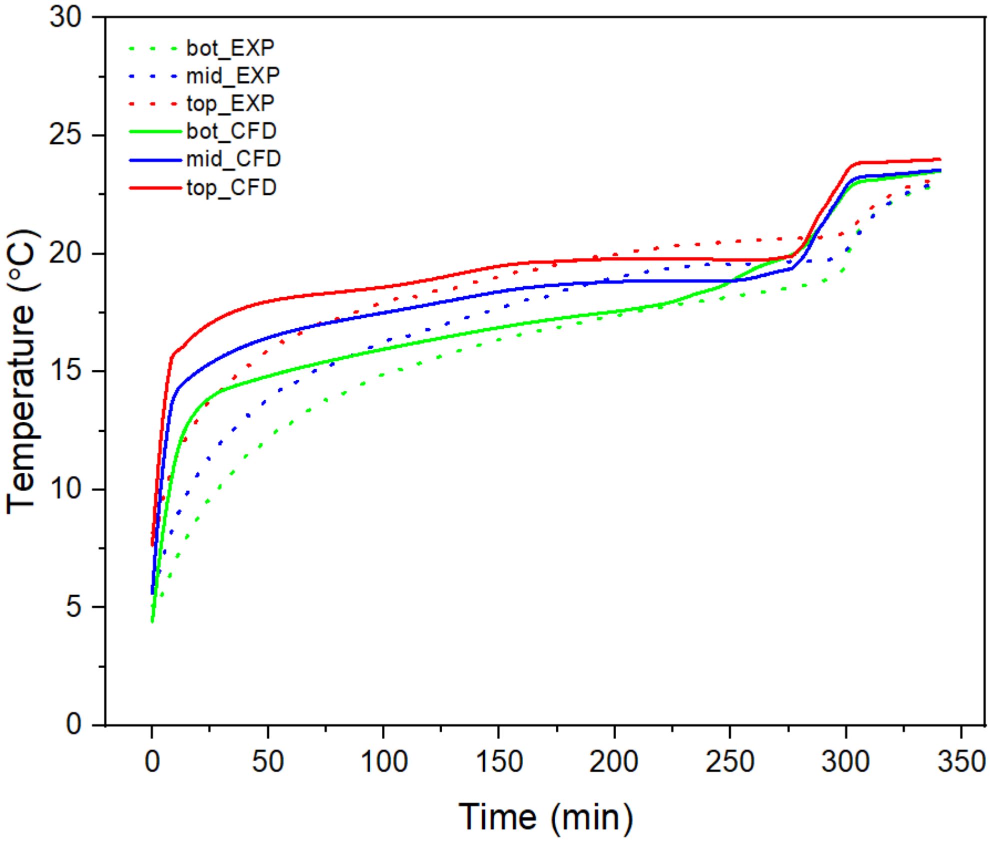

(a)

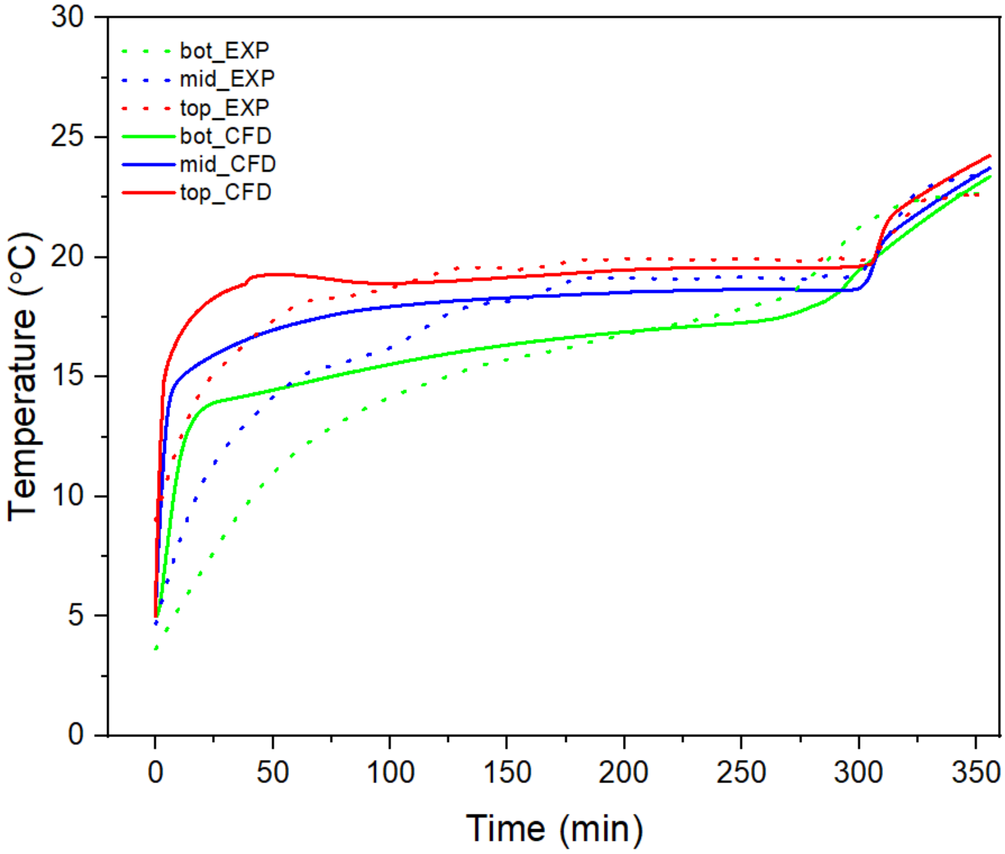

(b)

Figure 3.11 Temperature profiles at three measurement points obtained by experiment and simulation of (a) pyramidal and (b) tetrahedral panels to compare for validation.

3.7 Result and Discussion

3.7.1 Melting Time and Rate of Pyramidal and Tetrahedral Panels

The temperature and velocity contours depicted at the symmetrical vertical planes in two pyramidal protrusions and one tetrahedral protrusion are presented in Figure 3 at 50, 150, 250, and 300 min. The liquid fraction variations and the transient melting rate variations for the same simulation trials presented in Figure and Figure 3 are plotted in Figure . For the pyramidal panel, the phase change was 80% and 100% completed at 219 min and 292 min, respectively; for the tetrahedral panel, the phase change was 80% and 100% completed at 245 min and 353 min, respectively. This indicates that the pyramidal panel took 26 min less than the tetrahedral panel to reach 80% melting, while 61 min less to reach 100% melting. Therefore, for the entire melting process, the average melting rate of the pyramidal panel (0.582 g min^{-1}) is 20.75% higher than that of the tetrahedral panel (0.482 g min^{-1}). Although the effective heat transfer area of the tetrahedral panel is 21.6% higher than that of the pyramidal panel, a lower melting rate of the tetrahedral panel was observed. It is potentially attributed to its thicker base, which is 0.67 cm thicker than that of the pyramidal panel. Furthermore, according to the velocity contours presented in Figure 3, the velocity magnitude of the air adjacent to the base is lower than that of the air adjacent to the geometrical protrusions. This reveals that the thermal boundary layer adjacent to the geometrical protrusions is thinner than that adjacent to the base enhancing the heat transfer between the ambient air and the PCMs in the protrusions. This indicates the importance of the geometrical protrusions design. In addition, the average melting rate uniformed against the effective heat transfer area of the pyramidal panel (0.00251 g min^{-1} cm^{-2}) is 46.8% higher than that of the tetrahedral panel (0.00171 g min^{-1} cm^{-2}).

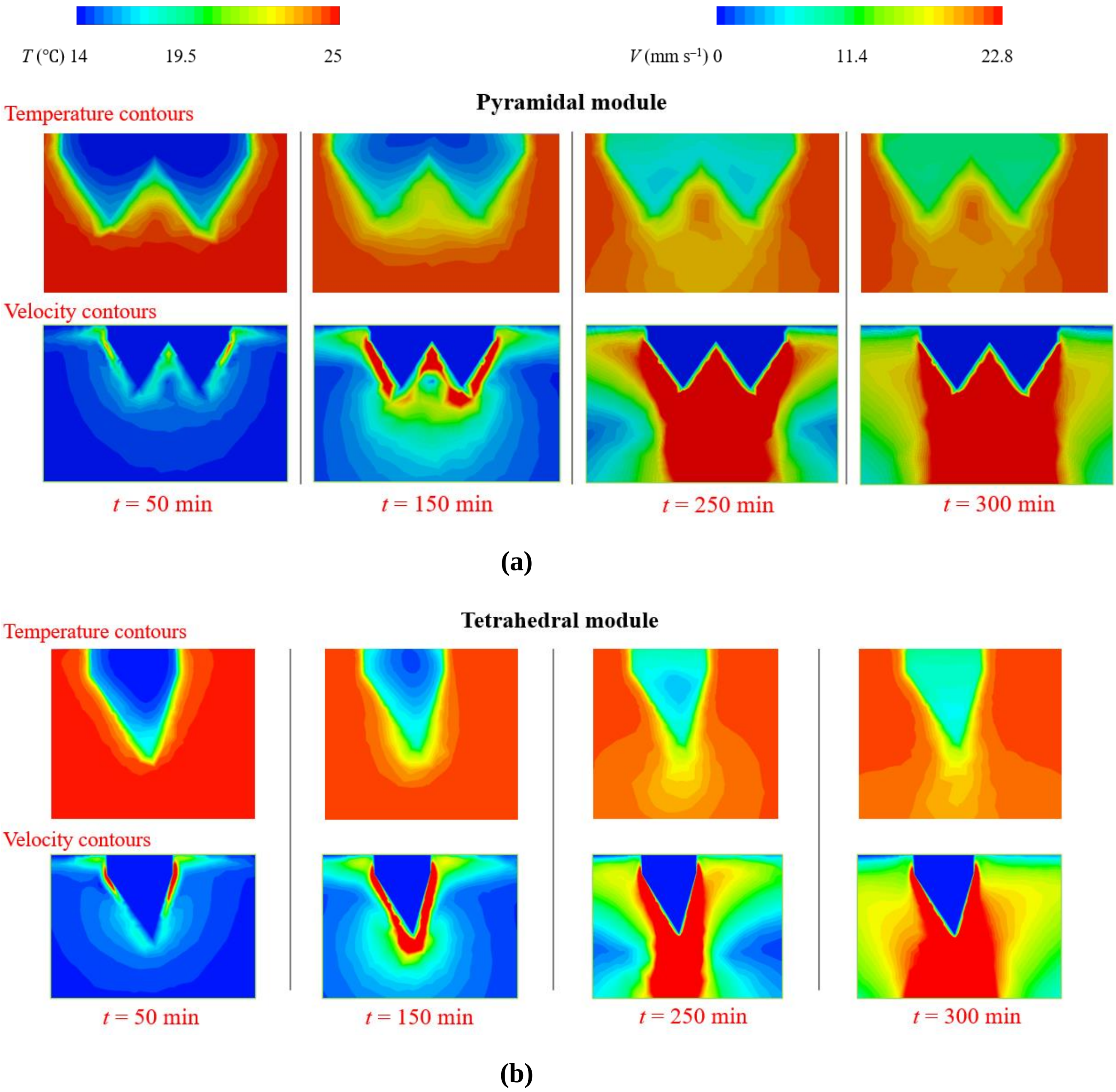

Figure 3.12 Temperature and velocity contours for (a) pyramidal and (b) tetrahedral panels depicted at different times.

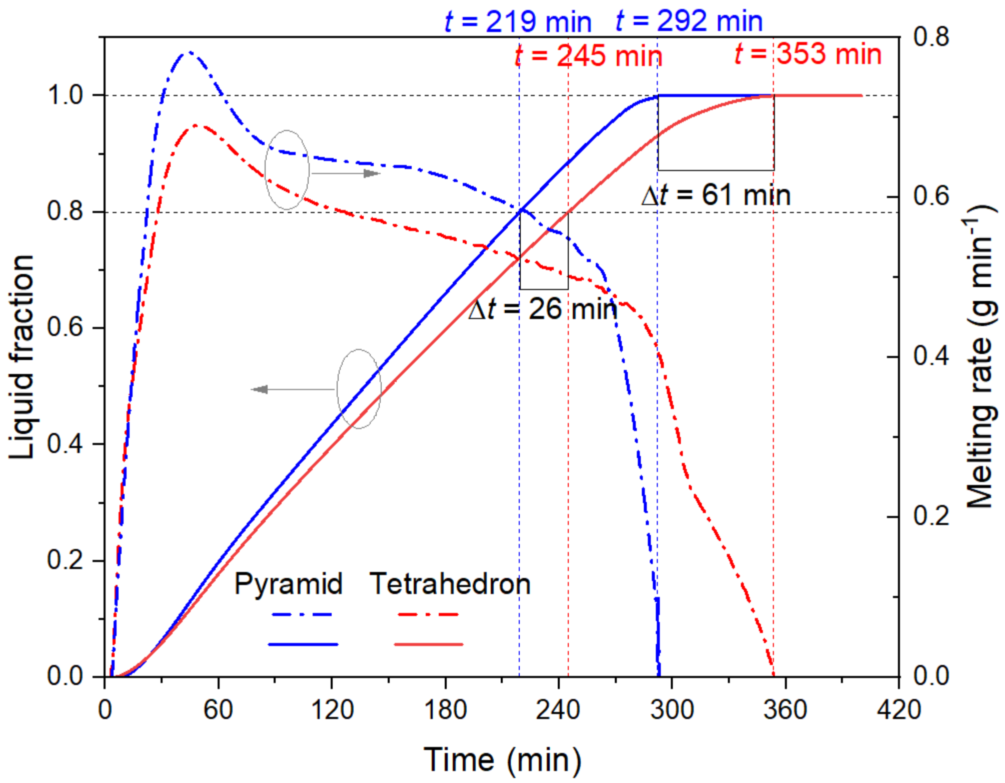

Figure 3.13 Liquid fraction variations (left axis, solid lines) and transient melting rate variations (right axis, dash-dot lines) of pyramidal and tetrahedral panels, with the time indicated for 80% and 100% melting.

3.7.2 Effects of The Initial Temperature Difference Between the Ambient Air and PCMs

The effects of the initial temperature difference between the ambient air and PCMs are investigated in this section. The initial temperature of PCMs was 5°C constant while the initial temperature of the ambient air was varied. As can be seen from Figure (a), the melting time for reaching both 80% and 100% of the liquid fraction decreases as the initial temperature difference increases. For the same panel, the difference in the melting time for reaching 80% and 100% of the liquid fraction also decreases as the initial temperature difference increases. Comparing the pyramidal and tetrahedral panels, the difference in the melting time for reaching the same liquid fraction decreases as the initial temperature difference increases. It is worthwhile noting that when the initial temperature difference is 30 K, it took almost the same melting time for the pyramidal and tetrahedral panels to reach the same liquid fraction. This reveals that when the initial temperature difference is large enough, the melting time will be less affected by the geometric features.

The liquid fraction variations of the PCM are plotted in Figure (b), from which a strong dependence can be observed on the initial temperature difference. Under the same initial temperature difference, the average melting rate of pyramidal panel is always higher than that of tetrahedral panel. For the same panel, the average melting rate increases in a relatively linear manner as the initial temperature difference increases. The average melting rate increases at approximately 0.0357 g min^{-1} K^{-1} and 0.0397 g min^{-1} K^{-1} with respect to the increment of initial temperature difference for the pyramidal and tetrahedral panels, respectively. Therefore, the average melting rate of the tetrahedral panel is 11.2% more sensitive to the temperature difference increment compared to that of the pyramidal panel, despite the latter always exhibiting a larger melting rate. The average melting rate of the pyramidal panel is 32.2%, 21%, 11%, and 3.91% higher than that of the tetrahedral panel when the initial temperature difference is 15, 20, 25 and 30 K, respectively. This further confirms that the increase of initial temperature difference would reduce the performance difference between pyramidal and tetrahedral panels in terms of the average melting rate.

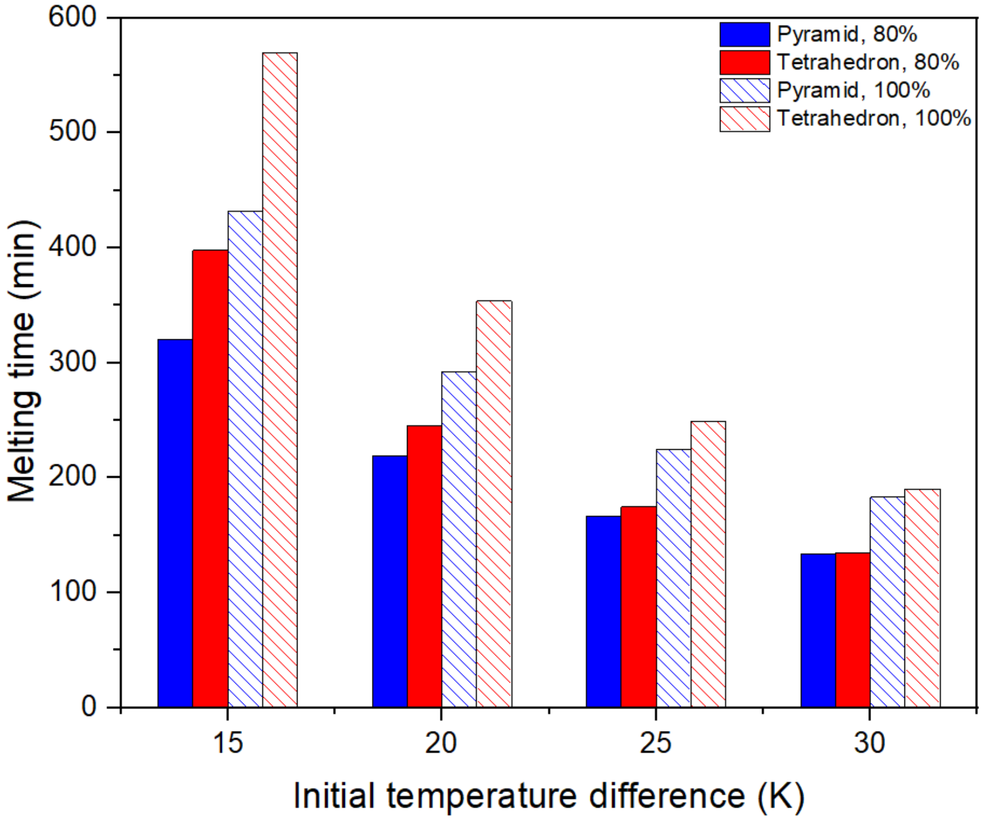

(a)

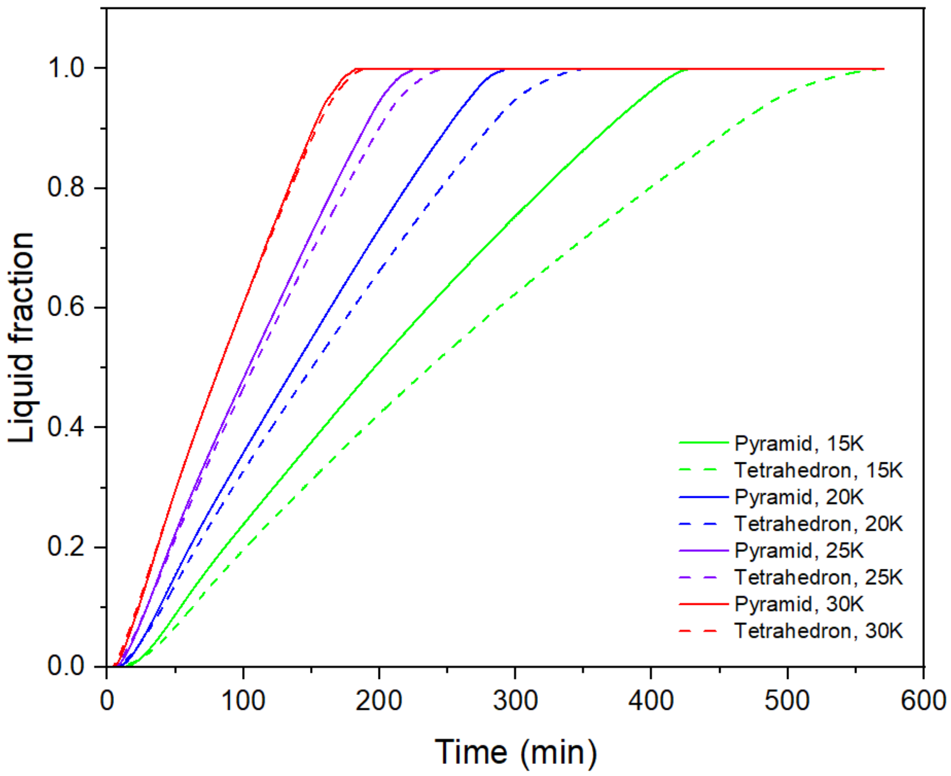

(b)

Figure 3.14 (a) The melting time for liquid fractions 80% and 100% against the initial temperature difference between the ambient air and PCMs; (b) the variations of liquid fraction of the PCM bulk.

3.7.3 Effects of Shell Thickness of the Panel

The shell thickness of the panel is another factor to consider in the implementation. The appropriate selection of shell thickness is essential, as a thin shell will reduce the robustness of the panel which may result in leakage if broken, while a thick shell will inhibit the heat transfer and slow down the melting. To study the effects of shell thickness, the initial temperature of the PCMs and ambient air was set to 5℃ and 25℃, respectively. Shell thicknesses of 1, 3 and 5 mm were selected. As shown in Figure (a), for both pyramidal and tetrahedral panels, the melting time for reaching both 80% and 100% of the liquid fraction increases as the shell thickness increases. However, the increment in melting time is marginal. This result indicates that a thicker shell slightly worsens the heat transfer resulting in slightly longer melting times (when considering the same shell material for all cases).

The results suggest that the average heat transfer rate decreases as the shell thickness increases for both pyramidal and tetrahedral panels. Under the same shell thickness, the average heat transfer rate of the pyramidal panel is always higher than that of the tetrahedral panel (as per discussion in Section 3.7.2). The average heat transfer rate of the pyramidal panel is 20.9%, 20.1%, and 18.3% higher than that of the tetrahedral panel, when the shell thickness is 1, 3 and 5 mm, respectively. This reveals that the difference in the average heat transfer rate between two panels decreases as the shell thickness increases. Thus, a thick shell might not be desirable since it reduces the effect of geometric feature on the thermal performance. When the shell thickness is increased from 1 to 3 mm, the average heat transfer rate decreases by 4.69% and

3.95% for pyramidal and tetrahedral panels, respectively; when the shell thickness increases from 3 to 5 mm, the average heat transfer rate decreases by 6.29% and 4.72% for pyramidal and tetrahedral panels, respectively. This reveals that the average heat transfer rate does not decrease linearly with respect to the shell thickness for both pyramidal and tetrahedral panels. In addition, the liquid fraction variations of the PCM bulks are plotted in Figure (b), showing that the discrepancies in liquid fraction resulting from different shell thickness is minor.

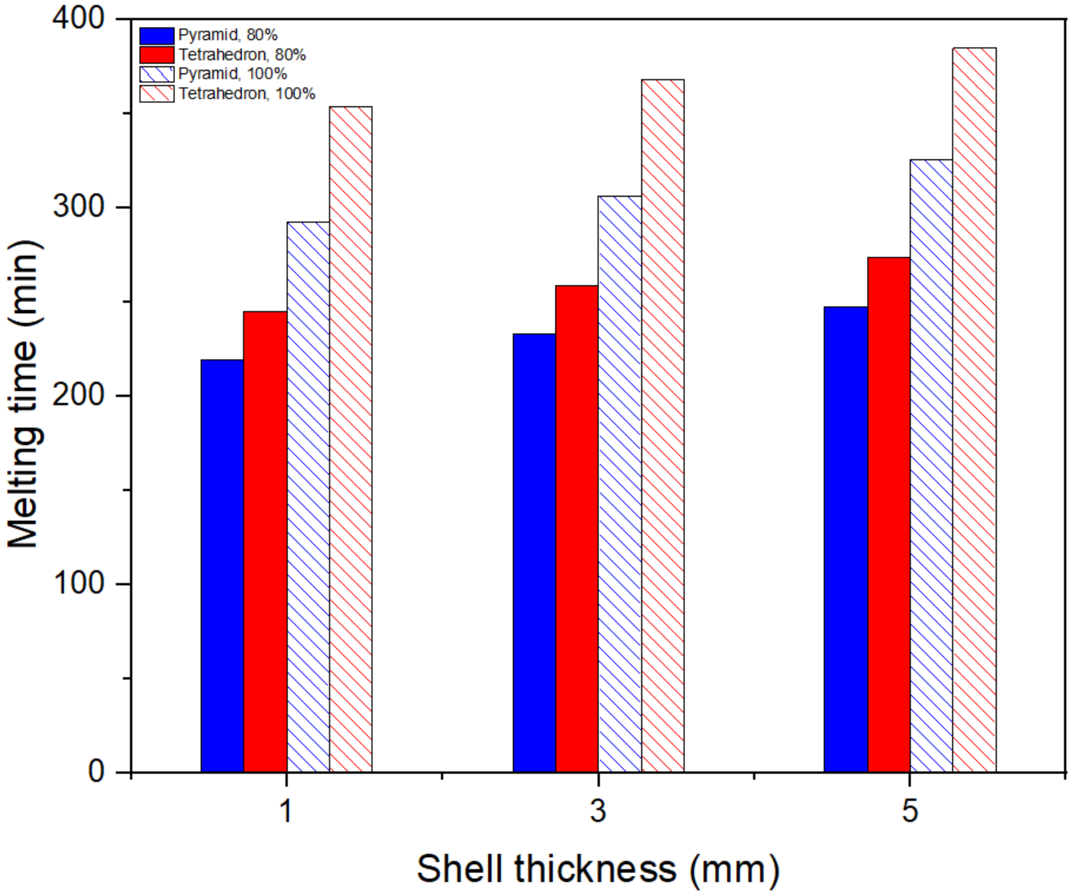

(a)

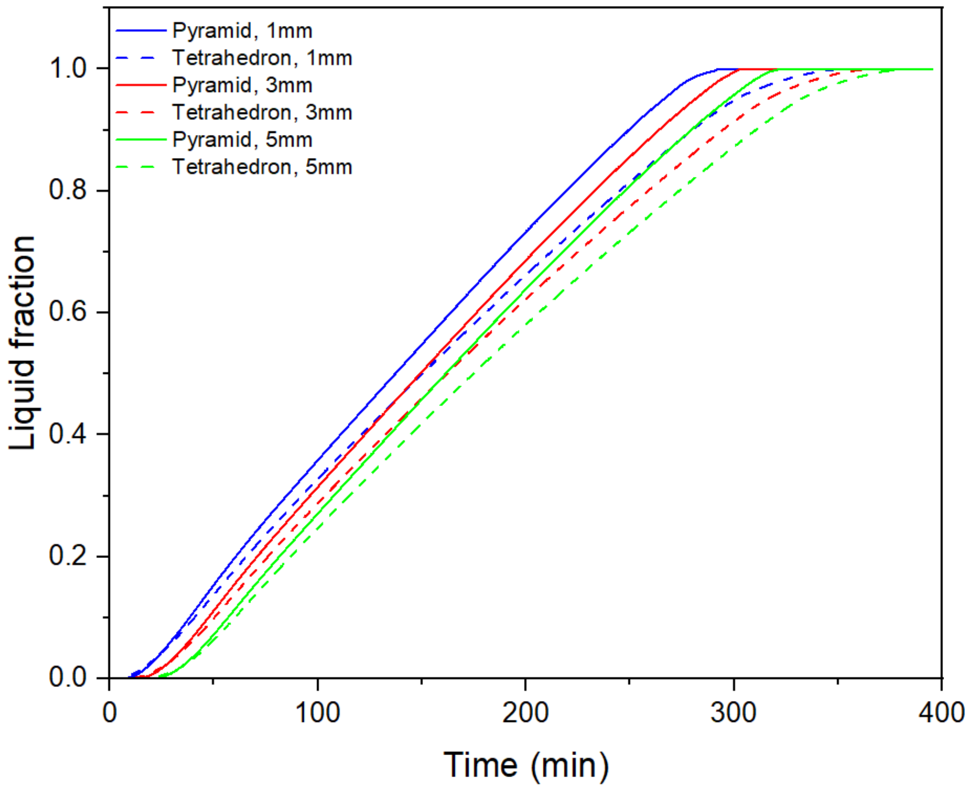

(b)

Figure 3.15 (a) The melting time for liquid fractions 80% and 100% against the shell thickness of the panel; (b) the variations of liquid fraction of the PCM bulk.

3.7.4 Effects of the Distance Between the Panel Base and Ceiling Surface

When there is a gap between the panel base and the ceiling surface, natural convection in the gap is allowed and the effective heat transfer area is increased as heat transfer also occurs through the base surface of the panel. In this case, the effective heat transfer area increases by 47.7% and 25.4% for the pyramidal and tetrahedral panels, respectively. To investigate the effects of distance between the panel base and ceiling surface, the initial temperature of the PCMs and ambient air was set to 5℃ and 25℃, respectively. Distances of 5, 10 and 15 cm were selected, and the simulated results are contrasted to the zero-distance condition in Figure.

As shown in Figure, when the distance between the panel base and ceiling surface is increased from 0 to 5 cm, there is a substantial drop on the melting time for reaching both 80% and 100% liquid fractions for both pyramidal and tetrahedral panels. This is because the effective heat transfer area is increased, and the conjugate heat transfer is therefore enhanced. As a result, the melting time is reduced significantly with an average melting rate for the pyramidal panel increasing by 30.2%; the average melting rate increases by 21.2% for the case of tetrahedral panel. Furthermore, the melting time for reaching both 80% and 100% liquid fractions keeps decreasing when the distance is further increased to 10 and 15 cm, but the difference is rather negligible. These results suggest that the increase of the average melting rate of the pyramidal panel is higher than that of the tetrahedral panel, which could be expected as the increase of effective heat transfer area of the pyramidal panel is higher than that of the tetrahedral panel. In addition, for the pyramidal panel, the average heat transfer rate increases by 6.46% and 3.22%

when the distance is increased from 5 to 10 cm and from 10 to 15 cm. Similarly, for tetrahedral panel, the average heat transfer rate increases by 3.60% and 2.15% when the distance is increased from 5 to 10 cm and from 10 to 15 cm. These results elucidate the marginal effects of the distance between the panel base and ceiling surface on the heat transfer for distances larger than 5 cm. In addition, considering the space clearance in a real-world implementation, a high ceiling would be a requirement to implement a large distance between the panel base and the ceiling. Thus, for the case of the presented study, in which the ceiling height is 2.25 m, it is recommended that the PCM panel should be suspended no more than 5 cm to the ceiling.

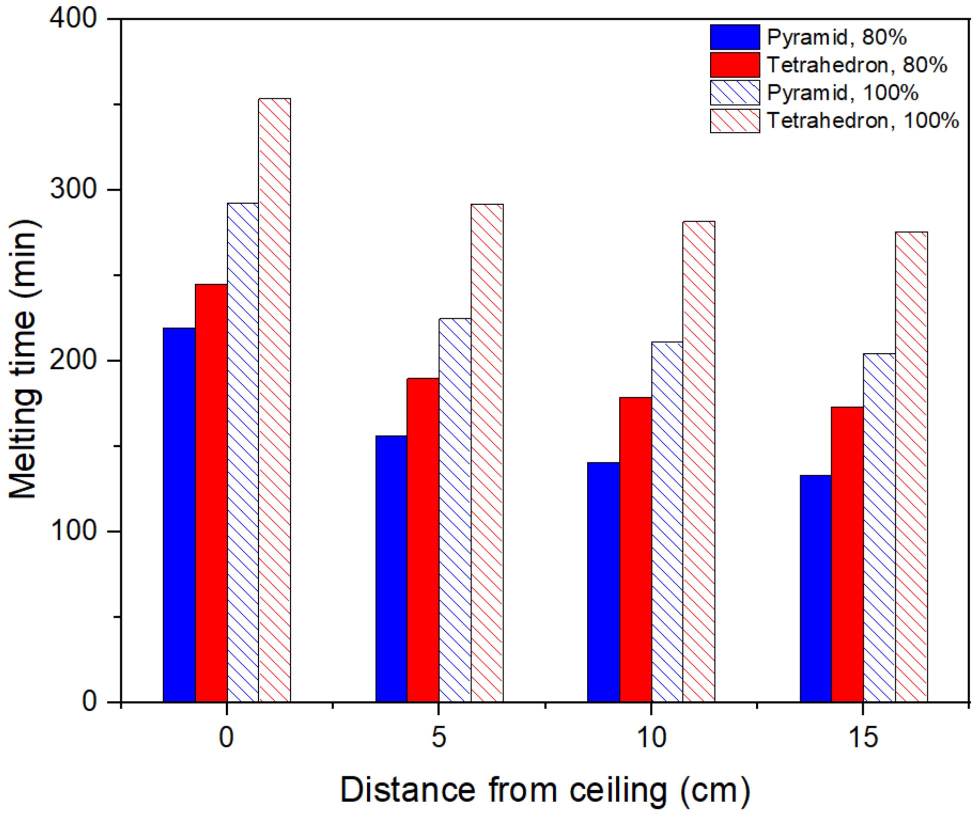

Figure 3.16 The melting time for liquid fractions 80% and 100% against the distance from the ceiling.

3.7.5 Effects of Protrusion-to-base Ratio

The protrusion-to-base ratio is another key factor that influences the thermal performance of the panel. From the velocity contours in Figure 3, the heat transfer between the ambient air and the protrusions is stronger than that between the ambient air and the base. Therefore, it would be worthwhile to investigate whether the PCM volume in the protrusions will enhance or impede the overall melting process. To study this, the initial temperature of the PCMs and ambient air was set to 5℃ and 25℃, respectively. 30%, 50%, and 70% were selected to be the PCM proportion in the protrusions to study, which represent the protrusion-to-base ratio of 3:7, 5:5, and 7:3, respectively. An indicative illustration of the panel with these three different protrusion-to-base ratios is presented in Figure, taking the pyramidal panels as an example. The area of the panel base surface and protrusion (i.e. pyramid or tetrahedron) base surface was kept the same, so the height of the protrusion will increase and the height of the base will decrease when the proportion is increased. Therefore, a larger proportion will result in a higher aspect ratio for the overall panel geometry. It is noted that the geometry features of the panel will change in this case: for the proportion of 30%, 50%, and 70%, the angle between the lateral edge and the base of the pyramid is 29.2°, 43.0°, and 52.6°, respectively; the angle between the lateral edge and the base of the tetrahedron is 40.3°, 54.7°, and 63.2°, respectively.

As shown in Figure , the melting time for reaching both 80% and 100% liquid fractions for both pyramidal and tetrahedral panels decreases as the PCM proportion increases. This reveals that the increase of the PCM proportion in the protrusions will facilitate the heat transfer between the ambient air and the PCM panel. When the PCM proportion increases, the protrusions will have a larger contact surface area with the ambient air. This confirms that the heat transfer is more dominant through the panel protrusions rather than the panel base. For pyramidal panel, the average melting rate increases by 7.58% and 10.7% when the PCM proportion is increased from 30% to 50% and 50% to 70%, respectively; the average melting rate increases by 11.1% and 13.5% for the case of tetrahedral panel when the PCM proportion is increased from 30% to 50% and 50% to 70%, respectively. This reveals that the increase of the average melting rate is non-linear to the increase of the PCM proportion, the increment of average melting rate is larger when the PCM proportion is increased from 50% to 70% for both pyramidal and tetrahedral panels.

However, in the case of 70% proportion, the aspect ratio of the overall panel geometry will be relatively high, which means the height of the panel will also be relatively high and the tip of the protrusion will be sharp. In this case, the panel will be closer to the room participants and the sharp tip may bring some safety issues to the room participants. Thus, the high PCM proportion in the protrusions may not be desirable for real-world implementation although a higher average melting rate can be yielded. In addition, the increase of PCM proportion in the protrusions would facilitate the heat transfer for the tetrahedral panel better than the pyramidal panel, as a same increase in the PCM proportion yields a larger increase in the average melting rate for the tetrahedral panel.

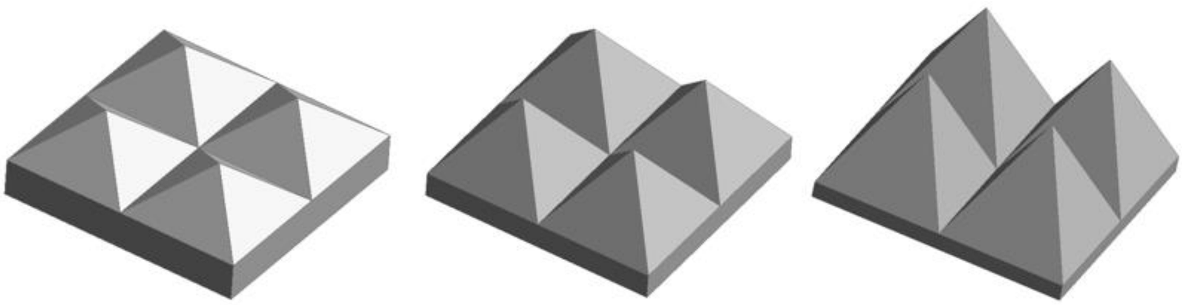

Figure 3.17 Geometry of the pyramidal panels with various protrusion-to-base ratios.

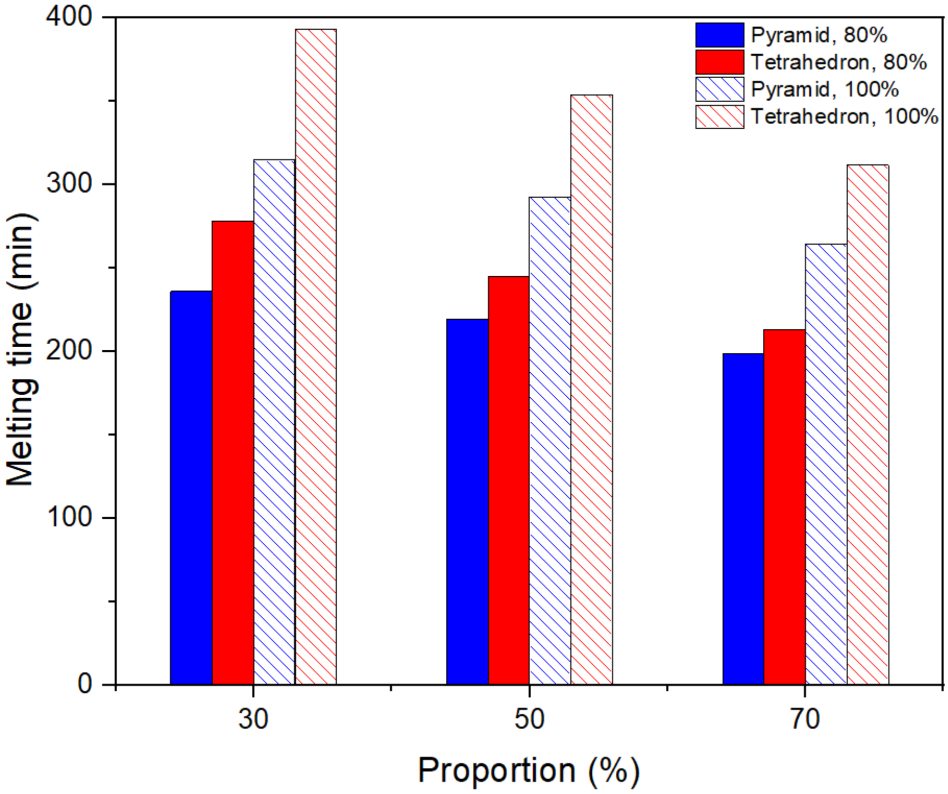

Figure 3.18 The melting time for liquid fraction 80% and 100% against the PCM proportion in the geometrical protrusions.

3.7.6 Effects of the Gaps Between Protrusions

Adding a gap between protrusions would increase the effective heat transfer area between the PCM panel and the ambient air. To study this effect, the initial temperature of the PCMs and ambient air was set to 5℃ and 25℃, respectively. In this study, 3 mm and 5 mm were selected to be the gap widths, and the results are contrasted to the condition where there is no gap between the protrusions. The geometric features of the panel with gaps between protrusions are presented in Figure.

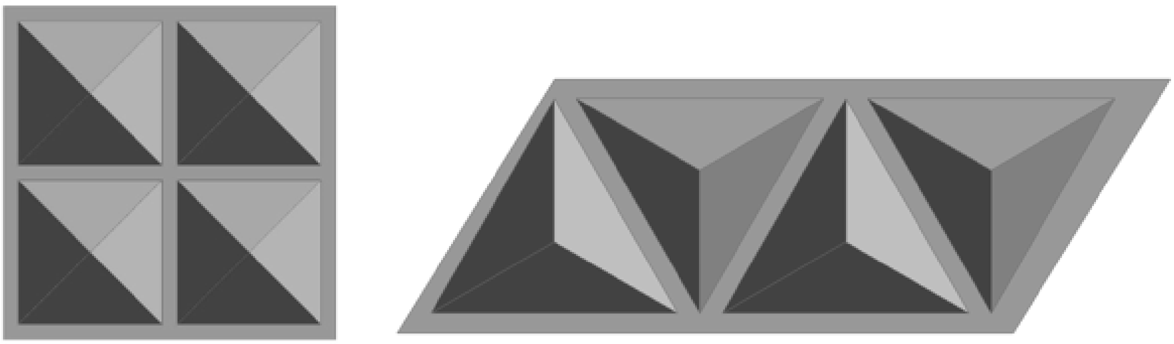

Figure 3.19 Geometry of the pyramidal (left) and tetrahedral (right) panel with gaps between protrusions.

As shown in Figure, the melting time for reaching both 80% and 100% liquid fraction decreases as the gap width between protrusions increases. However, the decrement is not very distinct as the effective heat transfer area does not increase too much. This is because the gap width is relatively small compared to the overall dimension of the panel. For the pyramidal panel, the average melting rate increases by 3.60% and 3.48% when the gap width increases from 0 to 3 mm and from 3 to 5 mm, respectively; for the tetrahedral panel, the average melting rate increases by 4.16% and 2.59% when the gap width increases from 0 to 3 mm and from 3 to 5 mm, respectively. Thus, adding a thin gap between the protrusions would not facilitate the PCM melting significantly. It is also speculated that the melting time would significantly reduce if the gap width is relatively large with respect to the overall panel dimension.

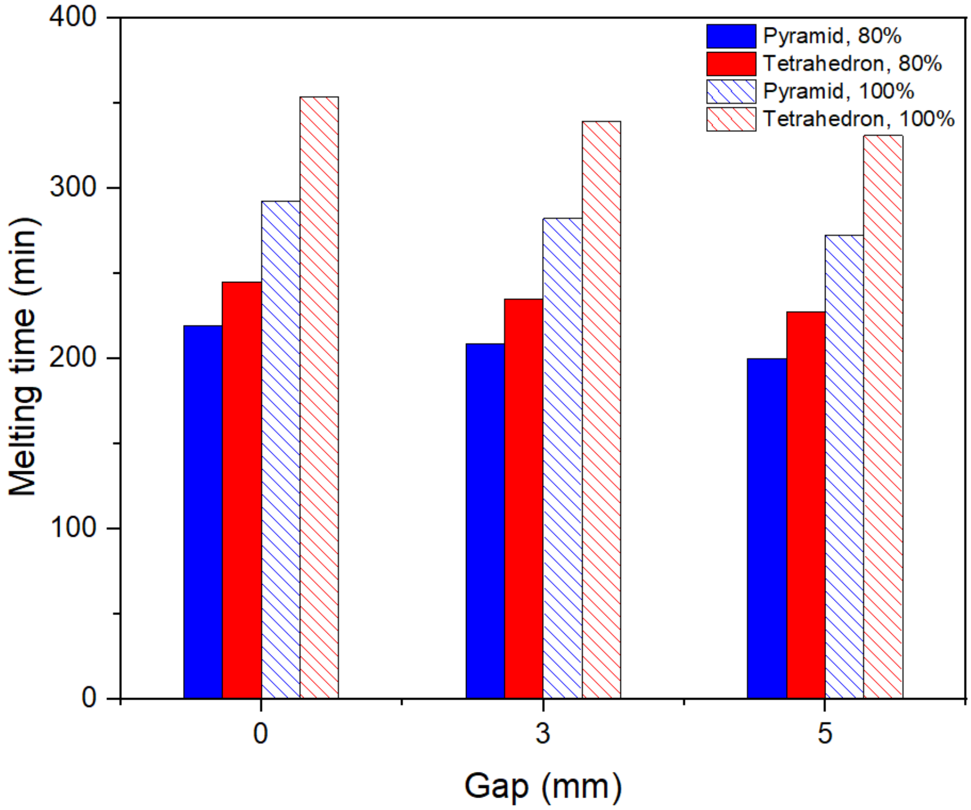

Figure 3.20 The melting time for liquid fractions 80% and 100% against the gap width.

3.7.7 Effects of the Panel Volume

The volume of the panel is another key influencing factor to study. If the panel has a small volume, it will be capable of only containing a small amount of PCMs, which cannot meet the required cooling capacity. In contrast, if the panel has a large volume, the encapsulated PCMs may not be able to melt or solidify entirely in line with the discharging and charging hours. To study the effect of panel volume, the initial temperature of the PCMs and ambient air was set to 5℃ and 25℃, respectively. Panel volumes of 250, 500 and 750 mL were analysed. The angle between the lateral edge and the base of the pyramid was kept at 43.0° for all the studied volumes, and that between the lateral edge and the base of the tetrahedron was kept at 54.7°. For pyramidal panels, the effective heat transfer area per volume is 0.928, 0.725, and 0.633

mL^{-1}, when the panel volume is 250, 500, and 750 mL, respectively; for tetrahedral panels, the effective heat transfer area per volume is 1.13, 0.895, and 0.782 mL^{-1}, when the panel volume is 250, 500, and 750 mL, respectively. As can be seen from Figure (a), the melting time for reaching both 80% and 100% liquid fractions for both pyramidal and tetrahedral panels increase as the panel volume increases. This is because the panel with a larger volume can contain more PCMs, and the total amount of latent heat is increased. It is worthwhile noting for the 750 mL tetrahedral panel, it took about 760 minutes to complete the melting, which is 115% longer than the 250 mL one and 56.1% longer than the 500 mL one.

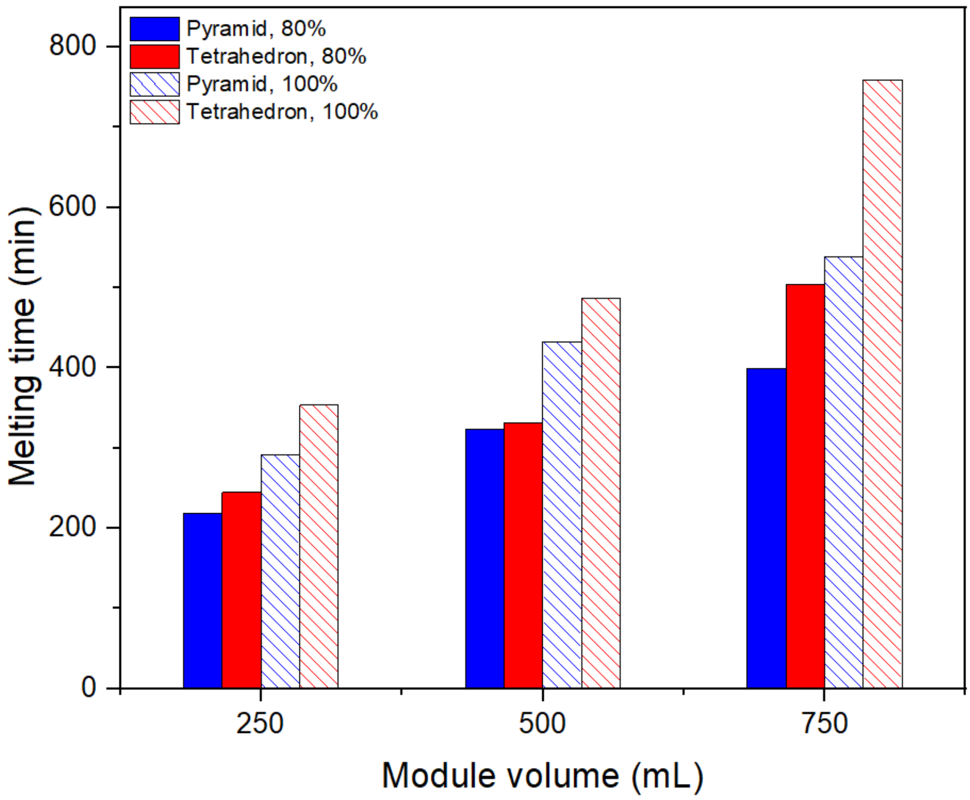

(a)

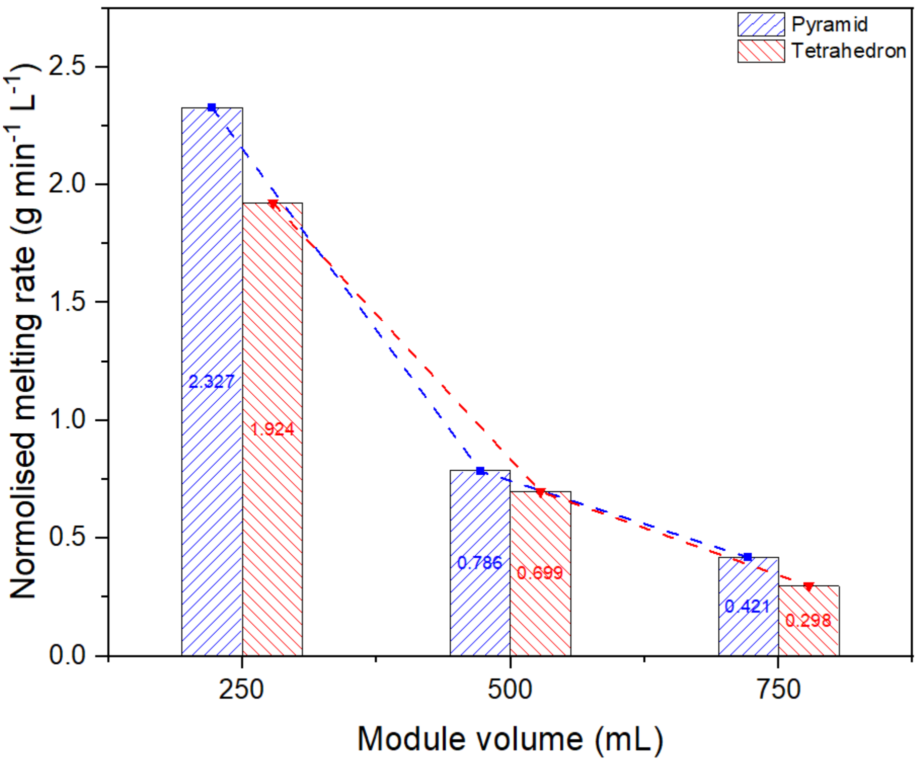

(b)

Figure 3.21 (a) The melting time for liquid fraction 80% and 100% against the panel volume; (b) the normalised melting rate against the panel volume.

Figure (b) shows the normalised melting rate for the pyramidal and tetrahedral panels with different volumes. The normalised melting rate for both pyramidal and tetrahedral panels decreases as the panel volume increases. For the pyramidal panel, the normalised melting rate decreases by 66.2% and 46.4% when the panel volume increases from 250 to 500 mL and from 500 to 750 mL, respectively; for the tetrahedral panel, the normalised melting rate decreases by 63.7% and 57.4% when the panel volume increases from 250 to 500 mL and from 500 to 750 mL. It is evident that the decrease of the normalised melting rate is not linear with respect to the linear increase of the panel volume for both pyramidal and tetrahedral panels. The decrement is more substantial when the panel volume increases from 250 to 500 mL than from 500 to 750 mL. The normalised melting rate of 250 mL pyramidal panel is 2.96 and 5.53 times higher than that of 500 and 750 mL pyramidal panel, respectively; while the normalised melting rate of 250 mL tetrahedral panel is 2.75 and 6.46 times higher than that of 500 and 750 mL tetrahedral panel, respectively. Therefore, the increase of the panel volume will result in a substantial decrease of the normalised melting rate, which is detrimental to the overall thermal performance for building thermal management. Hence, it would be necessary to distribute the PCMs into multiple small panels instead of encapsulating them within one single large panel.

3.7.8 Implications on Practical Implementation

The influencing factors studied from Section 3.7.3 to 3.7.7 correspond to the physical geometric configurations of the PCM ceiling panels. The simulation results can provide some implications to the real world design and implementation of such PCM ceiling panels. A general and brief summary on how to use the aforementioned findings from simulations to aid the practical design and implementation is provided in this section in Table 3. below.

Table 3.4. Implications of simulation results on practical design and implementation.

Influencing factor studied in simulation	Implication on practical design and implementation
Shell thickness	Although the thicker shell improves the panel robustness and prevents leakage, but it is less desirable considering the thermal performance as a thicker shell weakens heat transfer and increase the charging/discharging time.
Distance between panel base and ceiling surface	Suspending the panel from the ceiling surface benefits the thermal performance as it increases the effective heat transfer area. However, the gap between the panel base and ceiling surface is recommended to be 5 cm maximum.
Protrusion-to-base ratio	The higher protrusion-to-base ratio facilitates the heat transfer as the thermal boundary layer of the protrusions is thinner. However, the ratio is recommended to be 50:50 maximum, as the higher ratio results in sharp, hazardous panel tips, which might introduce safety issues to the building occupants.
Gaps between protrusions	Adding gaps between protrusions enlarged the effective heat transfer area, but the effect on thermal performance is not outstanding if the gap width is not large enough.
Panel volume	The increased panel volume can contain more PCMs, but the full charging or discharging of PCMs takes much longer time. For scenarios require high cooling loads, it is recommended to distribute the total PCM amount into multiple small panels instead of grouping them into large panels.

3.8 Chapter Conclusion

In this chapter, the melting behaviour of PCMs macro-encapsulated within a panel attached to the ceiling was studied. Conjugate heat transfer comprised of natural convection and heat conduction is considered. A numerical model of heat transfer through the ambient air, panel shell, and the PCM was built and validated. The validated model was employed to study the different influencing factors of the melting of the encapsulated PCMs, including initial temperature difference between ambient air and PCMs, panel shell thickness, distance to the ceiling, protrusion-to-base ratio, gap width, and panel volume. Melting rate, liquid fraction, and temperature were used as metrics to evaluate thermal performance. The main results of this chapter are concluded as below:

1) In all the cases studied, the melting time of pyramidal panels is always shorter than that of the tetrahedral panels, although the effective heat transfer area of the pyramidal panel is 21.6% less than that of the tetrahedral panel. This observation reveals that a thin panel base is desirable.

2) When the initial temperature difference increases (from 15 to 30 K), the difference of the melting time between the pyramidal and tetrahedral panels decreases. When the initial temperature difference is large enough (30 K) the melting time of the pyramidal and tetrahedral panels is almost the same.

3) The effect of the shell thickness on the thermal performance of the panel is insignificant for the thickness in a range of 1 to 5 mm.

4) Hanging the panel to the ceiling results in a shorter melting time as the effective heat transfer area is increased. It is recommended that the distance between the panel base and the ceiling surface should be 5 cm or larger, depending on the available space.

5) Changing the protrusion-to-base ratio and adding gaps between protrusions can enhance the thermal performance to some extent. The increase of the area of the protrusions is the key to facilitating the PCM melting due to the thinner thermal boundary layer around the protrusions.

6) The increase of the panel volume substantially reduces the normalised melting rate and increases the total melting time. Hence, it is suggested to distribute the large PCM volume into multiple smaller panels for rapid cooling supply.

These results complement the current body of knowledge about PCM-based ceiling applications for passive building indoor cooling. The recommended geometric, thermal, and spatial configurations can be used as a reference when it comes to real-world implementation. Some recommended future work includes the investigation of the thermal comfort brought by the PCM ceiling panels, and the simulations of the PCM panel array under real working conditions.

Chapter 4 – Study of PCM Ceiling Panel Array for Passive Cooling in an Outdoor Storage Enclosure

In Chapter 3, a CFD model was developed in the commercial software Ansys Fluent 2020 R2 and validated with the on-site experimental results. The effects of various geometric configurations on the panel thermal performance were also studied thoroughly. From the experimental and modelling results, the pyramidal panel manifested better thermal performance than the tetrahedral panel. Therefore, it is worthwhile to further explore the cooling effects of the pyramidal panel under the real working conditions. In this chapter, an experimental study will be presented to demonstrate the passive cooling efficacy of multiple pyramidal panels (i.e. pyramidal panel array) that cover the entire ceiling of the room. Some additional follow-up simulations will also be presented in this chapter.

As discussed in the previous chapters, although there has been substantial research on PCM ceilings for passive indoor cooling, the majority of them focuses on the commercial and residential buildings with either heavyweight or lightweight designs. The incorporation of PCM ceilings could provide extra thermal inertia against the temperature fluctuations in buildings. Besides, for building purposes of commercial and residential, internal heat gain from human activities and electrical appliance can be dominant. Studies have shown that PCM ceilings are promising passive cooling techniques to enhance indoor temperature uniformity and thermal comfort. However, there is not a known study focusing on the use of PCMs for passive indoor cooling of buildings with negligible thermal mass (i.e. worse than low-thermal-mass buildings), such as outdoor storage room, machine room, bike shed, dog shed, and garage. Opposite to high-thermal-mass buildings constructed with heavyweight materials or the low-thermal-mass buildings constructed with lightweight materials, these examples with negligible thermal mass manifest extremely short thermal lag time, which absorb and release heat quickly without buffering [108]. The indoor cooling of these enclosures is essential, especially for the cases when temperature-sensitive materials are stored or the ambient temperature is vital to machines' safe operation, where a moderate indoor temperature without overheating is a must. The indoor cooling of the enclosure can also potentially mitigate the thermal degradation of the stored materials, which yields a longer lifespan for the stored materials. Given the stand-alone storage enclosure is usually directly exposed under the outdoor environment, the major heat gain is direct solar irradiation, and the indoor temperature will be extremely sensitive to the external temperature as metal usually has high thermal conductivity but low thermal mass. Therefore, the incorporation of PCM ceiling panels to stand-alone enclosures with negligible thermal mass is important to enhance the thermal inertia of the enclosure, reduce the peak indoor temperature, and achieve a temperature-safe ambient for the stored materials or machines.

In this chapter, the author proposes a pioneering research work on a passive indoor cooling strategy of a stand-alone low-thermal-mass storage enclosure using PCM ceiling panels, where a PCM ceiling panel array is implemented to the ceiling of the enclosure. The PCMs are macro-encapsulated inside the panels with the geometric configuration of each panel to be pyramidal. The amount and layout of the PCM ceiling panels can be adjusted to offer great flexibility to match different cooling demands, building purposes, and climates. On-site experiments were conducted in the city of Canberra, Australia, and various parameters were measured and analysed to validate the effectiveness and indoor cooling performance of PCM ceiling panels for the stand-alone enclosure under different weather conditions. A further step of modelling the cooling performance of a single panel during PCM freezing and melting under constant or variable indoor temperature conditions was conducted. The work presented in this chapter extends the simulation work presented in Chapter 3 to the real-world application of using multiple PCM ceiling panels. The results will inform the applicability of the PCM ceiling panels for passive indoor cooling of stand-alone enclosures and other similar building applications.

4.1 Experimental Methodology

4.1.1 Selection of Phase Change Temperature

As the experiment was planned to be conducted on-site in a stand-alone outdoor storage enclosure (i.e. a metal shed) in the city of Canberra, Australia, and the season was selected to be the transitional period between summer and autumn (i.e. from February to May), the selection of the phase change temperature is essential. The selected phase change temperature must be in line with the local seasonal climate to ensure the balanced charging and discharging hours for the PCM ceiling panels. To this end, the indoor air temperature of the shed (without PCMs) was measured continuously for 213 hours (i.e. approximately nine days). The indoor air temperature variations of the shed are plotted in Figure , along with the outdoor temperature variations over the same time period. It is noted that the indoor temperature was always higher than the outdoor temperature during the measurement hours, on average by 16.4%. The indoor temperature is also fluctuating swiftly with the outdoor temperature without any lagging. Therefore, a goal of this study is to moderate indoor temperature as indicated by the temperature difference between indoor and outdoor and to reduce the fluctuation of indoor temperature. Although the aim of reducing ‘indoor-outdoor temperature difference’ sounds like a paradox for evaluating free cooling performance, it is a suitable metric in this study due to the aforesaid reasons and the lack of scientific control using an exact same shed without PCM ceiling panels. Based on the examination of the indoor and outdoor temperature variations, 20℃ is considered as an optimal phase change temperature for the presented study, at which the best-balanced charging and discharging hours can be achieved.

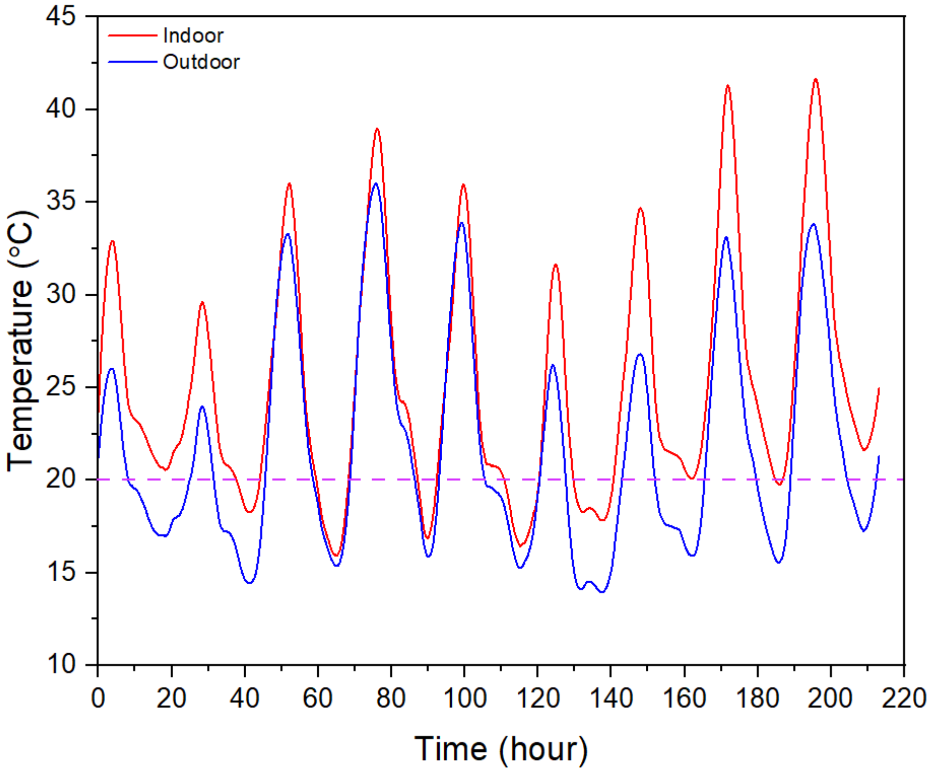

Figure 4.1 Indoor and outdoor temperature variations measured over nine consecutive days (8th/Feb - 17th/Feb, 2023).

Similar to the PCM preparation discussed in Chapter 3, to fulfil the desired phase change temperature, the eutectic mixture of capric and lauric acids (with mole proportion of 70:30) was adopted as the PCM for the presented study. In the study of Wang et al. [102], the freezing temperature was recognised as the phase change temperature, while the eutectics usually melts within a temperature band rather than isothermally. That means the melting temperature is a bit higher than the freezing temperature for eutectics, because of the nonexistence of the definitive lattice pattern [95]. Therefore, the eutectics of the capric and lauric acids (i.e. freezing temperature of 18℃) was considered as a good candidate for the experimental work in this chapter.

4.1.2 PCM Screening and Characterisation

The thermophysical properties of the developed PCM were measured using differential scanning calorimetry (DSC), with a cooling and heating rate of 10℃ min^{-1}. The phase change enthalpy of the PCM is 115 kJ kg^{-1}. The onset points are 17℃ and 20℃, which correspond to the freezing and melting temperature of the PCM, respectively. Other thermophysical properties are obtained from the previous work of Wang et al. [102]. The thermophysical properties are summarised in Table below.

Table 4.1 Thermophysical properties of the developed PCM.

Property	Value
Freezing temperature, K	290

Melting temperature, K	293
Density, kg m^{-3}	840
Thermal conductivity *l*, W m^{-1} K^{-1}	0.169
Thermal conductivity *s*, W m^{-1} K^{-1}	0.183
Specific heat *l*, kJ kg^{-1} K^{-1}	2.21
Specific heat *s*, kJ kg^{-1} K^{-1}	1.83
Latent heat of fusion, kJ kg^{-1}	115

4.1.3 PCM Ceiling Panels Preparation and Experimental Setup

A total of 25 panels were fabricated with 3D printing technique, each panel is hollow inside with a shell thickness of 2 mm. The material used for 3D printing is Acrylonitrile Butadiene Styrene (ABS). Each panel has an external volume of 1800 cm^3, which contains 1.44 kg of PCMs. The total mass of PCMs used in this experiment is 36 kg. The geometry of the panel can be deemed as a cuboid topped with four pyramids, and this selected panel geometry was the optimal geometry obtained from Chapter 3. The base surface of every panel was insulated during the experiment, so the effective heat transfer area is defined as the total panel surface area excluding the base area that is insulated. The major dimensions of the panel is labelled in Figure. The thermal and physical properties along with geometry features of the panel are summarised in Table .

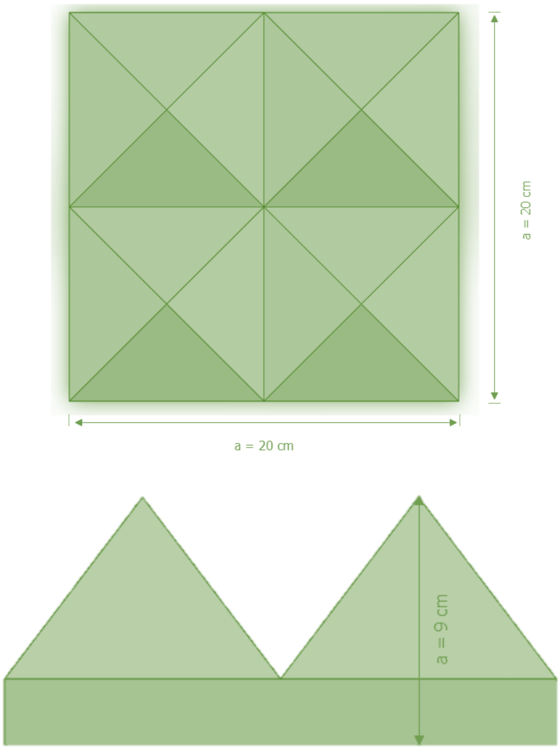

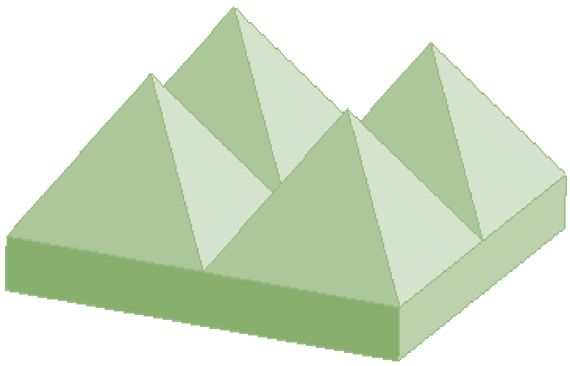

Figure 4.2 CAD design indicating the major dimensions (top, front, and isometric views).

Table 4.2 Thermophysical properties and geometric features of the panel.

Property	Result
Material	ABS plastic
Density, ρ	1070 kg m^{-3}
Thermal conductivity, λ	0.163 W m^{-1} K^{-1}
Specific heat, c_p	1.99 kJ kg^{-1} K^{-1}
Surface area to volume ratio	0.68 cm^{-1}
Effective heat transfer area	854.40 cm^2

The experiment was conducted in a stand-alone outdoor metal storage enclosure, shown in Figure (a), with a dimension of 1.48 m × 1.48 m × 1.9 m, where the major heat gain was direct solar irradiation and heat exchange with outdoor air. A metal mesh was mounted to the ceiling of the shed as a holder for the 25 PCM panels, and the metal mesh was supported by pinewood bars. A polyethylene foam with a thickness of 2 cm was sandwiched between the ceiling and the PCM panels, which covered the whole ceiling surface and set the base surfaces of the panels at nearly an adiabatic condition. Three Type-K thermocouples were fixed evenly along the central vertical axis of one of the pyramidal protrusions, as shown in Figure to measure the internal temperature variations. The apex, mid-point, and base measuring points represented 3/4, 1/2, and 1/4 of the height of the panel, respectively, taking the base surface of the panel as the reference. Three out of 25 panels were equipped with thermocouples, and they are placed from one corner to the center of the enclosure ceiling, as indicated in Figure (b). The nine thermocouples within the PCM panels were labelled as TC-1 to TC-9. There were another three thermocouples measuring the indoor air temperature (TC-A, TC-B, and TC-C) at the height of 1.35, 0.9, and 0.45 m, respectively, and one thermocouple measuring the outdoor air temperature (TC-D). The readings of the thermocouples were recorded by a digital data logger. The accuracy of the type-K thermocouples is ± 0.75%. The potential error of the experiment was mainly sourced from the measurement error of the type-K thermocouples and the possible minor deviation of the measurement points. A schematic diagram of the experimental setup is shown in Figure (a), and an on-site photo of the experimental setup is shown in Figure (a), with zoomed-in details of the ceiling panel array shown in Figure (b).

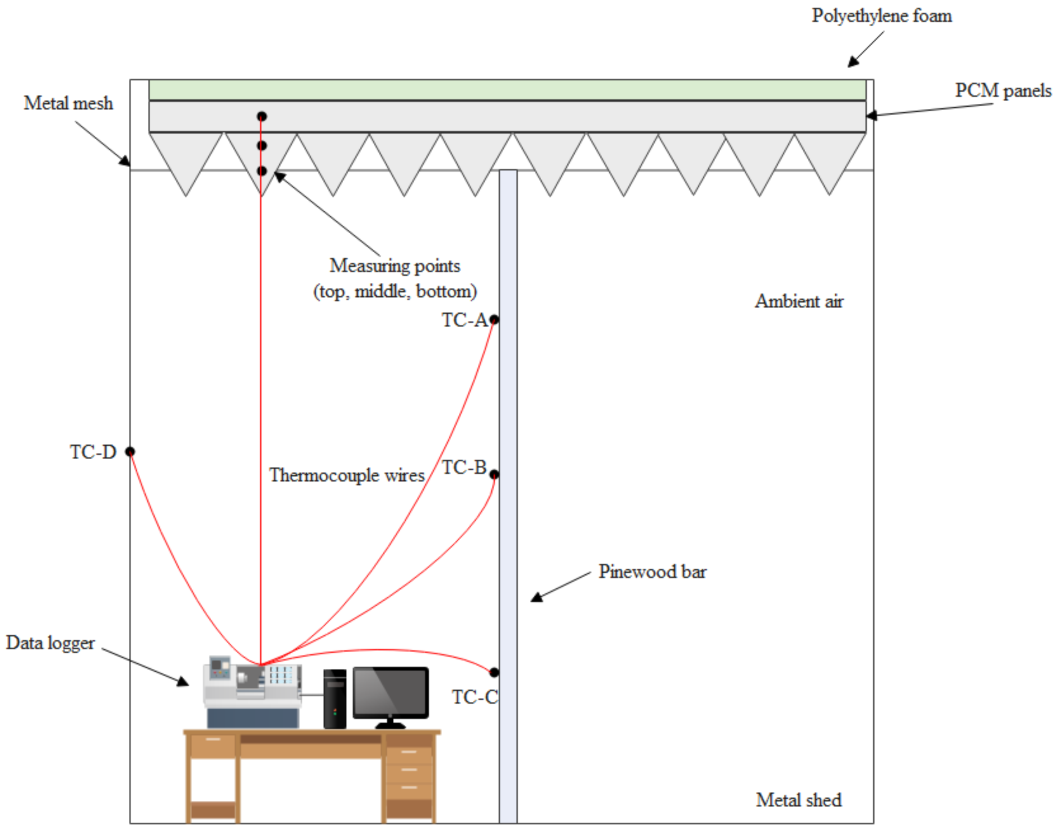

(a)

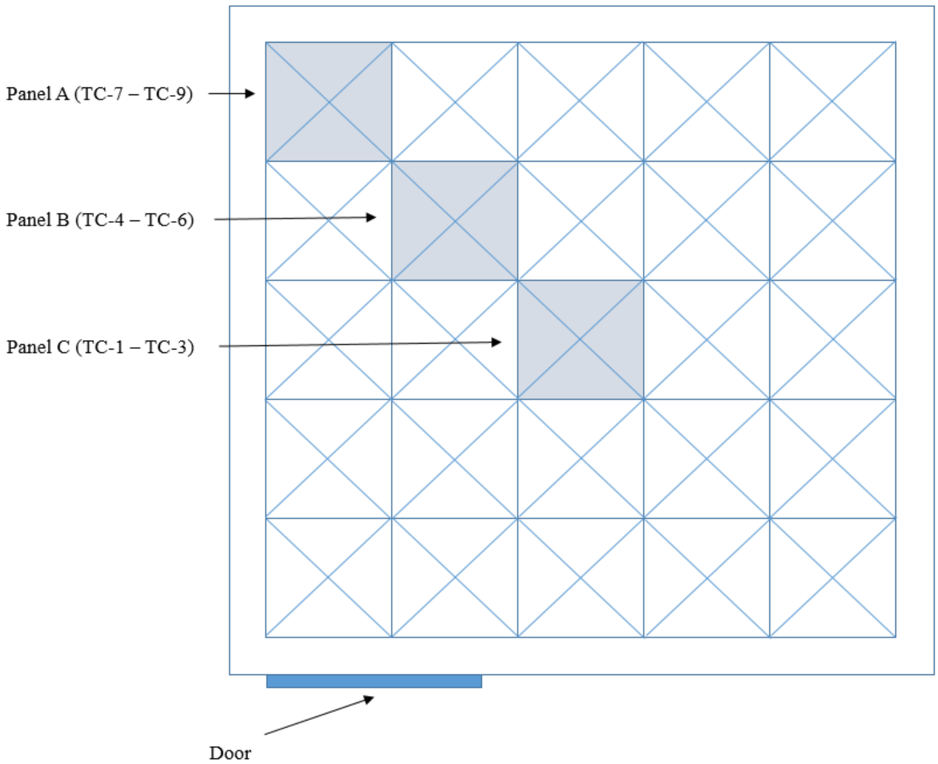

(b)

Figure 4.3 (a) Schematic of the experimental setup. (b) Floor plan of the PCM ceiling panel array.

(a)

(b)

Figure 4.4 (a) On-site photos of the experimental setup. (b) Zoomed-in details of the PCM panel array.

4.2 Numerical Modelling Methodology

The numerical modelling presented in this chapter was also implemented using the commercial software Ansys Fluent 2020 R2 with finite volume method. The mathematical model, engineering model, and assumptions were the same as those presented in Chapter 3, considering the conjugate heat transfer between the ambient air and panel shell, along with panel shell and PCMs. The detailed governing equations are also the same as those presented in Chapter 3. In this chapter, instead of the full-scale modelling of the entire PCM ceiling panel array, the melting and solidification processes of one individual panel (i.e. 1.44 kg PCMs) was modelled to save the computational resources and time. The boundary conditions of the model are defined as follows.

For the ambient air, the boundaries of the air domain (i.e. walls) are set to be either isothermal or temperature-time dependent for different trials. For the modelling of melting:

$$T_{\text{discharge\_1}} = T_{\text{eqv\_discharge}}$$

(4.1)

for the case that the air domain boundaries are isothermal, and

$$T_{\text{discharge\_2}} = -1.52 \times 10^{-4} t^2 + 0.058t + 20.79$$

(4.2)

for the case that the air domain boundaries are temperature-time dependent, where t represents the melting time in the unit of 'minutes' counting from 1 and T represents the temperature in the unit of 'degree Celsius'. The Equation (4.2) was obtained by applying a quadratic fitting to a selected segment in Figure . The $T_{\text{eqv\_discharge}}$ was obtained by computing the bounded area between the curve of Equation (4.2) and the horizontal line $y = 20$ (i.e. the melting temperature of the PCMs), then divided by time, which can be considered as the equivalent temperature (isothermal) to the time-dependent temperature described in Equation (4.2).

For the modelling of solidification:

$$T_{\text{charge\_1}} = T_{\text{eqv\_charge}}$$

(4)

for the case that the air domain boundaries are isothermal, and

$$T_{\text{charge\_2}} = 1.2 \times 10^{-5} t^2 - 0.0082t + 15.42$$

(5)

for the case that the air domain boundaries are temperature-time dependent, where t represents the solidification time in the unit of 'minutes' counting from 1 and T represents the temperature in the unit of 'degree Celsius'. The Equation (4.4) was obtained by applying a quadratic fitting to a selected segment in Figure . The $T_{\text{eqv\_charge}}$ was obtained by computing the bounded area between the curve of Equation (4.4) and the horizontal line $y = 17$ (i.e. the freezing temperature of the PCMs), then divided by time, which can be considered as the equivalent temperature (isothermal) to the time-dependent temperature described in Equation (4.4). The schematics of the air domain boundary conditions for both melting and solidification are presented in Figure below:

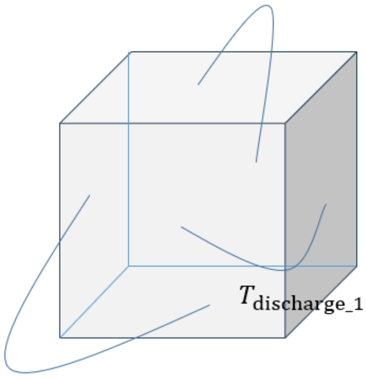
Melting – constant ambient temperature
$T_{\text{discharge\_1}} = T_{\text{eqv\_discharge}}$
$T_{\text{discharge\_1}} = T_{\text{eqv\_discharge}}$
$T_{\text{discharge\_1}} = T_{\text{eqv\_discharge}}$

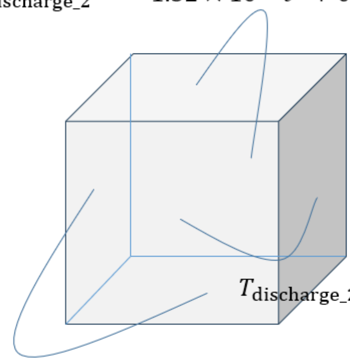
Melting – varying ambient temperature
$T_{\text{discharge\_2}} = -1.52 \times 10^{-4}t^2 + 0.058t + 20.79$
$T_{\text{discharge\_2}} = -1.52 \times 10^{-4}t^2 + 0.058t + 20.79$
$T_{\text{discharge\_2}} = -1.52 \times 10^{-4}t^2 + 0.058t + 20.79$

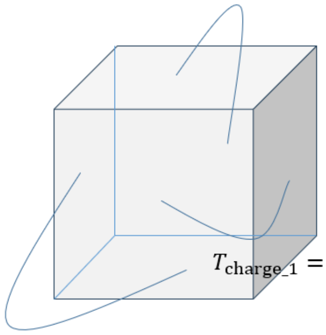
Solidification – constant ambient temperature
$T_{\text{charge\_1}} = T_{\text{eqv\_charge}}$
$T_{\text{charge\_1}} = T_{\text{eqv\_charge}}$
$T_{\text{charge\_1}} = T_{\text{eqv\_charge}}$

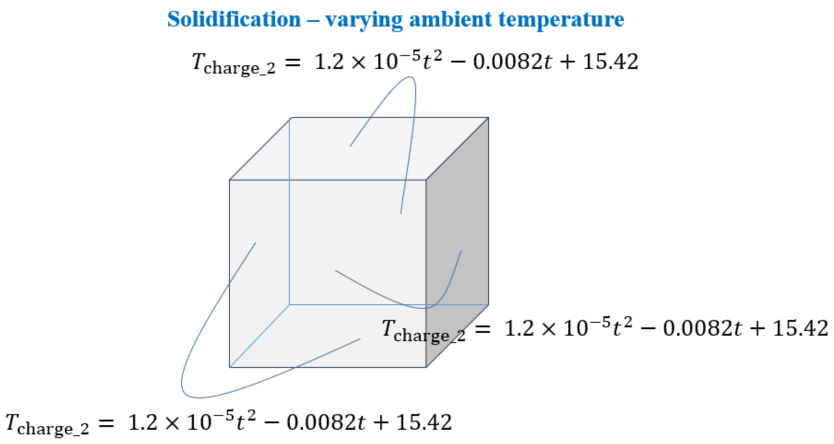

Figure 4.5 Schematics of air domain boundary conditions for the cases of melting and solidification under constant and varying ambient temperatures.

For the interface between PCMs and the panel shell:

$$\lambda_{\text{shell}} \nabla T_{\text{shell}} = \lambda_{\text{PCM}} \nabla T_{\text{PCM}} \tag{6}$$

where λ_{shell} and T_{shell} are the thermal conductivity and temperature of the panel shell, respectively, λ_{PCM} and T_{PCM} are the thermal conductivity and temperature of the PCMs, respectively.

The initial conditions are defined as follows.

For the ambient air, the initial conditions of the air domain (i.e. body) are defined in line with the boundary conditions. For the modelling of melting:

$$T = T_{\text{eqv\_discharge}}, u_i = 0, k = 0.3 \text{ m}^2\text{s}^{-2}, \varepsilon = 0.5 \text{ m}^2\text{s}^{-3} \tag{7}$$

for the case that the air domain boundaries are isothermal, and

$$T = T_{0\text{\_discharge}}, u_i = 0, k = 0.3 \text{ m}^2\text{s}^{-2}, \varepsilon = 0.5 \text{ m}^2\text{s}^{-3} \tag{8}$$

for the case that the air domain boundaries are temperature-time dependent, where $T_{0\text{\_discharge}}$ refers to the initial temperature of the air domain, which is set to 293 K.

For the modelling of solidification:

$$T = T_{\text{eqv\_charge}}, u_i = 0, k = 0.3 \text{ m}^2\text{s}^{-2}, \varepsilon = 0.5 \text{ m}^2\text{s}^{-3} \tag{9}$$

for the case that the air domain boundaries are isothermal, and

$$T = T_{0\_\mathrm{charge}}, u_i = 0, k = 0.3\ \mathrm{m^2 s^{-2}}, \varepsilon = 0.5\ \mathrm{m^2 s^{-3}} \tag{10}$$

for the case that the air domain boundaries are temperature-time dependent, where T_{0_charge} refers to the initial temperature of the air domain, which is set to 290 K.

For the PCMs:

$$T = T_{0,\mathrm{PCM}} \tag{11}$$

For the panel shell:

$$T = T_{0,\mathrm{shell}} \tag{12}$$

Here, $T_{0,\mathrm{PCM}}$ and $T_{0,\mathrm{shell}}$ refer to the initial temperatures of the PCMs and the panel shell. The initial temperatures for both the PCMs and the panel shell are set to 294 K for the case of solidification and 289 K for the case of melting.

4.3 CFD Modelling Results

The melting and solidification processes of one individual panel under both constant and varying ambient temperatures were simulated. The ambient temperature variations set in the CFD model were adopted from the measured indoor temperature variations, where the constant ambient temperature is equivalent to the varying temperatures over the same period of time. For the melting case, the equivalent constant ambient temperature was set to 24.42℃ and the initial temperature of the PCMs was set to 16℃, which is 1℃ lower than the solidus temperature of the PCMs. The melting processes over a total of 387 minutes were simulated. As shown in Figure , the PCM temperatures measured at apex, mid-point, and base measuring points under both varying and constant ambient temperatures are presented. The PCM temperature at the apex measuring points increased faster than that at the mid-point measuring point, then increased faster than that at the base measuring point. This was because the three measuring points encompass the vertical height of the panel, with the apex measuring point being closest to the ambient air and the base measuring point being closest to the ceiling surface (i.e. adiabatic). Therefore, the temperature rise at the three different measuring points was manifested with different speeds. Overall, the PCM temperature firstly rose from the initial temperature to the solidus temperature, which is the highest temperature that PCMs are maintained completely solid. This stage manifested the sensible heat of the solidus PCMs. After the PCMs reached the solidus temperature, the latent heat (i.e. phase change) stage was then triggered (at about 50 mins). As can be seen from Figure , the PCM temperature rose more slowly at the latent heat stage than the sensible heat stage and the phase change plateau was distinct. From Figure (left), the liquid fraction ended up to be 0.41–0.44 for both conditions. For the solidification case, the equivalent constant ambient temperature was set to 14.63℃ and the initial temperature of the PCMs was set to 21℃, which is 1℃ higher than the liquidus temperature of the PCMs. The solidification processes over a total of 769 minutes were simulated. As shown in Figure 4, the PCM temperatures measured at apex, mid-point, and base measuring points show the similar regularity as the melting case. The PCM temperature firstly dropped from the initial temperature to the liquidus temperature, which is the lowest temperature that PCMs are maintained completely liquid. This stage manifested the sensible heat of the liquidus PCMs, which was followed by the latent heat stage. From Figure (right), the liquid fraction ended up to be 0.49–0.51 for both conditions. In general, the comparisons of PCM temperature variations at apex, mid-point, and base measuring points and the liquid fraction variations for both melting and solidification cases reveal that the constant ambient temperatures set to the boundary condition for melting/solidification can be considered as a fair equivalence to the varying ambient temperatures for melting/solidification. The use of equivalent constant ambient temperature can save more than 50% of the computational time compared to the case with varying ambient temperatures.

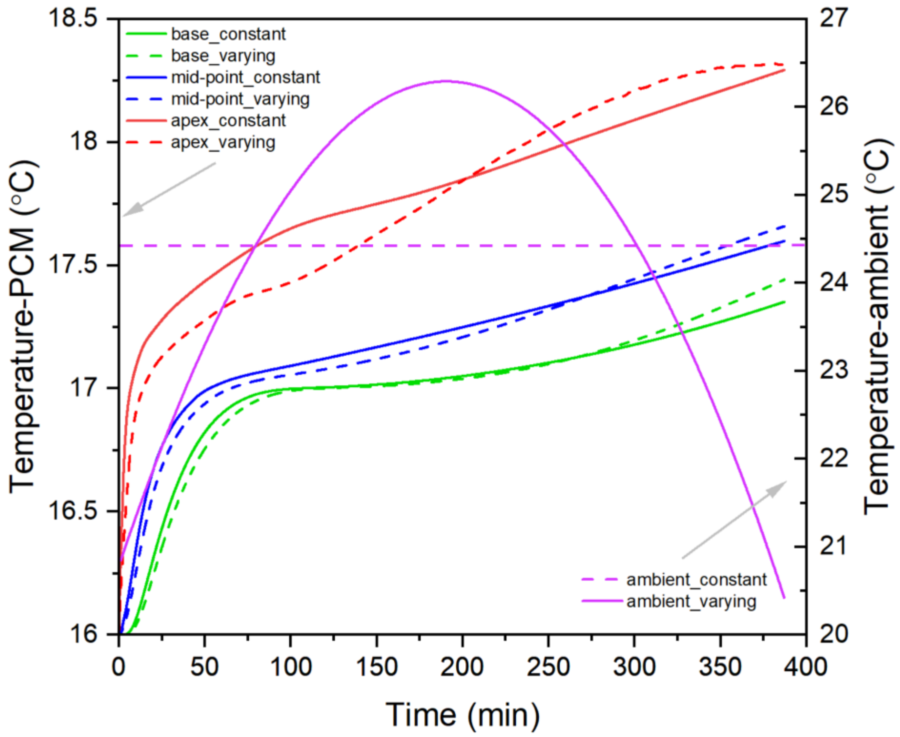

Figure 4.6 PCM temperature (left axis) and ambient air temperature (right axis) variations for the melting case.

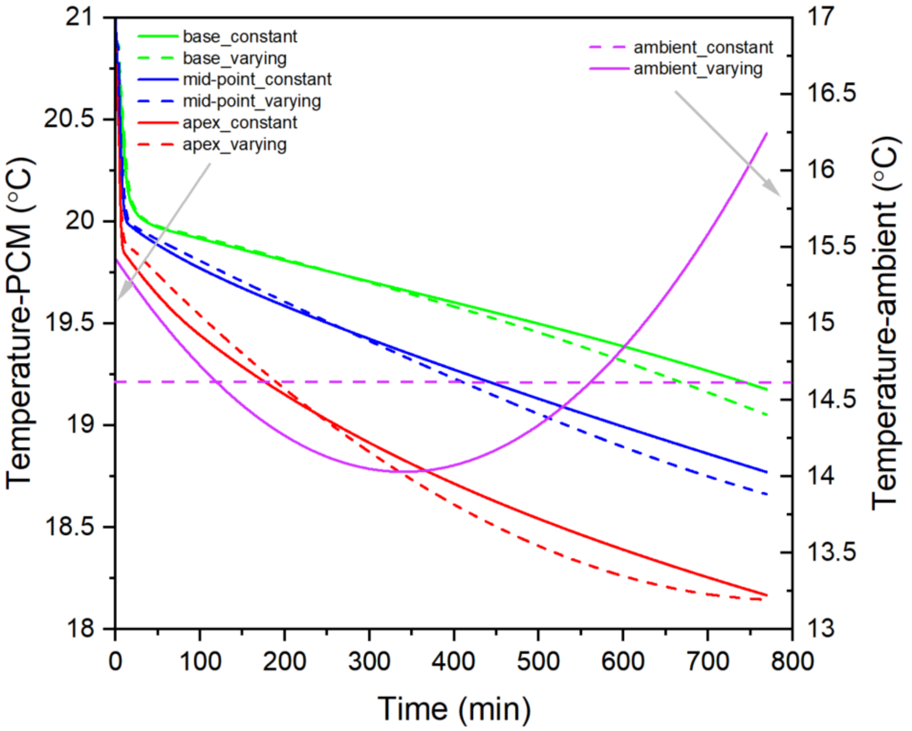

Figure 4.7 PCM temperature (left axis) and ambient air temperature (right axis) variations for the solidification case.

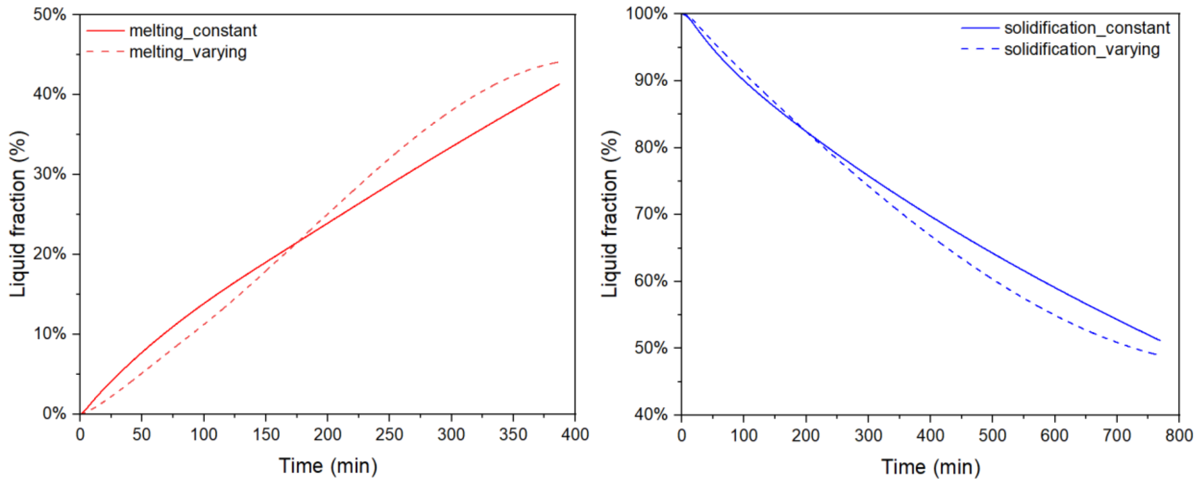

Figure 4.8 Liquid fraction variations for PCM melting (left) and solidification (right).

The temperature and velocity contours depicted at the symmetrical vertical planes in two pyramidal protrusions are presented in Figure and Figure for both constant and varying ambient temperatures. For the melting case, the contours are depicted at 120, 240, and 360 min. For the solidification case, the contours are depicted at 240, 480, 720 min. The time depiction for both melting and solidification cases encompasses the total simulated melting or solidification time (i.e. 387 minutes and 769 minutes). Based on the temperature and velocity contours, although the temperature and velocity distributions of the ambient air are very different for the constant and varying ambient temperatures, but those of the PCMs are very similar regardless of the ambient temperature condition. This again reveals that the phase change process of the PCMs can be rendered by the equivalent melting/solidification ambient temperatures properly. Notably, according to the velocity contours, in melting process of PCMs, there was a relatively strong time-dependent distinction on the air flow around the panel. However, there was no clear time-dependent distinction on the air flow around the panel for the solidification process of PCMs. This is because in the melting process, the air around the panel gets cooled down by the PCMs. The cold air is denser than the warmer air and therefore it sinks, which causes the temperature stratifications for the air around the panel. This phenomenon is further validated experimentally in section 4.4.

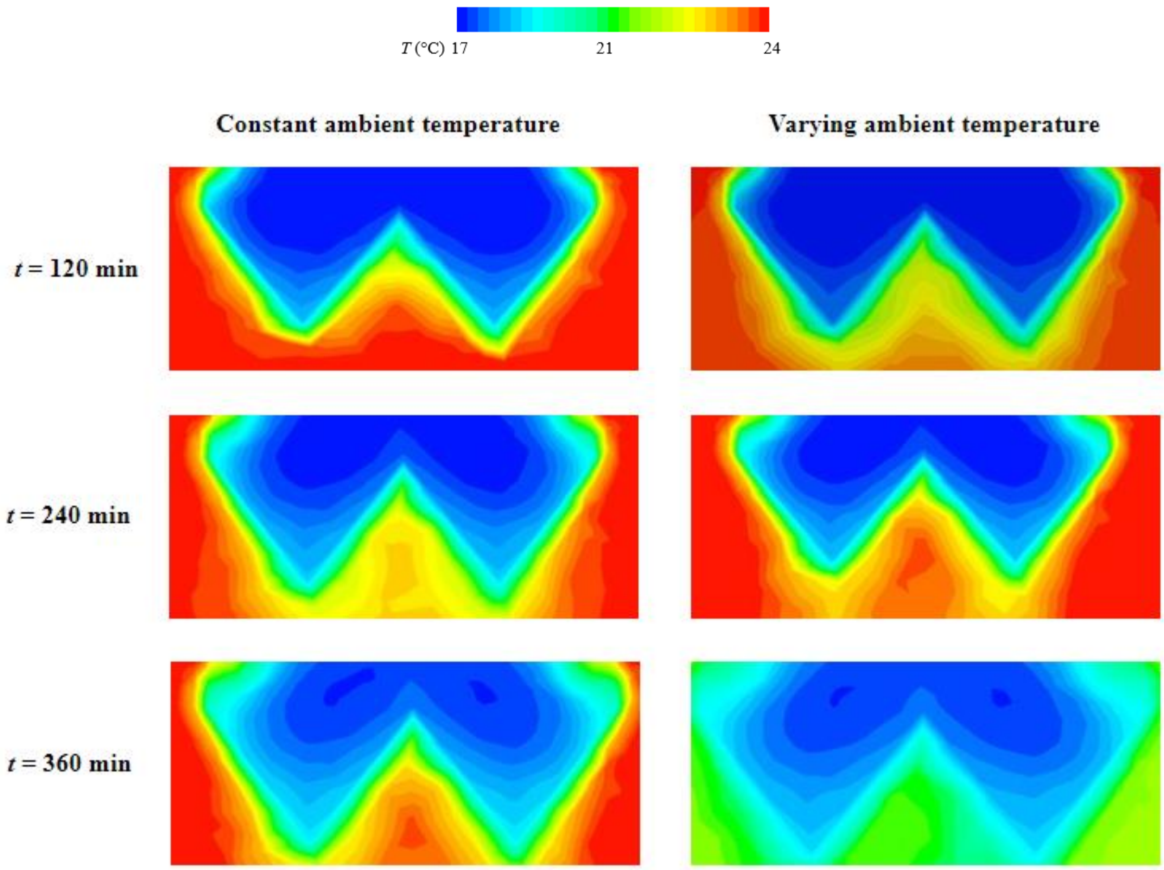

(a)

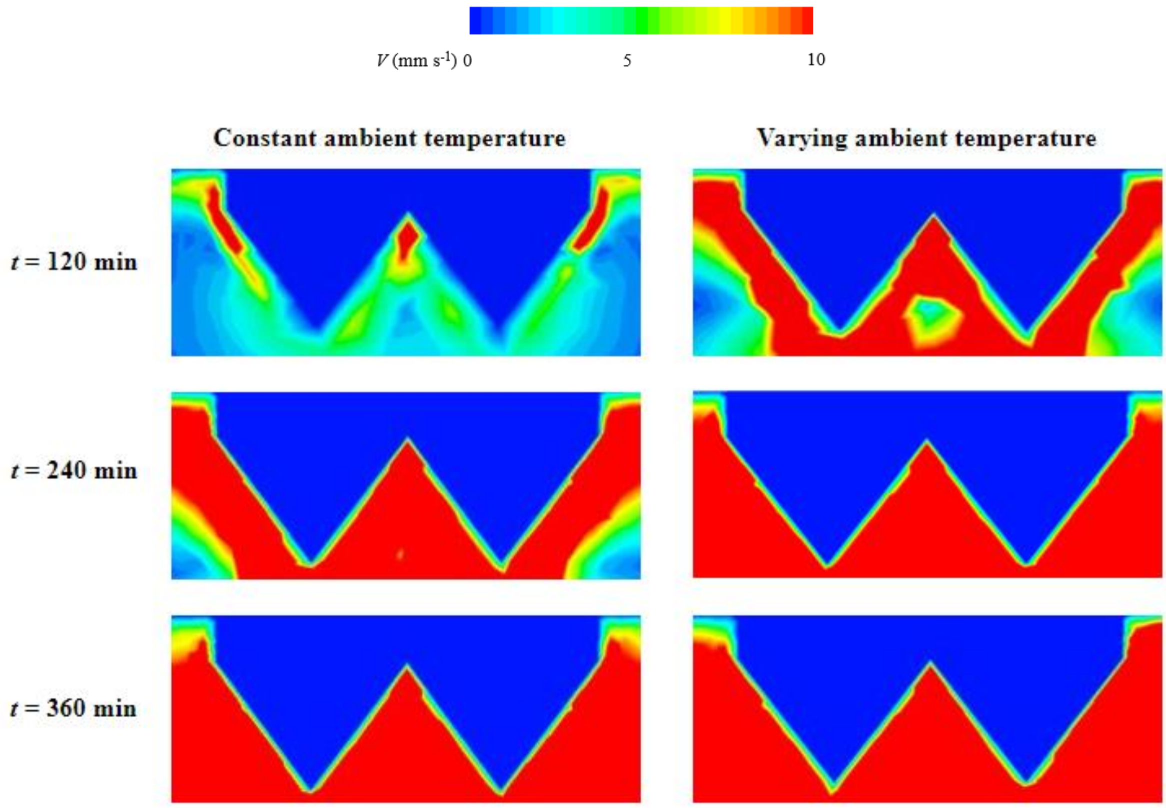

(b)

Figure 4.9 Temperature contours (a) and velocity contours (b) depicted during the melting of PCMs.

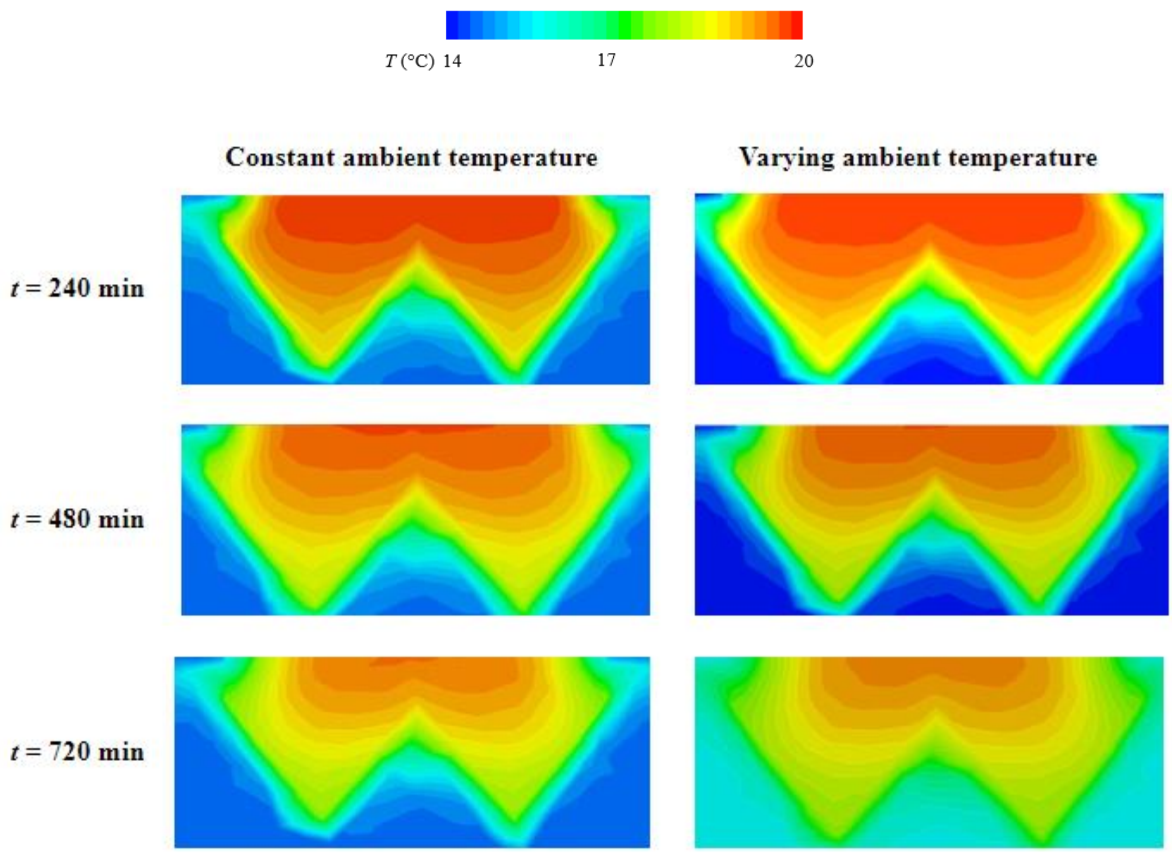
T (°C) 14
17
20
Constant ambient temperature
Varying ambient temperature
t = 240 min
t = 480 min
t = 720 min

(a)

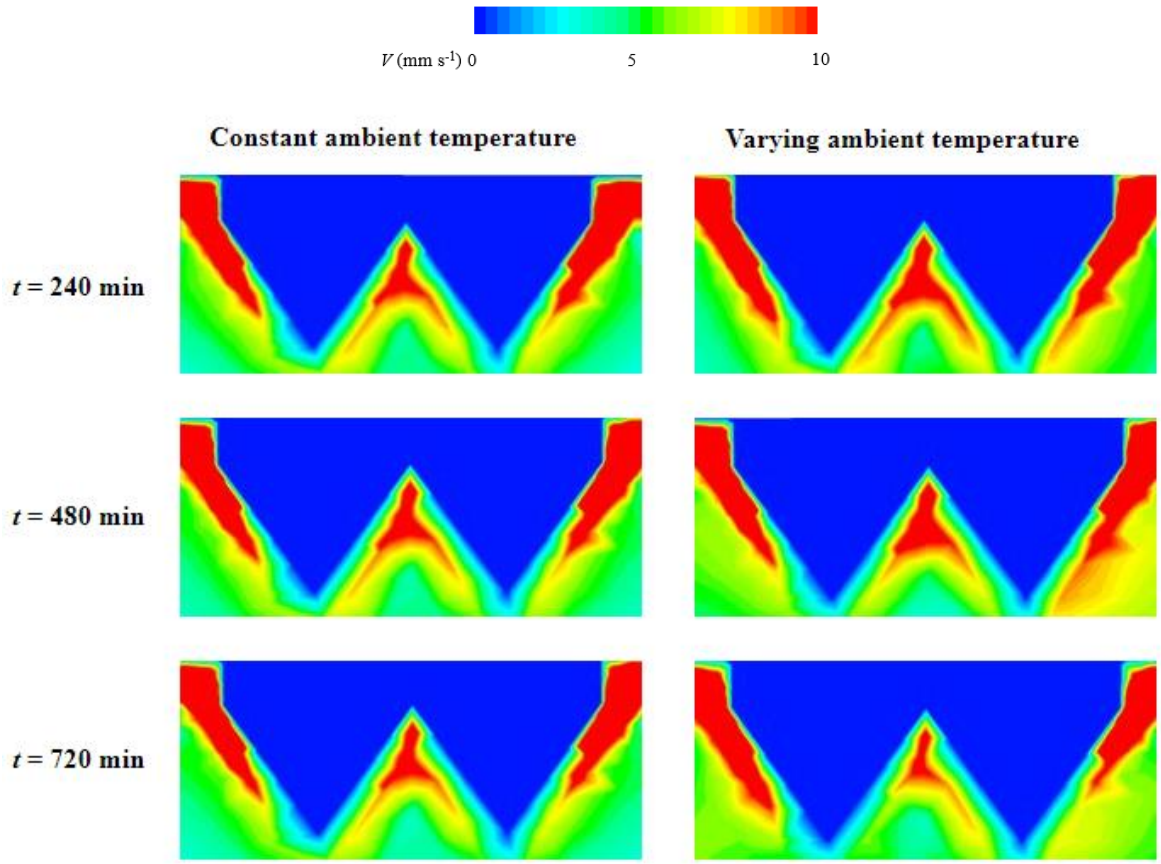

(b)

Figure 4.10 Temperature contours (a) and velocity contours (b) depicted during the solidification of PCMs.

4.4 Experimental Results

4.4.1 Heat Gain Analysis

To better understand the effects of solar irradiation on outdoor temperature variation, the solar irradiation and outdoor temperature variations over a day (i.e. from 18:00 to 18:00 next day) are plotted in Figure . As can be seen in Figure , the outdoor temperature started to rise from 7 am and reached the maximum in a day at 3:30 pm, then the temperature kept dropping as approaching the evening. Meanwhile, the solar irradiation started to rise from 7 am and reached the maximum in a day at noon. There was a 3.5-hour lag between the peak solar irradiation and the peak outdoor air temperature, which reveals the seasonal lag phenomenon [109].

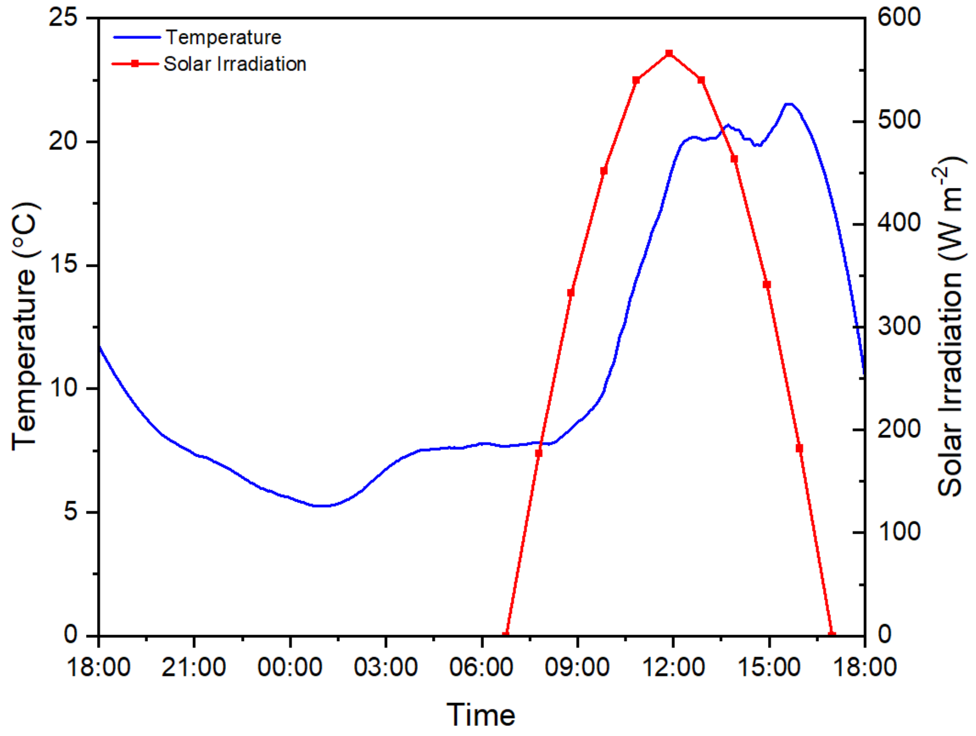

Figure 4.11 Solar irradiation and outdoor temperature variations over a full day.

The internal temperature variations of the three PCM panels equipped with thermocouples (i.e. PCM panel A, B, and C) over the same full day (i.e. from 18:00 to 18:00 next day) are plotted in Figure, along with the outdoor temperature and average indoor temperature over the same period of time. As shown in Figure, the internal temperature variations measured by nine thermocouples have the similar overall trend, but differ from each other slightly due to their different positioning within the PCM panels. TC-7, TC-8, and TC-9 were placed in panel A, corresponding to the base, mid-point, and apex measurement points, respectively. During the solidification stage (i.e. from 18:00 to 3:00 next day), the temperature of the PCM within panel A dropped fastest as panel A is placed at the corner of the shed and it has only two neighbour panels. Therefore, panel A is the most vulnerable panel to the outdoor low temperature. TC-4, TC-5, and TC-6 were placed in panel B, corresponding to the base, mid-point, and apex measurement points, respectively. The temperature of the PCM within panel B dropped slower than that within panel A during the solidification stage (i.e. from 18:00 to 3:00 next day) as panel B is positioned relatively far away from the corner of the shed, where the effect of the outdoor low temperature on the PCM solidification is less distinct. TC-1, TC-2, and TC-3 were placed in panel C, corresponding to the base, mid-point, and apex measurement points, respectively. The temperature of the PCM within panel C dropped the most slowly among the three panels during the solidification stage (i.e. from 18:00 to 3:00 next day) as panel C is positioned at the center of the shed. Hence, the effect of the outdoor low temperature on the PCM solidification of panel C is the least distinct. In addition, during the PCM solidification stage (i.e. from 18:00 to 3:00 next day), the average indoor temperature and outdoor temperature were always lower than the measured internal temperatures of PCMs. Conversely, during the PCM melting stage (i.e. from 9:00 to 16:00), the average indoor temperature and outdoor temperature were always higher than the measured internal temperatures of PCMs.

The internal temperature variations of PCM panel A, B, and C during this stage are magnified in the zoomed-in part of Figure. The very short phase change plateau, as can be seen from the zoomed-in part, indicates that the stored cooling capacity during the nighttime was not well released during the daytime as the heating period was not long enough. This indicates unbalanced thermal charging and discharging of PCM ceiling panels, which is inevitable during PCM passive cooling operations. Although the stored nighttime coolness was not fully discharged during the daytime, by comparing the indoor and outdoor temperature curves in both Figure and Figure, it can be seen that there was a delay between the peak indoor temperature and the peak outdoor temperature with the PCM ceiling, while the indoor temperature increased almost synchronously with the outdoor temperature without PCM due to the fact that the metal shed has almost negligible thermal mass. After the PCM ceiling panel was installed, the latent heat of PCMs effectively impeded the temperature rise of the indoor air, which manifested the improved overall thermal inertia of the system. Furthermore, during the latent heat stage, the temperature of the PCM was increasing within a temperature band rather than isothermally. This is because the developed PCMs are amorphous in the solid phase with nonexistence of the definitive lattice pattern [95].

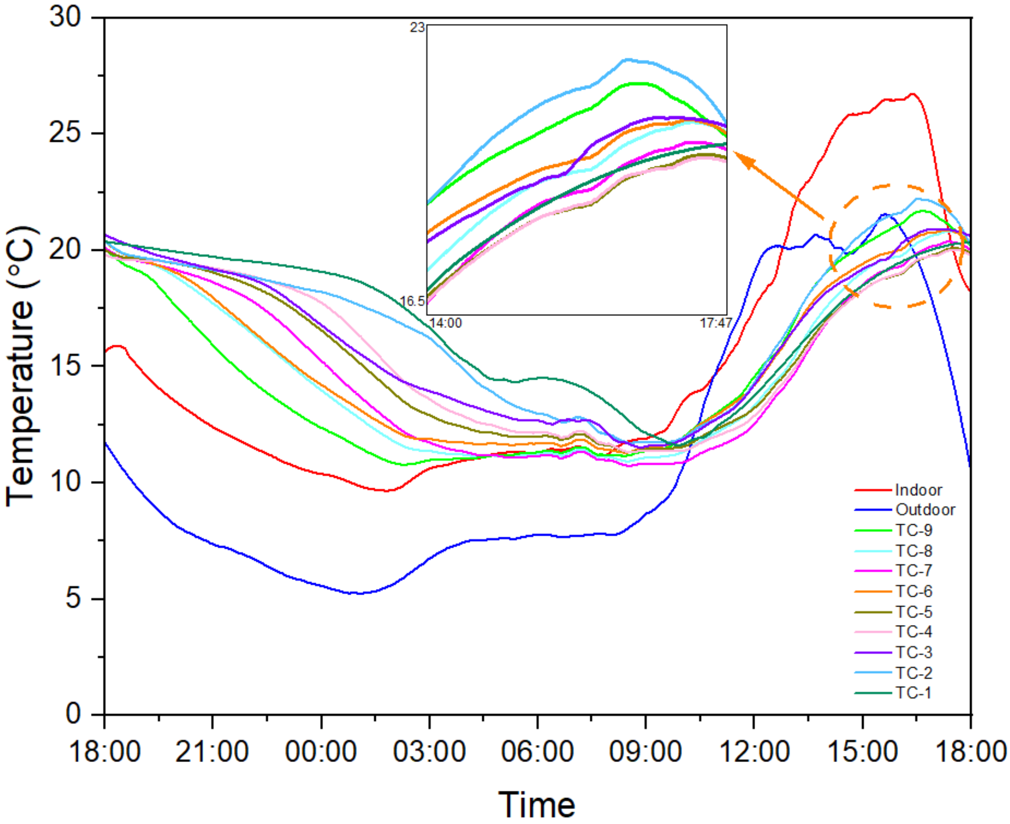

Figure 4.12 Internal PCM, indoor, and outdoor temperature variations.

4.4.2 Cooling Effect of the PCM Ceiling Panels

The average indoor and outdoor temperatures of two similar days are compared before and after the installation of PCM ceiling panels. The daily average temperatures, diurnal average temperatures, and nocturnal average temperatures are considered. The daily average indoor-outdoor temperature difference means the average of indoor-outdoor temperature difference over 24 hours; the diurnal average indoor-outdoor temperature difference means the average indoor-outdoor temperature difference over the daytime (6 am to 6 pm); the nocturnal average indoor-outdoor temperature difference means the average indoor-outdoor temperature difference over the nighttime (6 pm to 6 am next day). As shown in Figure, the daily average indoor-outdoor temperature difference was 4.3℃ without PCM while 0.5℃ with PCM. The reduction of daily average indoor-outdoor temperature difference was 88.4%. The diurnal average indoor-outdoor temperature difference was 4.8℃ and 3.5℃ without and with PCM, respectively. The reduction of diurnal average indoor-outdoor temperature difference was 27.1%. The nocturnal average indoor-outdoor temperature difference was 3.8℃ and 0.3℃ without and with PCM, respectively. The reduction of nocturnal average indoor-outdoor temperature difference was 92.1%. The results reveal that the PCM ceiling panel can effectively reduce the daily, diurnal, and nocturnal average indoor-outdoor temperature difference (i.e. lower indoor temperature), which shaves the peak temperatures within the metal storage enclosure. The higher reduction of nocturnal average indoor-outdoor temperature difference than diurnal difference again elucidates the unbalanced charging and discharging of the PCM ceiling panels.

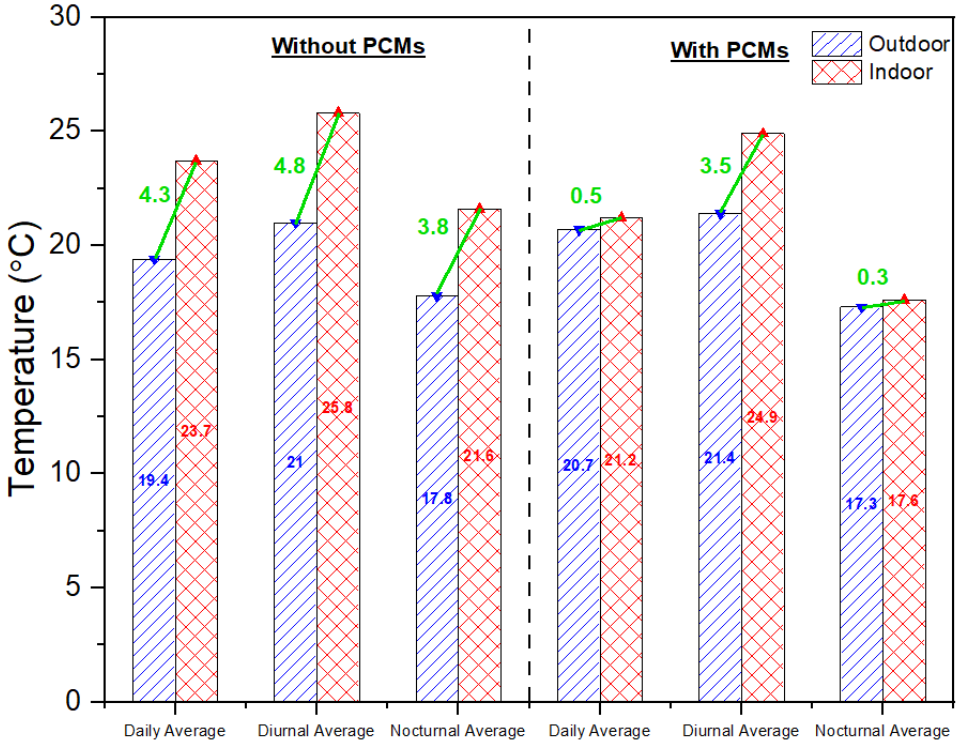

Figure 4.13 Daily, diurnal, and nocturnal average indoor-outdoor temperature difference without and with PCM ceiling panels of two similar days.

To further illustrate the effects of outdoor temperature on the PCM ceiling performance, the average daily indoor-outdoor temperature difference before and after the installation of PCM ceiling panels is plotted against different average daily outdoor temperatures. As can be seen from Figure, without PCM the average daily indoor-outdoor temperature difference (i.e.

$T_{indoor\_avg} - T_{outdoor\_avg}$) was in the range of 4.0–5.1°C. It increased with the rise of the outdoor temperature, indicating a higher indoor temperature increasing rate at a higher outdoor air temperature. This is because a higher average outdoor temperature in general leads to lower the indoor-outdoor heat exchange without PCMs thus the heat is accumulated inside the enclosure, enlarging the indoor temperature. However, at the same time the resulted higher indoor-outdoor temperature difference will improve heat transfer to some extent from the indoor air to the ambient, and therefore the overall result was a slight increase of the temperature difference with the outdoor temperature rise. From Figure 4, with PCM the average daily indoor-outdoor temperature difference, in contrast, decreased with the increased outdoor temperature with a range of -6–4.4°C. It reveals that the PCM ceiling panels provide decent indoor temperature controlling to the metal storage enclosure, and the PCM cooling performance is better at higher outdoor temperatures as the discharge of cooling (melting) is more effective. Moreover, notably, without PCM, the average daily indoor-outdoor temperature difference was always positive, which means the indoor temperature was always higher than the outdoor temperature (as shown in Figure). However, with PCM panels, the average daily indoor-outdoor temperature difference can be sometime negative, which indicates that the indoor temperature was lower than the outdoor temperature in some periods, indicating better indoor temperature reduction. In addition, the average daily indoor-outdoor temperature difference against total daily solar irradiation is also plotted in Figure. Therefore, PCM ceiling panels are effective complements of thermal mass to the metal storage enclosure, which moderate the temperature sensitivity of its indoor ambient to external conditions.

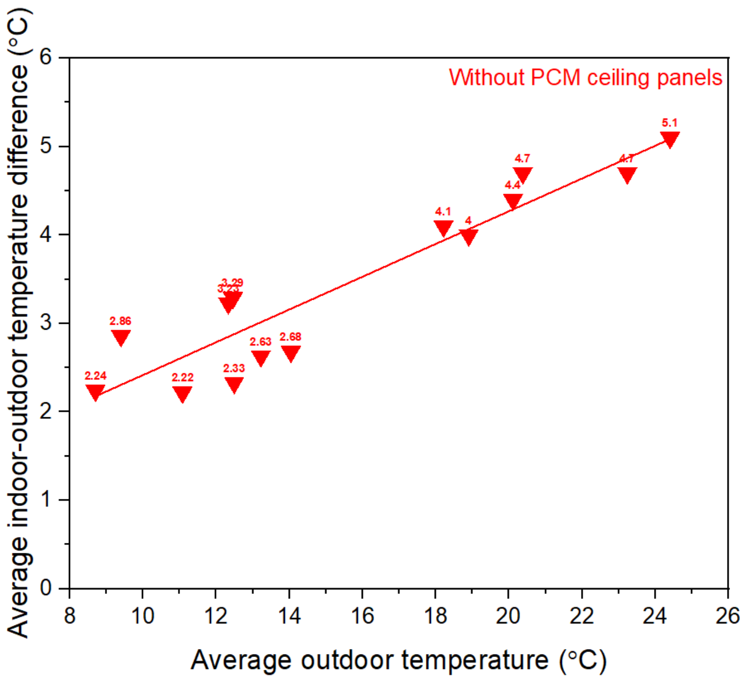

Figure 4.14 Average daily indoor-outdoor temperature difference against average daily outdoor temperature without PCM ceiling panels.

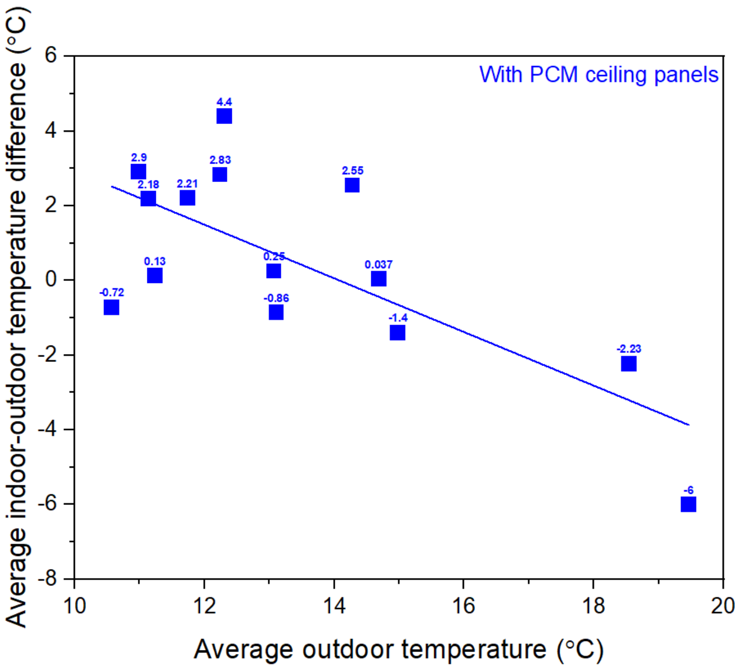

Figure 4.15 Average daily indoor-outdoor temperature difference against average daily outdoor temperature with PCM ceiling panels.

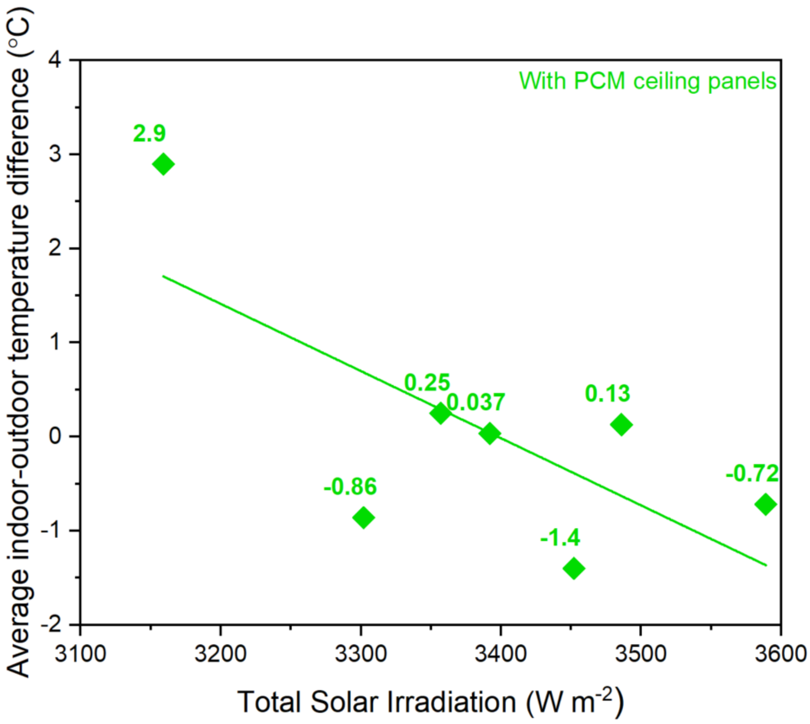

Figure 4.16 Average daily indoor-outdoor temperature difference against total daily solar irradiation with PCM ceiling panels.

4.4.3 Temperature Distribution in Vertical Direction

The indoor temperature variations over the same full day as Figure measured at three different vertical positions in the shed (i.e. high, mid, and low) by TC-A, TC-B, and TC-C are plotted in Figure , along with the outdoor temperature variation over the same period of time. As can be seen from Figure , over the same period of time, the indoor temperatures were higher than the outdoor temperature except for between 11:00 and 12:30. During this 1.5 hours, the PCM was melting, which lower the indoor temperature and brought the cooling effect. The lower-indoor-temperature periods only happened in cases with PCM, in contrast to Figure without PCM. The three vertical positions were 'high, TC-A, 1.35 m', 'mid, TC-B, 0.9 m', and 'low, TC-C, 0.45 m', respectively. During the entire course of time period shown in Figure , the temperature variation curves of the 'high, TC-A, 1.35 m' almost coincided with that of the 'mid, TC-B, 0.9 m', while the temperature measurements of the 'low, TC-C, 0.45 m' were 10.67% lower than that of 'mid, TC-B, 0.9 m' on average and 9.91% lower than 'high, TC-A, 1.35 m' on average. It reveals that thermal expansion causes a temperature gradient distribution in the vertical direction in the shed in both freezing and melting. It also shows that warmer-air area has better homogeneity than the colder-air area in the vertical direction. To further illustrate the temperature homogeneity in the vertical areas, the relative discrepancy at 'low, TC-C, 0.45 m' was found and compared to that of 'high, TC-A, 1.35 m' over a total of nine days. The relative discrepancy is defined as following:

$$\mathrm{RD}_{\mathrm{avg-low}} = \frac{\sum_{i=0}^{N} \frac{\left|T_{\mathrm{low}} - T_{\mathrm{avg}}\right|}{T_{\mathrm{avg}}} \times 100\%}{N} \tag{13}$$

$$\mathrm{RD}_{\mathrm{avg-high}} = \frac{\sum_{i=0}^{N} \frac{\left|T_{\mathrm{high}} - T_{\mathrm{avg}}\right|}{T_{\mathrm{avg}}} \times 100\%}{N} \tag{14}$$

where $\mathrm{RD}_{\mathrm{avg-low}}$ refers to the relative discrepancy between the average indoor temperature and indoor-low temperature; $\mathrm{RD}_{\mathrm{avg-high}}$ refers to the relative discrepancy between the average indoor temperature and indoor-high temperature; T_{low} refers to the indoor-low temperature; T_{high} refers to the indoor-high temperature; T_{avg} refers to the average indoor temperature; N represents the total amount of data pairs that compared.

As can be seen from Figure 3, over the nine days, the relative discrepancy at 'high, TC-A, 1.35 m' was between 2%–6%, with Day 3 (counting from leftmost) being an exception of 8.1%. The average relative discrepancy at 'high, TC-A, 1.35 m' was 4.17%. However, the relative discrepancy at 'low, TC-C, 0.45 m' was always higher than 6%, with Day 3 (counting from leftmost) being an extremum of 15.92%. The average relative discrepancy at 'low, TC-C, 0.45 m' is 8.72%, which was more than twice that of 'high, TC-A, 1.35 m'. This again confirms the poorer homogeneity at the vertical colder air section, as being away from the PCMs panels. The relative discrepancies were in general lower and more stable at higher-solar-irradiation days despite the outdoor temperature. It, however, requires more data in various weather to evidence the correlation between temperature homogeneity and solar irradiation.

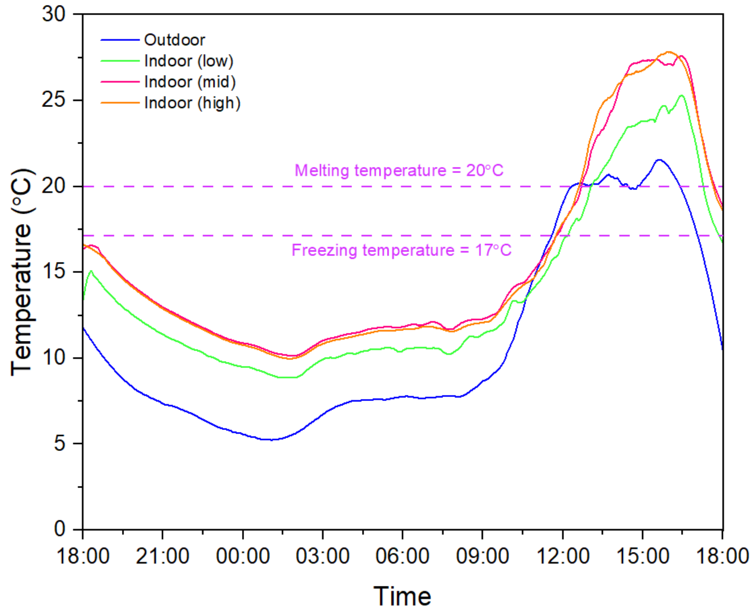

Figure 4.17 Indoor temperature variations measured at three vertical points and outdoor temperature variations.

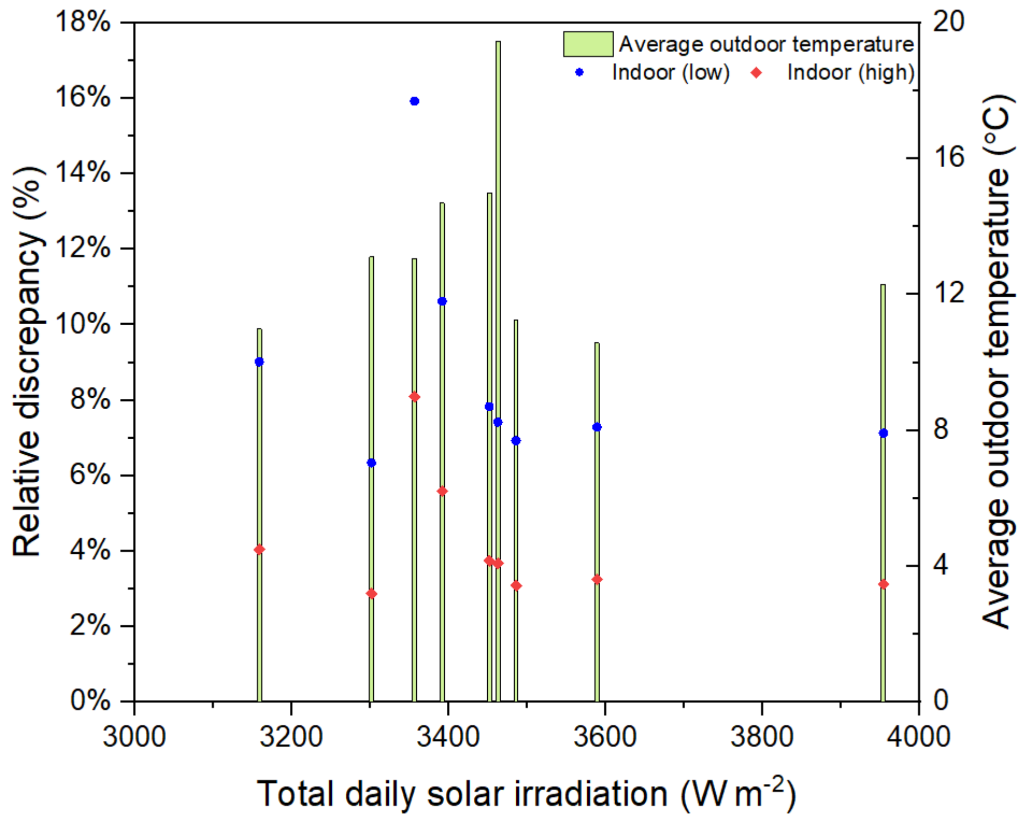

Figure 3.18 Relative discrepancy at indoor (low), indoor (high) positions and average outdoor temperature against total daily solar irradiation over nine days.

4.5 Chapter Conclusion

In this chapter, the experimental study on PCM ceiling panels for the indoor thermal management of an outdoor storage enclosure (i.e. a metal shed) with poor thermal mass was conducted. The solar irradiation was the main heat gain to the shed, and the conjugate heat transfer comprised of natural convection and heat conduction was considered for the PCM ceiling panels. The capability of PCM ceiling panels for indoor cooling was thoroughly investigated. In addition, the melting and solidification processes of one individual panel were simulated under both constant and varying ambient temperatures, with the constant ambient temperature being the equivalent of the varying ambient temperature. The main results and findings of this paper are concluded as below:

1) During the solidification process, the internal temperature of PCMs was always higher than the indoor and outdoor temperature. During the melting process, the internal temperature of PCMs was always lower than the indoor and outdoor temperature.
2) Under the similar daily weather, the PCM ceiling panels can smoothen the indoor temperature fluctuation by reducing the daily, diurnal, and nocturnal average indoor-outdoor temperature difference by 88.4%, 27.1%, and 92.1%, respectively.
3) Before the installation of PCM ceiling panels, the indoor temperature was always higher than the outdoor temperature. With the PCM ceiling panels, indoor temperature can sometimes be lower than the outdoor temperature, and the indoor-outdoor temperature difference was generally reduced.
4) There is a clear vertical temperature gradient due to the sinking of colder air from the PCM ceiling panels. The warmer-air section manifests better vertical homogeneity, which is consistent in both experimental and numerical results.
5) For the numerical modelling of PCM ceiling panels, using the equivalent constant ambient temperature as the boundary conditions is an appropriate substitution of the varying ambient temperature. This can save more than 50% of the computational time.

These results complement the current body of knowledge about PCM-based ceiling panels for passive building indoor cooling. This study is also a pioneer in the investigation of PCM ceiling panels in non-residential/commercial buildings. It proved that PCM ceiling panels are promising in this context. Some recommended future work includes the sealing improvement of macro-encapsulated PCM ceiling panels to avoid material leakage and facilitating more balanced charging and discharging of PCM ceiling panels.

Chapter 5 – Conclusion and Future Work

In conclusion, this study consolidated the optimisation of geometric configurations of PCM ceiling panels using CFD numerical modelling, where a CFD model was developed and validated using Ansys Fluent software bundle. The key novelty of this study is the exploration of thermal performance of PCM ceiling panels with the optimised geometric configuration under a special type of building envelope (i.e. metal shed) with negligible thermal mass, and this is the very first study focusing on this scope. The logic flow of the whole thesis is summarised in the paragraphs below.

The emerging lightweight-design buildings are advantageous than the conventional heavyweight-design buildings from the perspective of construction. However, for lightweight-design buildings, the lack of thermal mass is detrimental and the indoor temperature can be sensitive to the outdoor temperature swing. The indoor temperature fluctuation is not beneficial to the thermal comfort of the building occupants. Using HVAC system to achieve thermal comfort can be energy intensive, so more environmentally-friendly approaches are a must.

Thermal energy storage (TES) is a promising and common approach for building passive cooling. It can provide additional thermal mass to the existing building envelope, which can enhance the thermal inertia of the building envelope. As such, the building envelope can function as a thermal buffer to reduce the penetration of the heat from the exterior to the interior. In this case, the indoor temperature fluctuation can be dampened and the thermal comfort of the building occupants can be assured.

Phase change materials (PCMs) play a crucial role in TES, as PCMs can exchange a large amount of latent heat during the phase transition process within a small temperature band or isothermally. The natural temperature swing can be deployed to trigger the phase transition of the PCMs, which is in line with the charging and discharging process of a cooling system. The thermophysical properties of PCMs make it promising to be a great TES medium.

The selection of PCM is vital and should be dependent on the specific application. Properties such as phase change temperature, thermal conductivity, latent heat of fusion, and corrosivity need to be considered to ensure the optimal thermal performance can be achieved. The mixture of capric and lauric acids is suitable for the applications in buildings as the phase change temperature can be tweaked by introducing different additives, and the available phase change temperature range is in line with the purpose of free cooling. Furthermore, the mixture of capric and lauric acids are non-toxic and non-corrosive, which is beneficial from the perspective of safety.

In this work, we investigated the PCM-based ceiling panels for building indoor passive cooling. A computational fluid dynamics (CFD) model was developed and validated with on-site experiment to simulate the discharging (i.e. melting) process of the panel. In addition, the effects of geometric configurations on the thermal performance of the panel are further studied using the CFD model. The analysis of the different geometric configurations can inform the design consideration when it comes to the real-world implementations.

To further investigate the cooling efficacy of multiple PCM ceiling panels (i.e. PCM ceiling panel array), an on-site experiment was carried out in an outdoor storage enclosure (i.e. a metal shed) with negligible/poor thermal mass, with solar irradiation being the major source of heat gain. The cooling efficacy of the PCM ceiling panels was assessed by using the metrics such as average daily indoor-outdoor temperature difference and indoor vertical temperature distribution. It was concluded that PCM ceiling panels can provide decent indoor temperature regulation capability, which are feasible to be implemented in real-world applications.

This thesis provides a thorough investigation on PCM-based ceiling panels for indoor passive cooling, considering the conjugate heat transfer between the ambient air and panel shell, then panel shell and PCMs. The experiment program conducted in the outdoor storage enclosure was also a pioneering study on the building envelope with negligible thermal mass.

5.1 Main Findings

The main findings of the thesis are summarised below:

- When the panel external volume is 250 mL, the average melting rate of the pyramidal panel is 20.75% higher than that of the tetrahedral panel. Although the tetrahedral panel has a 21.6% larger effective heat transfer area than the pyramidal panel, the resultant lower average melting rate is because its thicker base (0.67 cm thicker than the pyramidal panel). From the numerical modelling results, the panel protrusion has a thinner thermal boundary layer than the panel base, which yields a stronger heat transfer through the protrusions rather than the base. The average melting rate uniformed against the effective heat transfer area of the pyramidal panel is 46.8% higher than that of the tetrahedral panel.
- The melting time for reaching both 80% and 100% of the liquid fraction decreases as the initial temperature difference between the PCMs and air increases. For the same panel, the difference in the melting time for reaching 80% and 100% of the liquid fraction also decreases as the initial temperature difference increases. When the initial temperature difference is large enough, the melting time will be less affected by the geometric features.
- For the same type of shell material, a thicker panel shell slightly worsens the heat transfer and results in slightly longer melting times. The difference in the average heat transfer rate between the pyramidal and tetrahedral panels decreases as the shell thickness increases. Therefore, a thick shell will reduce the effect of geometric features on the thermal performance, and therefore it might not be desirable.
- Adding a distance between the base of the panel and the ceiling surface can significantly reduce the melting time. However, For the distances larger than 5 cm, the effects on the melting will be marginal. From the perspective of real-world implementation, a high-ceiling room may be necessary if the panels are suspended from the ceiling.
- The increase of the PCM proportion in the panel protrusions will facilitate the heat transfer between the ambient air and the PCM panel. The larger contact surface area between the protrusions and air is the key for the enhanced heat transfer. However, a higher protrusion-to-base ratio also means a sharper tip for the panel, which might bring safety issues.

- Adding a gap between the protrusions can increase the heat transfer area as well. However, a thin gap (3–5 mm) between the protrusions would not facilitate the PCM melting significantly. It is speculated that the melting time would significantly reduce if the gap width is relatively large with respective to the overall panel dimension.
- The increase of the panel volume will result in a substantial decrease of the normalised melting rate, which is detrimental to the discharging process of the panel. It would be necessary to distribute the PCMs into multiple small panels instead of encapsulating them within one single large panel.

From the simulations, the geometric configuration of the macro-encapsulated PCM ceiling panels plays a pivotal role to the thermal performance, because the geometry of the panels will impact the thermal boundary layers and therefore the discharging process. In practical implementation, the selection of panel geometry should be carefully considered, and the main findings in Chapter 3 can be used as a reference.

- For the on-site experiment carried out in the outdoor storage enclosure, during the solidification process, the internal temperature of PCMs was always higher than the indoor and outdoor temperature. During the melting process, the internal temperature of PCMs was always lower than the indoor and outdoor temperature.
- The cooling efficacy of PCM ceiling panels can be evident by several experimental results: Under the similar daily weather, the PCM ceiling panels can smoothen the indoor temperature fluctuation by reducing the daily, diurnal, and nocturnal average indoor-outdoor temperature difference by 88.4%, 27.1%, and 92.1%, respectively. Before the installation of PCM ceiling panels, the indoor temperature was always higher than the outdoor temperature. With the PCM ceiling panels, indoor temperature can sometimes be lower than the outdoor temperature, and the indoor-outdoor temperature difference was generally reduced.
- There is a clear temperature gradient/stratification in the vertical direction within the shed due to the density differential between warmer and colder air. That is, the colder air sinks from the ceiling to the floor while the warmer air rises from the floor to the ceiling. The upper section of the shed with warmer air manifests better vertical temperature homogeneity, which is consistent in both experimental and numerical results. This phenomenon is also beneficial for the nature of PCM ceiling panels for indoor cooling, as the building occupants stay on the floor, which is in line with the incoming direction of the cold air.

Through the experiment, it is evident that the PCM ceiling panel array can provide adequate cooling efficacy to the outdoor storage enclosure with low thermal mass. The cooling efficacy was measured by the parameters such as average indoor-outdoor temperature difference and the temperature distribution in the vertical direction within the shed. Overall, the cooling efficacy provided by the PCM ceiling panel array can be deemed as considerable based on the analysis.

5.2 Future Work

The numerical modelling of the single PCM ceiling panel is time-consuming and also requires a lot of computational resources. Therefore, it would be vital to develop a computational strategy to model the full-scale condition (i.e. PCM ceiling panel array) which is less demanding on the time and resources.

In the studied case, the charging and discharging of the PCM ceiling panels relied solely on the natural temperature swing. This would easily result in an unbalanced charging and discharging for the ceiling panels. If the full discharging cannot be achieved, then the cooling effect will be impacted. Thus, a more controlled charging and discharging behaviour would be desirable, so that the effects of weather can be mitigated.

For the macro-encapsulation of PCMs in the presented study, 3D printing using polymer plastic was employed as the technique to produce the panel. However, the leakage might occur if the panels are mounted on the ceiling for a certain period of time due to the material degradation or mechanical impact. Hence, a more sealed encapsulation approach would be a must for real-world implementation of the PCM ceiling panels.

Usually, the low thermal conductivity of PCMs (especially organic PCMs) and the panel shell material would also hinder the thermal performance of the PCM ceiling panels. Thus, increasing the thermal conductivity of the PCMs and panel shell material could also be a direction of future work, where miscellaneous approaches of heat transfer enhancement can be investigated and explored.

5.3 Epilogue

The passive building thermal management strategies have been researched for several decades. They are effective countermeasures to the environmental issues raised by the over utilisation of the active HAVC systems. PCMs have a broad application in passive building cooling when being incorporated into various building envelopes. The latent heat of fusion of PCMs during the phase change process can yield decent storage of thermal energy, which can be in line with the charging and discharging of the cooling system. As such, PCMs are recognised as outstanding complements to the thermal mass of the building envelope, which result in a better thermal inertia. We have confidence that the work presented in this thesis contributes significantly to this field of research.

Bibliography

[1] "237218984-Morfologia-Vegetal-Goncalves-E-G-Lorenzi-2007-pdf .pdf," Energy US., 2017. [Online]. Available: www.eia.gov/forecasts/ieo/pdf/0484(2016).pdf .

[2] "IEA Online Data Services," [Online]. Available: http://data.iea.org/ieastore/statslisting. asp .

[3] "ENERGY SAVER," [Online]. Available: https://www.energy.gov/energysaver/air-conditioning. [Accessed 28 January 2022].

[4] A. Diaz, "Australia's air conditioning usage statistics 2022," Finder, 19 January 2023. [Online]. Available: https://www.finder.com.au/energy/aircon-statistics#:~:text=South%20Australians%20are%20the%20most,down%20from%2060%25%20in%202020..

[5] "4 Negative Environmental Impacts Of Air Conditioners," EcoMENA, 13 October 2021. [Online]. Available: https://www.ecomena.org/air-conditioning-negative-impacts-on-environment/.

[6] N. Artmann, H. Manz and P. Heiselberg, "Climatic potential for passive cooling of buildingsby night-time ventilation in Europe," *Applied Energy* , no. 84, pp. 187-201, 2007.

[7] D. Zhou, C. Zhao and Y. Tian, "Review on thermal energy storage with phase change materials (PCMs) in building applications," *Applied Energy* , no. 92, pp. 593-605, 2012.

[8] Y. Fan, Y. Zhao, J. F. Torres, F. Xu, C. Lei, Y. Li and J. Carmeliet, "Natural convection over vertical and horizontal heated flat surfaces: A review of recent progress focusing on underpinnings and implications for heat transfer and environmental applications," *Physics of Fluids,* no. 33, p. 101301, 2021.

[9] M. Rida and S. Hoffmann, "The influence of macro-encapsulated PCM panel's geometry on heat transfer in a ceiling application," *ADVANCES IN BUILDING ENERGY RESEARCH,* 2021.

[10] Y. Zhang, K. Lin, Q. Zhang and H. Di, "Ideal thermophysical properties for free-cooling (or heating) buildings with constant thermal physical propertymaterial," *Energy and Buildings,* no. 38, pp. 1164-1170, 2006.

[11] N. Soares, J. Costa, A. Gaspar and P. Santos, "Review of passive PCM latent heat thermal energy storage systems towards buildings' energy efficiency," *Energy and Buildings,* no. 59, pp. 82-103, 2013.

[12] "ALTERNATE CONSTRUCTION SYSTEMS," HIAGreenSmart, March 2013. [Online]. Available: https://www.abis.com.au/wp-content/uploads/2013/03/alternateconstructionsystems002.pdf. [Accessed 24 January 2022].

[13] "2016 Concrete Manual MCS," [Online]. Available: https://www.virginiadot.org/VDOT/Business/asset_upload_file578_118183.pdf. [Accessed 31 January 2022].

[14] I. Asadi, P. Shafigh, Z. F. B. A. Hassan and N. B. Mahyuddin, “Thermal conductivity of concrete – A review,” *Journal of Building Engineering,* no. 20, pp. 81-93, 2018.

[15] “Thermal mass,” greenspec, [Online]. Available: https://www.greenspec.co.uk/building-design/thermal-mass/. [Accessed 31 January 2022].

[16] P. Hoes, M. Trcka, J. Hensen and B. Bonnema, “Investigating the potential of a novel low-energy house concept with hybrid adaptable thermal storage,” *Energy Conversion and Management,* no. 52(6), pp. 2442-2447, 2011.

[17] A. Alnuaimi, S. Natarajan and T. Kershaw, “The comfort and energy impact of overcooled buildings in warm climates,” *Energy & Buildings,* no. 260, p. 111938, 2022.

[18] D. K. Bhamare, M. K. Rathod and J. Banerjee, “Passive cooling techniques for building and their applicability in different climatic zones—The state of art,” *Energy & Buildings,* no. 198, pp. 467-490, 2019.

[19] X. Wang, S. Yang, H. Zhang, X. Xu, C. D. Wood and W. Lipinski, “Amine infused hydrogel-based CO2 gas storage technology for CO2 hydrate-based cold thermal energy storage,” *Journal of CO2 Utilization,* no. 53, p. 101705, 2021.

[20] D. Asimakopoulos and M. Santamouris, “Passive Cooling of Buildings,” London, Routledge, 2013.

[21] J. Heier, C. Bales and V. Martin, “Combining thermal energy storage with buildings - a review,” *Renewable and Sustainable Energy Reviews,* no. 42, pp. 1305-1325, 2015.

[22] S. Hasnain, “Review on sustainable thermal energy storage technologies, part 1: Heat storage materials and techniques,” *Energy Conversion and Management,* no. 39(11), pp. 1127-1138, 1998.

[23] E. Hahne, “STORAGE OF SENSIBLE HEAT,” in *ENERGY STORAGE SYSTEMS*, Stuttgart, University of Stuttgart.

[24] l. Sarbu and C. Sebarchievici, “A Comprehensive Review of Thermal Energy Storage,” *Sustainability,* 2018.

[25] R. Baetens, B. Jelle and A. Gustavsen, “Phase change materials for building applications: a state-of-the-art review,” *Energy Build,* no. 42, p. 1361–8, 2010.

[26] H. Sarier and E. Onder, “Organic phase change materials and their textile applications: An overview,” *Thermochimica Acta,* no. 540, pp. 7-60, 2012.

[27] S. Hasnain, “Review on sustainable thermal energy storage technologies, Part I: heat storage materials and techniques,” *Energy Conversion and Management,* no. 39(11), pp. 1127-1138, 1998.

[28] F. Souayfane, F. Fardoun and P.-H. Biwole, “Phase change materials (PCM) for cooling applications in buildings: A review,” *Energy and Buildings,* no. 129, pp. 396-431, 2016.

[29] A. Abhat, “Low temperature latent heat thermal energy storage: heat storage materials,” *Solar Energy,* no. 30, 1983.

[30] J. Kosny, N. Shukla and A. Fallahi, “Cost Analysis of Simple Phase Change Material-Enhanced Building Envelopes in Southern U.S. Climates,” 2013.

[31] Y. Zhang and Y. Jiang, “A simple method, the T-history method, of determining the heat of fusion, specific heat and thermal conductivity of phase-change materials,” *Measur Sci Technol,* no. 10, pp. 201-5, 1999.

[32] H. Hong, K. S. Kim and Y.-S. Kim, “Accuracy improvement of T-history method for measuring heat of fusion of various materials,” *Int J Refrig,* no. 27, pp. 360-6, 2004.

[33] H. J. Peck, J.-J. Kim, C. Kang and H. Hong, “A study of accurate latent heat measurement for a PCM with a low melting temperature using T-history method,” *Int J Refrig,* no. 29, pp. 1225-32, 2006.

[34] M. Parsazadeh and X. Duan, “Numerical and statistical study on melting of nanoparticle enhanced phase change material in a shell-and-tube thermal energy storage system,” *Applied Thermal Engineering,* no. 111, pp. 950-960, 2017.

[35] R. E. Murray and D. Groulx, “Experimental study of the phase change and energy characteristics inside a cylindrical latent heat energy storage system: Part 1 consecutive charging and discharging,” *Renewable Energy,* no. 62, pp. 571-581, 2014.

[36] X. Py, R. Olives and S. Mauran, “Paraffin/porous graphite-matrix composite as a high and constant power thermal storage material,” *International Journal of Heat Mass Transfer,* no. 44, pp. 2727-37, 2001.

[37] K. Boomsma, D. Poulikakos and F. Zwick, “Metal foams as compact high performance heat exchangers,” *Mech Mater,* no. 35, pp. 1161-76, 2003.

[38] K. Nakaso, H. Teshima, A. Yoshimura, S. Nogami, Y. Hamada and J. Fukai, “Extension of heat transfer area using carbon fiber cloths in latent heat thermal energy storage tanks,” *Chemical Engineering and Processing: Process Intensification* , no. 5, pp. 879-885, 2008.

[39] U. Stritih, “Heat transfer enhancement in latent heat thermal storage system for buildings,” *Energy and Buildings,* no. 11, pp. 1097-1104, 2003.

[40] Y. Zhang, G. Zhou , K. Lin, Q. Zhang and H. Di, “Application of latent heat thermal energy storage in buildings: state-of-the-art and outlook,” *Building and Environment,* no. 42(6), pp. 2197-2209, 2007.

[41] F. Agyenim, N. Hewitt, P. Eames and M. Smyth, “A review of materials, heat transfer and phase change problem formulation for latent heat thermal energy storage systems (LHTESS),” *Renewable and Sustainable Energy Reviews* , no. 14(2), pp. 615-628, 2010.

[42] R. Baetens, B. P. Jelle and A. Gustavsen, “Phase change materials for building applications: A state-of-the-art review,” *Energy and Buildings* , no. 42, p. 1361–1368, 2010.

[43] M. Farid, A. Khudhair, S. Ali and K. Razack, “A review on phase change energy storage: materials and applications,” *Energy Conversion and Management* , no. 45, pp. 1597-1615, 2004.

[44] V. Tyagi and D. Buddhi, “PCM thermal storage in buildings: a state of art,” *Renewable and Sustainable Energy Reviews,* no. 11(6), pp. 1146-1166, 2007.

[45] A. Khudhair and M. Farid, “A review on energy conservation in building applications with thermal storage by latent heat using phase change materials,” *Energy Conversion and Management,* no. 45(2), pp. 263-275, 2004.

[46] Y. Zhang, K. Lin, R. Yang, H. Di and Y. Jiang, “Preparation, thermal performance and application of shape-stabilised PCM in energy efficient buildings,” *Energy Build,* no. 38, pp. 1262-9, 2006.

[47] “How Are Bricks Made?,” brickhunter, 5 February 2021. [Online]. Available: https://brickhunter.com/blog/how-are-bricks-made#:~:text=The%20main%20ingredient%20of%20most,colour%20of%20the%20end%20product.. [Accessed 31 May 2023].

[48] M. Mahdaoui, S. Hamdaoui, A. A. Msaad, T. Kousksou, T. E. Rhafiki, A. Jamil and M. Ahachad, “Building bricks with phase change material (PCM): Thermal performance,” *Construction and Building Materials,* no. 269, p. 121315, 2021.

[49] E. Elnajjar, “Using PCM embedded in Building Material for thermal management: performance assessment study,” *Energy Build,* no. 151, pp. 28-34, 2017.

[50] R. Saxena, D. Rakshit and S. Kaushik, “Phase change material (PCM) incorporated bricks for energy conservation in composite climate: a sustainable building solution,” *Sol. Energy,* no. 183, pp. 276-284, 2019.

[51] J. Yang, Y. Zhang and J. He, “Experimental study on heat transfer process of phase change contrete hollow block,” *New Build. Master,* no. 47(06), pp. 128-131, 2020.

[52] Y. Gao, F. He, X. Meng, Z. Wang, M. Zhang, H. Yu and W. Gao, “Thermal behavior analysis of hollow bricks filled with phase-change material (PCM),” *Journal of Building Engineering,* no. 31, p. 101447, 2020.

[53] V. R. V., P. R. and V. R. V., “PCM-mortar based construciton materials for energy efficient buildings: A review on research trends,” *Energy and Buildings,* no. 158, pp. 95-122, 2018.

[54] C. Guardia, G. Barluenga and I. Palomar, “PCM Cement-Lime Mortars for Enhanced Energy Efficiency of Multilayered Building Enclosure under Different Climatic Conditions,” *Materials (Basel),* no. 13(18), p. 4043, 2020.

[55] F. Orsini, P. Marrone, S. Santini, L. Sguerri, F. Asdrubali, G. Baldinelli, F. Bianchi and A. Presciutti, “Smart Materials: Cementitious Mortars and PCM Mechanical and Thermal Characterization,” *Materials (Basel),* no. 14(15), p. 4163, 2021.

[56] S. Lucas, L. Senff, V. Ferreira, J. d. A. Barroso and J. Labrincha, “Fresh state characterisation of lime mortars for latent heat storage,” *Applied Rheology,* no. 20, p. 63162, 2010.

[57] R. Shadnia, L. Zhang and P. Li, “Experimental study of geopolymer mortar with incorporated PCM,” *Construction and Building Materials* , no. 84, pp. 95-102, 2015.

[58] S. Cunha, J. Aguiar and F. Pacheco-Torgal, “Effect of temperature on mortars with incorporation of phase change materials,” *Construction and Building Materials* , no. 98, pp. 89-101, 2015.

[59] A. Adesina, “Use of phase change materials in concrete: current challenges,” *Renewable Energy and Environmental Sustainability,* no. 4, 2019.

[60] Y. Shen, S. Liu, C. Zeng, Y. Zhang, Y. Li, H. Xiaojing, L. Yang and X. Yang, “Experimental thermal study of a new PCM-concrete thermal storage block (PCM-CTSB),” *Construction and Building Materials,* no. 293, p. 123540, 2021.

[61] I. I. Hakim, N. Putra and P. D. Agustin, “Measurement of PCM-Concrete Composites Thermal Properties for Energy Conservation in Building Material,” in *API Conference Proceedings,* 2020.

[62] D. Niall, O. Kinnane, R. P. West and S. McCormack, “Mechanical and thermal evaluation of different types of PCM-concrete composite panels,” *Journal of Structural Integrity and Maintenance,* vol. 2, no. 2, pp. 100-108, 2017.

[63] H. Yu, C. Li, K. Zhang, Y. Tang, Y. Song and M. Wang, “Preparation and thermophysical performance of diatomite-based composite PCM wallboard for thermal energy storage in buildings,” *Journal of Building Engineering* , no. 32, p. 101753, 2020.

[64] H. Wang, W. Lu, Z. Wu and G. Zhang, “Parametric analysis of applying PCM wallboards for energy saving in high-rise lightweight buildings in Shanghai,” *Renewable Energy,* no. 145, pp. 52-64, 2020.

[65] G. Evola, L. Marletta and F. Sicurella, “A methodology for investigating the effectiveness of PCM wallboards for summer thermal comfort in buildings,” *Building and Environment,* no. 59, pp. 517-527, 2013.

[66] H. Yu, C. Li, K. Zhang, Y. Tang, Y. Song and M. Wang, “Preparation and thermophysical performance of diatomite-based composite PCM wallboard for thermal energy storage in buildings,” *Journal of Building Engineering,* no. 32, p. 101753, 2020.

[67] K. Biswas, J. Lu, P. Soroushian and S. Shrestha, “Combined experimental and numerical evaluation of a prototype nano-PCM enhanced wallboard,” *Applied Energy,* no. 131, pp. 517-529, 2014.

[68] F. Kuznik, J. Virgone and K. Johannes, “In-situ study of thermal comfort enhancement in a renovated building equipped with phase change material wallboard,” *Renewable Energy,* no. 36, pp. 1458-1462, 2011.

[69] Q. Wang, R. Wu, Y. Wu and C. Zhao, “Parametric analysis of using PCM walls for heating loads reduction,” *Energy & Buildings,* no. 172, pp. 328-336, 2018.

[70] W. He, C. Yu, J. Yang, B. Yu, Z. Hu, D. Shen, X. Liu, M. Qin and H. Chen, “Experimental study on the performance of a novel RC-PCM-wall,” *Energy & Buildings,* no. 199, pp. 297-310, 2019.

[71] S. H. Choi, J. Park, H. S. Ko and S. W. Karng, “Heat penetration reduction through PCM walls via bubble injections in buildings,” *Energy Conversion and Management,* no. 221, p. 113187, 2020.

[72] J. Xie, W. Wang, P. Sang and J. Liu, "Experimental and numerical study of thermal performance of the PCM wall with solar radiation," *Construction and Building Materials,* no. 177, pp. 443-456, 2018.

[73] S. Duan, L. Wang, Z. Zhao and C. Zhang, "Experimental study on thermal performance of an integrated PCM Trombe wall," *Renewable Energy,* no. 163, pp. 1932-1941, 2021.

[74] R. Ansuini, R. Larghetti, A. Giretti and M. Lemma, "Radiant floors integrated with PCM for indoor temperature control," *Energy and Buildings,* no. 43, pp. 3019-3026, 2011.

[75] L. Royon, L. Karim and A. Bontemps, "Optimization of PCM embedded in a floor panel developed for thermal management of the lightweight envelope of buildings," *Energy and Buildings,* no. 82, pp. 385-390, 2014.

[76] X. Jin and X. Zhang, "Thermal analysis of a double layer phase change material floor," *Applied Thermal Engineering,* no. 31, pp. 1576-1581, 2011.

[77] S. Lu, B. Liang, X. Li, X. Kong, W. Jia and L. Wang, "Performance Analysis of PCM Ceiling Coupling with Earth-Air Heat Exchanger for Building Cooling," *Materials (Basel),* no. 13, p. 13, 2020.

[78] J. Riffat, C. Kutlu, E. Tapia-Brito, Y. Su and S. Riffat, "A preliminary experimental study of a novel incorporation of chilled ceiling with phase change materials and transparent membrane cover," *International Journal of Low-Carbon Technologies,* vol. 17, pp. 258-265, 2022.

[79] M. Velasco-Carrasco, Z. Chen, J. L. Aguilar-Santana and S. Riffat, "Experimental Evaluation of Thermal Energy Storage (TES) with Phase Change Materials (PCM) for Ceiling Tile Applications," *Future Cities and Environment,* vol. 6, no. 1, p. 11, 2020.

[80] M. Koschenz and B. Lehmann, "Development of a thermally activated ceiling panel with PCM for application in lightweight and retrofitted buildings," *Energy and Buildings,* no. 36, pp. 567-578, 2004.

[81] J. Quesada Allerhand, O. Berk Kazanci and B. W. Olesen, "Energy and thermal comfort performance evaluation of PCM ceiling panels for cooling a renovated office room," in *CLIMA 2019 Congress*, Romania, 2019.

[82] M. Rida and S. Hoffmann, "The influence of macro-encapsulated PCM panel's geometry on heat transfer in a ceiling application," *Advances in Building Energy Research,* vol. 16, no. 4, pp. 445-465, 2021.

[83] H. Jamil, M. Alam, J. Sanjayan and J. Wilson, "Investigation of PCM as retrofitting option to enhance occupant thermal comfort in a mordern residential building," *Energy and Buildings,* no. 133, pp. 217-229, 2016.

[84] T. Silva, R. Vicente, C. Amaral and A. Figueiredo, "Thermal performance of a window shutter containing PCM: Numerical validation and experimental analysis," *Applied Energy,* no. 179, pp. 64-84, 2016.

[85] E. M. Alawadhi, "Using phase change materials in window shutter to reduce the solar heat gain," *Energy and Buildings,* no. 47, pp. 421-429, 2012.

[86] T. Silva, R. Vicente, F. Rodrigues, A. Samagaio and C. Cardoso, “Performance of a window shutter with phase change material under summer Mediterranean climate conditions,” *Applied Thermal Engineering,* no. 84, pp. 246-256, 2015.

[87] B. Durakovic and M. Torlak, “Experimental and numerical study of a PCM window model as a thermal energy storage unit,” *International Journal of Low-Carbon Technologies,* vol. 12, no. 3, pp. 272-280, 2016.

[88] D. Li, Y. Wu, C. Liu, G. Zhang and M. Arici, “Energy investigation of glazed windows containing Nano-PCM in different seasons,” *Energy Conversion and Management,* no. 172, pp. 119-128, 2018.

[89] M. F. L. King, P. N. Rao, A. Sivakumar, V. K. Mamidi, S. Richard, M. Vijayakumar, K. Arunprasath and P. M. Kumar, “Thermal performance of a double-glazed window integrated with a phase change material (PCM),” *Materials Today: Proceedings,* no. 50, pp. 1516-1521, 2022.

[90] D. Kumar, M. Alam and J. G. Sanjayan, “Retrofitting Building Envelope Using Phase Change Materials and Aerogel Render for Adaptation to Extreme Heatwave: A Multi-Objective Analysis Considering Heat Stress, Energy, Environment, and Cost,” *Sustainability,* no. 13, p. 10716, 2021.

[91] D. Bentz and R. Turpin, “Potential application of phase change materials in concrete technology,” *Cem Concr Compos,* no. 29, p. 527–32, 2007.

[92] Y. Zhang, M. V. Bozorg, J. F. Torres, Y. Zhao and X. Wang, “Dynamic melting of encapsulated PCM in various geometries driven by natural convection of surrounding air: A modelling-based parametric study,” *Journal of Energy Storage,* vol. 48, p. 103975, 2022.

[93] dreamstime, “Continuous line drawing of business situation - man sitting in office chair thinking,” OneLineStock, [Online]. Available: https://www.dreamstime.com/continuous-line-drawing-business-situation-man-sitting-office-chair-thinking-continuous-line-drawing-flat-vector-image139662580. [Accessed 7 November 2022].

[94] “How to Draw a Sitting Person,” HOWTODRAWFORKIDS, [Online]. Available: https://howtodrawforkids.com/how-to-draw-a-sitting-person/. [Accessed 7 November 2022].

[95] R. W. Douglas, “amorphous solid,” Britannica, 31 July 2019. [Online]. Available: https://www.britannica.com/science/amorphous-solid/additional-info#contributors. [Accessed 22 December 2022].

[96] J. F. Torres, D. Henry, A. Komiya and S. Maruyama, “Bifurcation analysis of steady natural convection in a tilted cubical cavity with adiabatic sidewalls,” *Journal of Fluid Mechanics,* vol. 756, pp. 650-688, 2014.

[97] J. F. Torres, F. Ghanadi, Y. Wang, M. Arjomandi and J. Pye, “Mixed Convection and Radiation From An Isothermal Bladed Structure,” *International Journal of Heat and Mass Transfer,* vol. 147, p. 118906, 2020.

[98] ANSYS, “ANSYS,” 23 January 2009. [Online]. Available: https://www.afs.enea.it/project/neptunius/docs/fluent/html/th/node352.htm. [Accessed 16 August 2022].

[99] "LatLong.net," [Online]. Available: https://www.latlong.net/place/canberra-australia-29466.html. [Accessed 13 September 2021].

[100] "Climate - Australia - Average weather, temperature, rainfall, when to go, what to pack," [Online]. Available: https://www.climatestotravel.com/climate/australia. [Accessed 16 September 2021].

[101] "Past Weather in Canberra, Australian Capital Territory, Australia — May 2020," [Online]. Available: https://www.timeanddate.com/weather/australia/canberra/historic?month=5&year=2020. [Accessed 16 September 2021].

[102] X. Wang, X. Zhai, T. Wang, H. Wang and Y. Yin, "Performance of the capric and lauric acid mixture with additives as cold storage materials for high temperature cooling application," *Applied Thermal Engineering,* no. 58, pp. 252-260, 2013.

[103] M. V. Bozorg, M. H. Doranehgard, K. Hong and Q. Xiong, "CFD study of heat transfer and fluid flow in a parabolic trough solar receiver with internal annular porous structure and synthetic oil-Al2O3 nanofluid," *Renewable Energy,* vol. 145, pp. 2598-2614, 2020.

[104] A. Mwesigye, Z. Huan and J. P. Meyer, "Thermal performance and entropy generation analysis of a high concentration ratio parabolic trough solar collector with Cu-Therminol®VP-1 nanofluid," *Energy Conversion and Management,* vol. 120, pp. 449-465, 2016.

[105] S. S. Hosseini, A. Ramiar and A. A. Ranjbar, "Numerical investigation of natural convection solar air heater with different fins shape," *Renewable Energy,* vol. 117, pp. 488-500, 2018.

[106] G. Kuznetsov, V. Maksimov and M. Sheremet, "Natural convection in a closed parallelepiped with a local energy source," *Journal of Applied Mechanics and Technical Physics,* vol. 54, pp. 588-595, 2013.

[107] S. Patankar, Numerical Heat Transfer and Fluid Flow, CRC Press, 1980.

[108] A. Government, "Thermal mass," YourHome, [Online]. Available: https://www.yourhome.gov.au/passive-design/thermal-mass#:~:text=Materials%20such%20as%20concrete%2C%20bricks,to%20have%20low%20thermal%20mass.. [Accessed 21 June 2023].

[109] C. Gregory, "Seasonal Lag: The relationship between incoming sunlight and temperatures on earth," 10 January 2021. [Online]. Available: https://www.rochesterfirst.com/weather/weather-blog/seasonal-lag-the-relationship-between-incoming-sunlight-and-temperatures-on-earth/. [Accessed 9 May 2023].

[110] S. Lu, B. Liang, X. Li, X. Kong, W. Jia and L. Wang, "Performance Analysis of PCM Ceiling Coupling with Earth-Air Heat Exchanger for Building Cooling," *Materials (Basel,* no. 13, p. 13, 2020.

[111] S. Yang, Y. Zhang, Y. Zhao, J. F. Torres and X. Wang, "PCM-based ceiling panels for passive cooling in buildings: A CFD modelling," *Energy & Buildings,* no. 285, p. 112898, 2023.

[112] X. Wang, X. Zhai, T. Wang, H. Wang and Y. Yin, "Performance of the capric and lauric acid mixture with additives as cold storage materials for high temperature cooling application," *Applied Thermal Engineering,* no. 58, pp. 252-260, 2013.

Appendix – Abstract of Publications

Energy & Buildings 285 (2023) 112898

Contents lists available at ScienceDirect

Energy & Buildings

journal homepage: www.elsevier.com/locate/enb

PCM-based ceiling panels for passive cooling in buildings: A CFD modelling

Shufan Yang [a], Yuxuan Zhang [a], Yongling Zhao [b], Juan F. Torres [a], Xiaolin Wang [a,*]

[a] School of Engineering, The Australian National University, Canberra, ACT 2601, Australia
[b] Department of Mechanical and Process Engineering, ETH Zürich, 8092 Zürich, Switzerland

ARTICLE INFO

Article history:
Received 22 December 2022
Revised 10 February 2023
Accepted 12 February 2023
Available online 15 February 2023

Keywords:
Phase change materials
Thermal energy storage
Passive cooling
Computational fluid dynamics
Natural convection
Conjugate heat transfer

ABSTRACT

To relieve the upsurge of the energy demand associated to building indoor cooling, passive cooling employing phase change materials (PCMs) has been proposed as a promising technique to stabilise indoor air temperature fluctuation and reduce building energy demand. PCMs can exchange a large amount of latent heat during the melting and solidification processes, which can be utilised in line with the discharging and charging processes of a cooling system. The use of encapsulated PCM ceiling panels in buildings has immense application potential for passive cooling, which has attracted investigations in recent years. The geometry selection of the PCM ceiling panel is vital as it determines the exposed surface area to the surrounding air and the natural convection, and therefore the heat transfer rate to/from the PCM, which generally suffers from low thermal conductivity. This paper builds on the geometric optimisation of enclosed PCM capsules driven by natural convection, aiming to investigate the phase change behaviour and thermal performance of encapsulated PCM ceiling panels of different geometries. Here, the presented study focuses on the conjugate heat transfer phenomena through the surrounding air, panel shell, and PCM. A mixture of lauric, capric, and oleic acids was selected as PCM encapsulated in a thin-shell enclosure made of acrylonitrile butadiene styrene plastic, which forms the aesthetic panels attached to the ceiling. A computational fluid dynamics model was validated using full-scale experimental data and further employed to analyse the discharging process and design considerations of the PCM ceiling panels. The effects of various influencing factors were explored, such as panel volume, the initial temperature difference between PCMs and surrounding air, shell thickness, and geometrical features. The results indicate that the panel comprised of a pyramid array is more advantageous than the tetrahedral-based panel in terms of thermal performance, where the average melting rate is 20.8 % higher when the panel volume is 250 mL. In addition, tweaking the geometric features of the panel will largely impact its thermal performance as the effective heat transfer area and natural convection conditions are varied. Finally, it was found that hanging the panel to the ceiling will effectively enhance the heat transfer compared to directly attaching it to the ceiling. The results complement the knowledge body of macro-encapsulated PCM ceiling panels in terms of thermal performance and geometric optimisation. The effects of geometric features on the thermal performance of the PCM ceiling panels are studied in a more holistic manner.

1. Introduction

In recent decades, there has been an increasing energy demand for building indoor cooling, especially for those with emerging construction techniques. The lightweight-design buildings have reduced thermal mass compared to the conventional buildings [1], therefore the indoor temperature is more sensitive to heat gain and the thermal comfort for building occupants cannot be guaranteed due to the temperature fluctuations. Air conditioning energy consumption is overwhelming, which brings environmental challenges such as depletion of the ozone sphere, intensification of global warming, and greenhouse effect [2]. In the United States, 6 % of the total electricity production is consumed by air conditioners, which creates a cost of 29 billion to homeowners annually. This also results in an annual carbon dioxide emission of approximately 117 million metric tons [3]. To mitigate the energy demand sourced from indoor space cooling, passive cooling techniques have attracted increased interest recently. Passive cooling technologies employ the low-temperature ambient as a cooling sink

* Corresponding author.
E-mail address: xiaolin.wang@anu.edu.au (X. Wang).

https://doi.org/10.1016/j.enbuild.2023.112898
0378-7788/© 2023 Elsevier B.V. All rights reserved.